

AN EXPERIMENTAL AND NUMERICAL STUDY OF UTILIZING STEEL FIBER AND
GFRP IN BRIDGE DECKS UNDER BENDING

by

SAM KAFAJI

A DISSERTATION

Presented to the Faculty of the Graduate School of The University of Texas at Arlington

In Partial Fulfillment of the Requirements for the Degree

DOCTOR OF PHILOSOPHY



The University of Texas at Arlington

College of Engineering

Civil Engineering, December 2023

Copyright © by Sam Kafaji 2023

All Rights Reserved



ACKNOWLEDGEMENTS

I wish to convey my profound appreciation to all the distinguished individuals and esteemed organizations whose unwavering support and contributions have played an indispensable role in the successful culmination of my doctoral research.

Foremost among those to whom I owe a debt of gratitude is my esteemed supervisor, Dr. Raad Azzawi. His continuous encouragement, unwavering enthusiasm, and steadfast support have been the cornerstone of this research endeavor. Without his invaluable guidance, this project would have faced formidable challenges in reaching its conclusion. Dr. Azzawi's mentorship has enriched my academic journey and made me a more accomplished researcher.

Additionally, I extend my heartfelt thanks to Dr. Nur Yazdani, whose technical expertise and expert counsel were instrumental in the progress of this research project. I am equally appreciative of the contributions of Dr. Warda Ashraf and Dr. Bill Carroll, whose generous allocation of time, extensive knowledge, and constructive feedback during the evaluation of my research significantly elevated the quality of my dissertation.

I would also like to express my gratitude to my dear friends, Ahmed Alateeq, Ahmed Shlash, and Sadat Morshed, along with my colleagues and the faculty and staff of the department. Their camaraderie and support made my tenure at the University of Texas at Arlington a truly enriching experience.

Finally, I wish to extend my heartfelt thanks to my family, particularly my beloved wife, Hala Aldnan, and my children, for their unwavering understanding, love, encouragement, and assistance throughout my academic journey and the challenges it presented. I am equally indebted to my father, Neamah AlKhafaji, whose unwavering support has been a constant source of strength and motivation for me.

Sam Kafaji

December 2023

ABSTRACT

AN EXPERIMENTAL AND NUMERICAL STUDY OF UTILIZING STEEL FIBER AND GFRP IN BRIDGE DECKS UNDER BENDING

Sam Kafaji

The University of Texas at Arlington, 2023

Advisor: Dr. Raad Azzawi

The process of laying and tying conventional reinforcement is a time-consuming task when building a bridge deck, especially while ensuring the proper cover. To speed up the construction process, the bridge construction industry should look into replacing conventional reinforcing bars with steel fibers. This could be a significant breakthrough in bridge construction. Despite numerous experiments and research conducted on the bending strength of reinforced concrete decks, there are still several factors that require further exploration. This experiment focuses on utilizing steel fiber reinforced concrete (SFRC) in a multiple-span concrete bridge deck to investigate the opportunities of using SFRC as the main reinforcement and reducing construction time by eliminating the need for tying and tying reinforcement. SFRC does not require this, making the process much quicker. To evaluate the behavior of the SFRC decks, it was necessary to compare them to conventional reinforced concrete decks (RC) in terms of load-displacement, bending strength, ductility, crack behavior, and crack widths. In this study, two groups of concrete bridge decks were tested. The first group consisted of six decks, two of which were cast-in-place and reinforced with steel fiber as the main reinforcement, along with supplementary steel wire mesh (SFRC-CIP). The other two decks had similar reinforcement to the first two decks but were precast (SFRC-PC). These decks were compared with the last two cast-in-place decks reinforced

by conventional steel bars designed per AASHTO LRFD (RC). The second group also had six decks, with two cast-in-place decks reinforced with steel fiber as the main reinforcement and supplementary GFRP mesh (SFRC-GFRP-CIP). The other two decks had similar reinforcement but were precast (SFRC-GFRP-PC). These decks were compared with the last two cast-in-place decks of this group that were reinforced by GFRP bars designed per AASHTO LRFD and ACI-440 code (GFRP). The study used concrete with a compressive strength of 4000 psi, and all decks were tested under flexural loads. Load-displacement curves ($P-\Delta$) were recorded as a tool to measure the ductility index (μ_E) (Spadea et al. and Hason 2021).

The result showed that the flexural stiffness behavior of the SFRC concrete deck specimens was improved, and load-carrying capacity increased compared to RC and GFRP decks. Moreover, crack width and crack were reduced since the SFRC decks offer more concrete ductility than the RC and GFRP decks, meaning less future maintenance and corrosion. Therefore, utilizing steel fiber in concrete mixtures could be a significant step in speeding up bridge construction since it saves time for laying, tying, and verifying clear cover, in addition to increasing the lifespan of bridge decks.

TABLE OF CONTENTS	
ACKNOWLEDGEMENTS.....	iii
ABSTRACT.....	v
List of Figures.....	xii
List of Tables.....	xviii
Chapter 1.....	1
INTRODUCTION	1
1.1 Overview	1
1.2 Steel Fiber	3
1.3 GFRP	5
1.4 Research Objectives.....	6
1.5 Dissertation outlines.....	7
Chapter 2.....	8
LITERATURE REVIEW	8
2.1 Overview	8
2.2 Steel Fiber	8
2.3 GFRP	21
Chapter 3.....	26
MATERIALS AND CONCRETE STANDARD TESTS.....	26
3.1 Materials.....	26

3.1.1	Cement	26
3.1.2	Non-shrink Grout	26
3.1.3	Coarse aggregate	27
3.1.4	Fine aggregate	27
3.1.5	Mixing water	27
3.1.6	Steel bars	27
3.1.7	Steel fiber	27
3.1.8	GFRP bars	29
3.1.9	Concrete	30
3.2	Concrete Standard Test	30
3.2.1	Slump Test	32
3.2.2	Comprehensive Strength Test	33
3.2.3	Split Tensile Test	36
3.2.4	Flexural Test	39
3.2.5	Modulus of Elasticity Test	44
3.2.6	Poisson's Ratio	48
3.3	Conclusion of concrete standard test results	52
Chapter 4	53
CONCRETE DECK SPECIMENS PREPARATION AND EXPERIMENT WORK		53
4.1	Overview	53

4.2	Dimensions of deck case study	54
4.2.1	Concrete Girders design.....	55
4.2.2	Deck design.....	56
4.2.3	Specimen preparation.....	66
4.2.4	Experimental Work.....	66
4.2.5	Specimen testing.....	73
Chapter 5	76
FINITE ELEMENT MODELING (FEM)	76
5.1	Overview	76
5.1.1	Initial Numerical Modeling.....	76
5.1.2	Precast Girders	77
5.1.3	Concrete Decks	78
5.1.4	Concrete and Steel Properties	82
5.2	Material properties	82
5.3	Boundary Conditions.....	88
5.4	Interaction.....	89
5.5	Results	91
5.6	Conclusions of the FE Modeling.....	91
Chapter 6	93
RESULTS AND DISCUSSIONS OF SFRC-CIP & SFRC-PC vs. RC	93

6.1	Results Presentation	93
6.1.1	Reference RC Concrete Decks.....	94
6.1.2	SFRC-CIP Concrete Decks.....	97
6.1.3	SFRC-PC Concrete Decks	101
6.2	Results Comparison.....	104
6.2.1	Load – Displacement Characteristics.....	106
6.2.2	Ductility Index	107
6.2.3	Stress-Strain Characteristics	108
6.2.4	Crack Width.....	108
Chapter 7	112
RESULTS AND DISCUSSIONS OF SFRC-GFRP-CIP & SFRCR-GFRP-PC vs. GFRP...		112
7.1	Results Presentation	112
7.1.1	Reference GFRP	112
7.1.2	SFRC-GFRP-CIP	115
7.1.3	SFRC-GFRP-PC	119
7.2	Results Comparison.....	122
7.2.1	Load – Displacement Characteristics.....	122
7.2.2	Ductility Index	123
7.2.3	Stress-Strain Characteristics	124
7.2.4	Crack Width.....	125

Chapter 8	128
CONCLUSIONS AND RECOMMENDATIONS	128
8.1 Conclusions	128
8.1.1 SFRC-CIP Concrete Decks vs RC Concrete Decks	128
8.1.2 SFRC-PC Concrete Decks vs RC Concrete Decks.....	129
8.1.3 SFRC-GFRP-CIP Concrete Decks vs GFRP Concrete Decks	130
8.1.4 SFRC-GFRP-PC Concrete Decks vs GFRP Concrete Decks.....	130
8.2 Recommendations and Future Research	132
References.....	134
Abbreviations.....	141
Appendix A.....	145
Appendix B	148
Appendix C	155

LIST OF FIGURES

Figure 2 - 1 Load–deformation plot for horizontal and vertical displacement of 24-in. SFRCP versus RCP (AbulMaali et al. 2012).....	11
Figure 2 - 2 Load–deformation plot for vertical displacement of 36-in. (AbulMaali et al. 2012)	12
Figure 2 - 3 Variation of Compressive strength with respect to % of fiber content (Milind V. Mohod 2012).....	13
Figure 2 - 4 Variation of Flexural strength with respect to % of fiber content (Milind V. Mohod 2012).....	13
Figure 2 - 5 Load deflection curves of the tested road pavement slabs. (Fattouh et al. 2023).....	15
Figure 2 - 6 Visual appearance of beam specimens exposed to 10% Cl–solution:	17
Figure 2 - 7 Cracks in specimens after exposure to 10% Cl–solution:.....	18
Figure 3 - 1 Type I/II Cement.....	26
Figure 3 - 2 Non-Shrinkage Grout.....	27
Figure 3 - 3 Hooked-end Dramix 4D Steel Fiber (Bekaert, 2023)	28
Figure 3 - 4 Hooked-end Dramix 4D Steel Fiber	29
Figure 3 - 5 Glass Fiber Reinforced Polymer Bars (GFRP).....	29
Figure 3 - 6 Concrete Standard Specimens in The Curing Room.....	32
Figure 3 - 7 Slump Test for Plain Concrete and SFRC.....	33
Figure 3 - 8 Compression Test for Plain Concrete and SFRC.....	34
Figure 3 - 9 Ultimate Load of Compressive Test Results of Plain Concrete.....	34
Figure 3 - 10 Ultimate Load of Compressive Test Results of SFRC.....	35
Figure 3 - 11 Ultimate Compressive Strength Test Results of Plain Concrete.....	35

Figure 3 - 12 Ultimate Compressive Strength Test Results of SFRC Concrete	36
Figure 3 - 13 Tensile Test Machine	36
Figure 3 - 14 Tensile Test of Plain Concrete and SFRC.....	37
Figure 3 - 15 Ultimate Load of Tensile Test Results of Plain Concrete.....	38
Figure 3 - 16 Ultimate Load of Tensile Test Results of SFRC.....	38
Figure 3 - 17 Ultimate Tensile Strength Test Results of Plain Concrete.....	39
Figure 3 - 18 Ultimate Tensile Strength Test Results of SFRC.....	39
Figure 3 - 19 Flexure Test Machine.....	40
Figure 3 - 20 Flexure Test of Plain Concrete and SFRC	41
Figure 3 - 21 Ultimate Load of Flexure Test Results of Plain Concrete	42
Figure 3 - 22 Ultimate Load of Flexure Test Results of SFRC	42
Figure 3 - 23 Ultimate Load of Flexure Test Results of SFRC	43
Figure 3 - 24 Ultimate Load of Flexure Test Results of SFRC	43
Figure 3 - 25 Modulus of Elasticity Test Machine	44
Figure 3 - 26 Modulus of Elasticity of Plain Concrete	46
Figure 3 - 27 Modulus of Elasticity of SFRC.....	46
Figure 3 - 28 Stress-Strain Curves of Plain Concrete.....	47
Figure 3 - 29 Stress-Strain Curves of SFRC.....	48
Figure 3 - 30 Initial and Final Length and Diameter of Cylinder.....	50
Figure 3 - 31 Poisson's Ratio Test Results of Plain Concrete	51
Figure 3 - 32 Poisson's Ratio Test Results of SFRC	51
Figure 4 - 1 Case Study Details	55

Figure 4 - 2 Sketch of Pre-Cast Concrete Girder.....	56
Figure 4 - 3 Pre-Cast Concrete Girder	56
Figure 4 - 4 AASHTO LRFD Concrete Deck Design Details.....	58
Figure 4 - 5 Formworks and Bottom Layer Reinforcement of AASHTO LRFD Concrete Deck	58
Figure 4 - 6 Steel Fiber Reinforcement Cast-In-Place Concrete Deck Details (SFRC-CIP).....	59
Figure 4 - 7 Steel Fiber Reinforcement Precast Concrete Deck Details (SFRC-PC)	60
Figure 4 - 8 Precast Deck and Girders before Grouting	61
Figure 4 - 9 Precast Deck and Girders After Grouting	62
Figure 4 - 10 Reinforcement Details of GFRP Decks	63
Figure 4 - 11 Formworks and Bottom Layer Reinforcement of GFRP Bars.....	64
Figure 4 - 12 Reinforcement Details of SFRC-GFRP-CIP Deck	65
Figure 4 - 13 Reinforcement Details of SFRC-GFRP-PC Deck.....	65
Figure 4 - 14 Concrete Decks Formworks and Casting.....	66
Figure 4 - 15 400 Kips MTS Testing Machine.....	67
Figure 4 - 16 Load Cell.....	68
Figure 4 - 17 Steel Plate as a Tire Contact Area.....	69
Figure 4 - 18 Load Distribution Steel Beam.....	70
Figure 4 - 19 Linear Variable Differential Transformer Sensor	71
Figure 4 - 20 Strain Gauges	72
Figure 4 - 21 Data Acquisition System.....	73
Figure 4 - 22 Schematic Testing Setup	74
Figure 4 - 23 400 Kips MTS Testing Machine and Test Configuration.....	75

Figure 5 - 1 Model View of the Concrete Decks	77
Figure 5 - 2 FE Model of Girders	78
Figure 5 - 3 FE Model of RC Decks.....	79
Figure 5 - 4 FE Model of SFRC-PC	80
Figure 5 - 5 FE Model of GFRP	81
Figure 5 - 6 FE Model of SFRC-GFRP-PC	82
Figure 5 - 7 Menu of Material Density	83
Figure 5 - 8 Menu of Material Elastic Properties	84
Figure 5 - 9 Concrete Damage Plasticity Menu.....	86
Figure 5 - 10 Compressive Behavior Menu.....	86
Figure 5 - 11 Tensile Behavior Menu	87
Figure 5 - 12 Concrete Compression Damage Menu.....	87
Figure 5 - 13 Concrete Tension Damage Menu.....	88
Figure 5 - 14 Boundary conditions of numerical simulation	89
Figure 5 - 15 Stresses shape / location.....	90
Figure 5 - 16 Deflection shape / location.....	90
Figure 5 - 17 XY Data Field Output and S-S Curve.....	91
Figure 6 - 1 Load-Displacement Curve of RC-1 Deck.....	95
Figure 6 - 2 Load-Displacement Curve of RC-2 Deck.....	95
Figure 6 - 3 Stress-Strain Curve of RC-1 Deck	96
Figure 6 - 4 Stress-Strain Curve of RC-2 Deck	97
Figure 6 - 5 RC Concrete Deck Specimen.....	97

Figure 6 - 6 Load-Displacement Curve of SFRC-CIP-1 Deck.....	98
Figure 6 - 7 Load-Displacement Curve of SFRC-CIP-2 Deck.....	99
Figure 6 - 8 Stress-Strain Curve of SFRC-CIP-1 Deck.....	100
Figure 6 - 9 Stress-Strain Curve of SFRC-CIP-2 Deck.....	100
Figure 6 - 10 SFRC-CIP Concrete Deck Specimen.....	101
Figure 6 - 11 Load-Displacement Curve of SFRC-PC-1 Deck.....	102
Figure 6 - 12 Load-Displacement Curve of SFRC-PC-2 Deck.....	102
Figure 6 - 13 Stress-Strain Curve of SFRC-PC-1 Deck.....	103
Figure 6 - 14 Stress-Strain Curve of SFRC-PC-2 Deck.....	104
Figure 6 - 15 SFRC-PC Concrete Deck Specimen.....	104
Figure 6 - 16 Definition of the Ductility Index Estimation Curve.....	106
Figure 6 - 17 Crack Width Curves of RC, SFRC-CIP, SFRC-PC.....	110
Figure 6 - 18 Concrete Specimens Failure, (a, b) RC; (c, d) SFRC-CIP; (e, f): SFRC-PC.....	111
Figure 7 - 1 Load-Displacement Curve of GFRP-1 Deck.....	113
Figure 7 - 2 Load-Displacement Curve of GFRP-2 Deck.....	113
Figure 7 - 3 Stress-Strain Curve of GFRP-1 Deck.....	114
Figure 7 - 4 Stress-Strain Curve of GFRP-2 Deck.....	115
Figure 7 - 5 GFRP Concrete Deck Specimen.....	115
Figure 7 - 6 Load-Displacement Curve of SFRC-GFRP-CIP-1 Deck.....	116
Figure 7 - 7 Load-Displacement Curve of SFRC-GFRP-CIP-2 Deck.....	117
Figure 7 - 8 Stress-Strain Curve of SFRC-GFRP-CIP-1 Deck.....	118
Figure 7 - 9 Stress-Strain Curve of SFRC-GFRP-CIP-2 Deck.....	118

Figure 7 - 10 SFRC-GFRP-CIP Concrete Deck Specimen	119
Figure 7 - 11 Load-Displacement Curve of SFRC-GFRP-PC-1 Deck.....	120
Figure 7 - 12 Load-Displacement Curve of SFRC-GFRP-PC-2 Deck.....	120
Figure 7 - 13 Stress-Strain Curve of SFRC-GFRP-PC-1 Deck	121
Figure 7 - 14 Stress-Strain Curve of SFRC-GFRP-PC-2 Deck.....	122
Figure 7 - 15 SFRC-GFRP-PC Concrete Deck Specimen.....	122
Figure 7 - 16 Crack Width Curves of GFRP, SFRC-GFRP-CIP, and SFRC-GFRP-PC.....	126
Figure 7 - 17 Concrete Specimens Failure, (a, b) GFRP; (c, d) SFRC-GFRP-CIP; (e, f): SFRC-GFRP-PC	127

LIST OF TABLES

Table 3 - 1 Dramix 4D Steel Fiber Characteristics and Geometry	28
Table 3 - 2 Concrete Mix Design, Amounts for 1 Cubic Yard of Concrete	30
Table 3 - 3 Type and Number of Specimens for Standard Concrete Tests.....	31
Table 4 - 1 Concrete Decks with Various Types of Reinforcement	54
Table 4 - 2 AASHTO LRFD Reinforcement Details of RC Decks	57
Table 4 - 3 Reinforcement Details of GFRP Decks.....	62
Table 5 - 1 Modulus of Elasticity and Poisson's Ratio of Concrete Decks	84
Table 6 - 1 Load-Displacements of RC, SFRC-CIP, and SFRC-PC Decks	107
Table 6 - 2 Energy Absorbed, and Ductility Index of RC, SFRC-CIP, and SFRC-PC Decks ..	108
Table 6 - 3 Stress-Strain of RC, SFRC-CIP, and SFRC-PC Decks	108
Table 7 - 1 Load-Displacements of GFRP, SFRC-GFRP-CIP, and SFRC-GFRP-PC Decks	123
Table 7 - 2 Energy Absorbed, and Ductility Index of GFRP, SFRC-GFRP-CIP, and SFRC-GFRP-PC Decks.....	124
Table 7 - 3 Stress-Strain of GFRP, SFRC-GFRP-CIP, and SFRC-GFRP-PC Decks.....	125

CHAPTER 1

INTRODUCTION

1.1 Overview

For over 4500 years, fibers have been utilized to strengthen mixtures that are weak in tension. In ancient times, straw fibers were used in sun-dried mud bricks to create composites that had increased toughness, resulting in better resistance to cracking and an improved post-cracking response. With the innovation of Portland cement, concrete became a popular construction material. Engineers have long been engaged in endeavors aimed at mitigating the inherent shortcomings of concrete, particularly its notable deficiencies in terms of low tensile strength and high brittleness. Attempts were made to use fibers to reduce cracks. Notably, a seminal contribution to this ongoing pursuit was made by Joseph Lambot in 1847. Lambot's innovation entailed the incorporation of continuous fibers into the concrete mixture, typically shown in the form of wires or wire meshes. This innovative approach represented a pivotal step forward in concrete engineering, marking an early instance of addressing concrete's structural limitations through strategically integrating reinforcing elements. This led to the development of ferrocement and reinforced concrete, as known today (Naaman, 1985). In response to the inherent weakness of concrete regarding its tensile strength, the utilization of continuous steel bars as a reinforcing mechanism has proven to be notably efficacious. Nevertheless, the successful integration of discontinuous reinforcement, in the form of fibers, into the concrete matrix persists as a formidable challenge within the field of concrete engineering. Prior to the 1960s, advancements in the utilization of fiber reinforcement for concrete exhibited a measured pace of development. While certain research efforts had explained the conceptual framework for integrating fibers as reinforcing agents within concrete compositions, the

practical application of this knowledge remained conspicuously limited. However, a noteworthy turning point emerged with the inception of research endeavors focused on glass fibers, which transpired concurrently in the United States, the United Kingdom, and Russia during the formative years of the 1950s, as documented by the American Concrete Institute's Committee 544 in their report from 1982. This period marked a significant turning point in the path of concrete engineering, as it laid the foundation for subsequent innovations in the field of fiber reinforcement for concrete structures.

Fiber-reinforced concrete (FRC) has garnered substantial and pervasive scholarly and practical interest since its emergence in the early 1960s, constitutes a pivotal turning point in its evolutionary path. The contemporary landscape of the FRC field has been profoundly shaped by the introduction of diverse fiber variants that feature a range of types, dimensions, shapes, and colors. This evolutionary phase has engendered a rapid spreading in the FRC industry, resulting in a noteworthy expansion of its applications. These applications include a multifaceted spectrum of structural and architectural contexts, representing a profound transformation in the utilization of FRC within the broader field of construction and engineering. These types include:

- Glass Fibers
- Steel Fibers
- Polypropylene Fibers
- Natural Organic Fiber
- Carbon Fibers
- Other Fibers & Blends

Later, in the late 1970's and early 1980's, during the modern development of FRC, when the

testing equipment and analysis procedures became more quantitative and better qualitatively, the concept of energy absorption and ductility index was introduced. This equipment enabled the measurement of the toughness of materials. The major advantage of FRC was discovered, and it was the outstanding property of absorbing large amounts of energy compared to plain concrete. Even today, after more than six decades of research in this field, it can be said that the main benefit of FRC is its high fracture toughness. However, further research with different types, dosages of fibers, and admixtures targets the development of a composite with increased tensile and compressive strengths besides the fracture toughness. The production of a cement-based material having high tensile and compressive strengths and remarkable energy absorption capacity is no longer difficult. The incessant research in the field of FRC has led to the production of high-performance fiber-reinforced concrete (HPFRC), which shows a combination of excellent properties compared to other cementitious composites. The research involved using steel fibers as the primary reinforcement in the concrete mixture for concrete bridge decks. In addition, steel wire mesh was used as supplementary reinforcement. The bending strength of these decks was analyzed and compared with reference specimens that were reinforced with conventional steel bars. Another group of concrete decks was reinforced with steel fiber as the primary reinforcement and glass fiber reinforced polymer wire mesh as supplementary reinforcement.

1.2 Steel Fiber

Steel fiber reinforced concrete (SFRC) is a structural material that combines a cementitious matrix and a discontinuous reinforcement, consisting of small pieces of steel randomly distributed in the concrete mixture (Marcos-Meson et al. 2018). Some research shows that adding steel fiber to the concrete mixture reduces the shrinkage of concrete and decreases the

spacing between cracks and crack width of the concrete slab, in addition to increasing the tensile strength and ductility. (Hwang et al. 2017, Zhang et al. 2023 and Thomas et al. 2007). The use of steel fibers as a supplement or main reinforcement bars has become a wide solution for constructing many structures due to its overall high durability and good performance of tensile strength (Kamal and El-Refai 1987). Nevertheless, the total replacement of conventional steel reinforcement is still under investigation. In this research, steel fiber has been used as the main reinforcement in concrete bridge decks, replacing the conventional bars to investigate the behavior of these decks, including load deflection, stress-strain, crack widths, and energy absorption.

Advantages and Disadvantages of Steel Fibers in Concrete

Utilizing steel fiber in concrete has some advantages that can be summarized as follows:

- Enhanced ductility.
- Increase the load-bearing capacity of concrete.
- Reduction of concrete slab thickness.
- Load capacity is not diminished by concrete cracks.
- Increase the durability.
- Low maintenance costs.
- Improved flexural properties.
- Can be used on a fast-track schedule.
- Easier positioning of joints.
- Reduced site labor for managing steel reinforcement.
- Less corrosion.
- Increase impact and abrasion resistance.

- Even distribution of fibers throughout the concrete
- Better behavior of crack control systems.

However, there are some disadvantages of steel fibers in concrete as follows:

- Reduce workability.
- Possible balling during mixing for high steel dosage.
- Finishing difficulties.

1.3 GFRP

Glass fiber reinforced polymer (GFRP) is a composite material manufactured of a polymer matrix reinforced with glass fibers, carbon (CFRP), or aramid (AFRP). In this research, GFRP has been utilized as the main and supplementary reinforcement in the specimens. Typically, the polymer matrix is an epoxy resin that provides a bond to the fibers. Although the initial cost of GFRP reinforcement is higher than steel reinforcement, the total life cycle cost and maintenance of the structures reinforced with GFRP is significantly lower. (Goldston et al. 2016).

GFRP has been widely used for strengthening structural components, including sheet plates of GFRP as externally reinforced materials applied on the external surface of beams (Attari et al. 2012), slabs (Smith et al. 2011) and repair damaged reinforced concrete columns (Li et al. 2003). The use of GFRP in infrastructure projects is beneficial, especially for structures exposed to salt environments like marine or roads exposed to de-icing salts.

Advantages and Disadvantages of GFRP

Here are some of the advantages of using GFRP rebar in various applications:

- The constituents of GFRP include high-quality corrosion-resistant vinyl ester resin that increases the lifespan of a concrete structure.

- As compared with the conventional reinforcement bars, GFRP rebar is $\frac{1}{4}$ the weight of steel with two times the tensile strength of steel.
- Higher bond strength
- Corrosion-free, perfect for highly corrosive environments (exposed to water, salt, and humidity)
- Non-conductive
- Less labor, less freight, and faster and safer on-site handling
- Easy to cut and flexible
- Disadvantage:
- Low elastic modulus: it is not rigid enough and easily deformed in the structural application.
- Poor long-term temperature resistance. FRP cannot be used under high temperatures for a long time; it is generally only used under 100°C (212°F) (Hajiloo et al. 2028 and Correia et al. 2015).

1.4 Research Objectives

The objective of this research is to advance the knowledge of utilizing SFRC as the main reinforcement in bridge decks by comparing the results with decks reinforced with conventional bars (RC). The comparisons include load-deflection, ductility, stress-strain, and cracks. The following objectives were established:

- 1- Investigate the performance of cast-in-place (CIP) and precast (PC) SFRC decks with steel wire mesh under bending and compare it with the standard AASHTO Design decks.
- 2- Investigate the performance of cast-in-place (CIP) and precast (PC) SFRC decks with GFRP mesh under bending and compare it with the GFRP decks.

- 3- Perform numerical analysis and finite element model (FEM) by using ABAQUS software.
- 4- Provide conclusions and design recommendations for the utilization of SFRC in bridge decks.

1.5 Dissertation outlines

Chapter one presents the introduction and general overview of the steel fiber and GFRP that were used in this research.

Chapter 2 presents a literature review establishing the necessary background for the research in this dissertation, including the background of SFRC and GFRP.

Chapter 3 presents the standard material tests and the results of a preliminary investigation into the use of SFRC in concrete.

In Chapter 4, a case study was identified, which is a small part of a simply supported bridge, design, preparation, and experimental procedure of the specimens.

Chapter 5 presents the numerical analysis and results.

In Chapter 6 and Chapter 7, the analysis of experimental results was discussed, including load-deflection, ductility, stress-strain, and cracks width and spacing.

Chapter 8 presents conclusions and future recommendations.

CHAPTER 2

LITERATURE REVIEW

2.1 Overview

The literature review discusses the topics related to this research, i.e., utilizing steel fiber and GFRP in concrete bridge decks as the main reinforcement and the previous research related to it.

2.2 Steel Fiber

Steel fibers are one of the materials that have been used to reinforce the concrete, which is a non-continuous material that is spread randomly throughout the concrete mixture. This enhances the ductility of the concrete, similar to conventional reinforced steel bars.

This material has found widespread use in construction due to its ability to be produced in short lengths and added to concrete mixtures. This makes it ideal for creating thin and curved walls, such as concrete pipes (culverts) and intricate architectural details. It has also been used in bridge decks to reduce maintenance costs. The steel fibers used in this material exhibit less corrosion than conventional reinforcement, which is a common cause of deck failure in harsh environmental conditions. By minimizing the need for maintenance and traffic shutdowns, this material proves to be a cost-effective solution for construction projects. Various studies and research have been conducted to observe the behavior of steel fiber-reinforced concrete, including compression strength, bending strength, tensile strength, impact resistance, crack resistance, corrosion resistance, and heat resistance.

A full-scale steel fiber reinforced concrete bridge deck was tested to investigate the behavior under two-way action by McMahan in 2018. The deck was designed to reduce the amount of traditional reinforcing bars in a design controlled by service-limit criteria. The SFRC is

intended to reduce the strains in the steel at service limits. Loads were applied to simulate the single and tandem loads in the continuous spans of the bridge deck and a single tandem load in the overhang. A companion test program tested slab strips to establish the one-way flexural response with and without reinforcing bars. One-way strength was used in a yield-line analysis to predict the experimental capacity of the specimens. Theoretical capacities were significantly less than the experimental strength for interior loads where significant multiple-cracking effects were observed from the SFRC. In the overhang where membrane action and load redistribution were not possible, yield-line analysis predicted the experimental capacity. In 2020, Azzawi and Abolmaali conducted an experiment to test the strength of nine hollow concrete columns with square cross-sections. The concrete mix of the columns had different dosages of steel fiber (0.5%, 1.0%, and 1.5% volume fraction) and varying opening ratios (10% and 20% hollow ratio), with an eccentricity to column depth ratio of 0.75. The experiment calculated the first cracking load, lateral displacement, and ultimate load for each column and compared the results with similar columns made of ordinary reinforced concrete with and without a hole.

The results showed that the first cracking load reduction for columns with hollow ratios of 10% and 20% (C2-I, C-II) and without steel fibers was 28.88% and 49.70%, respectively, compared to the solid column (C1-I, C1-II). However, the addition of steel fibers significantly improved the mechanical response of the tested specimens, especially the cracking load. The cracking load for specimen C5-I (10% opening ratio with 1.5% steel fibers volume fraction) increased 2.346 times that of specimen C2-I (10% opening ratio without steel fibers). Similarly, for a specimen with a 20% opening ratio and 1.5% steel fibers volume fraction (C5-II), the cracking load increased 2.181 times compared to the same specimen without adding

steel fibers.

Furthermore, the ultimate load-carrying capacity for specimen C5-I (10% opening ratio with 1.5% steel fibers volume fraction) increased 1.094 times the cracking load for specimen C2-I (10% opening ratio without steel fibers). Similarly, for a specimen with a 20% opening ratio and 1.5% steel fibers volume fraction (C5-II), the ultimate load-carrying capacity increased 1.23 times compared to the same specimen without adding steel fibers.

In conclusion, the experiment showed that the addition of steel fibers enhanced the strength capacity and ductility of the columns and allowed them to absorb more energy compared to similar columns made of ordinary reinforced concrete.

Some have specifically studied the behavior of concrete pipes used as culverts after using steel fibers. In 2012, AbulMaali et al. conducted research on a concrete pipe reinforced with varying amounts of steel fibers and found that 82% of 24-inch diameter pipes and 94% of 36-inch diameter pipes exceeded ASTM C76 Class III requirements. Figures 2-1 and 2-2 show typical load–deflection graphs for 24-in and 36-in pipes, respectively. Figure 2-1 presents the test results for a 24-in. pipe produced by Northern Concrete Pipe with Wall B and (33 lb/yd³) fiber dosage. The results were compared with reinforced concrete pipes (RCP) produced simultaneously with the same diameter and concrete mixture design. For RCPs and steel fiber–reinforced concrete pipes (SFRCP), The relationship between the load and the vertical and lateral deformations is similar, with the two following each other closely. The data clearly shows that for RCPs, as the load increases, the stiffness degradation decreases at a constant negative rate, ultimately reaching its limit. The SFRCPs showed a different result. As the load increased to its maximum, the stiffness decreased with a negative slope at first. Then, the slope increased to zero and remained constant. This means that the rate of stiffness

degradation changed from negative to zero, which explains why the SFRCs can handle large lateral and vertical deformations without collapsing, even with cracks over ½ inch in size. In Figure 2-2, graphs are displayed for a 36-inch pipe with Wall C, which was manufactured by Northern Concrete Pipe (NCP-36-C-88). The RCP counterparts were tested at the same age and with the same mix design. The vertical load-deformation plots for both SFRCs and RCPs were like those shown in Figure 2-1 for the 24-inch pipe. The plot revealed that the SFRCs had smaller crack widths than the RCPs, both at ultimate load and ultimate deformation. These results demonstrate that SFRCs can withstand larger crack widths.

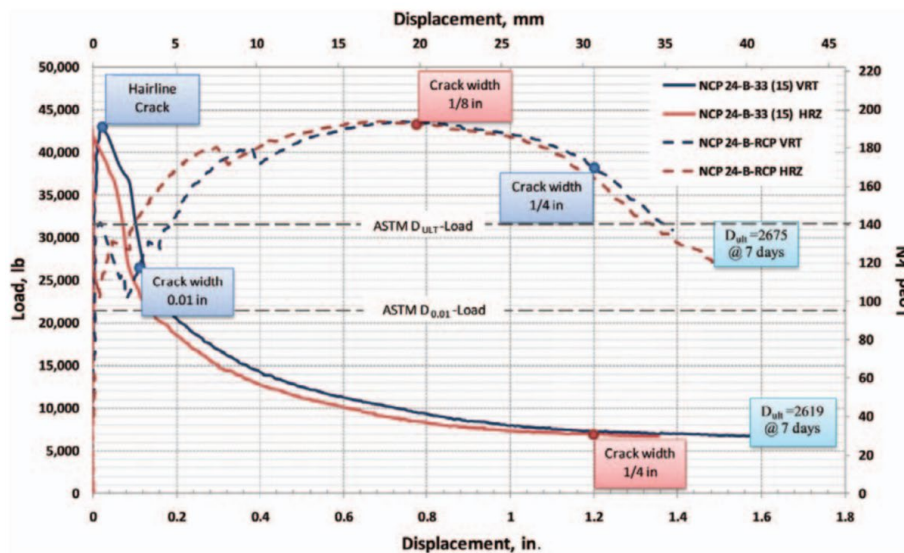


Figure 2 - 1 Load–deformation plot for horizontal and vertical displacement of 24-in. SFRCP versus RCP (AbulMaali et al. 2012)

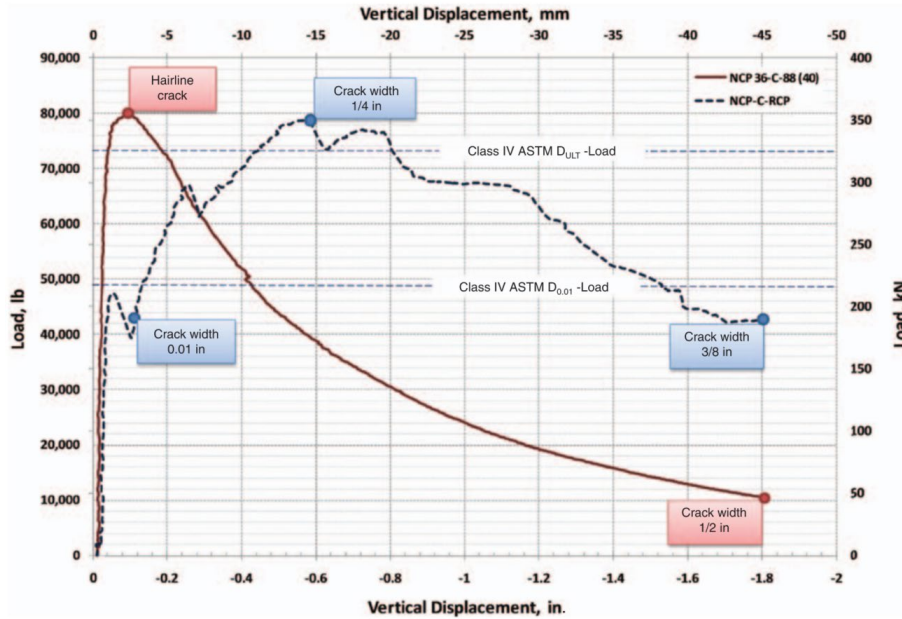


Figure 2 - 2 Load–deformation plot for vertical displacement of 36-in. (AbulMaali et al. 2012)

Milind V. Mohod 2012, studied the effect of fibers in different dosages (0.25%, 0.50%, 0.75%, 1%, 1.5%, and 2% by volume of cement) on concrete cubes of size 150mm x 150mm x 150mm that were examined the compressive strength and beams of size 500mm x 100mm x 100mm were examined flexural strength. Through research, it was discovered that the optimum dosage of steel fibers to add to concrete is 1% for cube compressive strength and 0.75% for beam flexural strength. This led to a noticeable enhancement in the mechanical properties of the concrete beam, as shown in Figure 2-3 and 2-4.

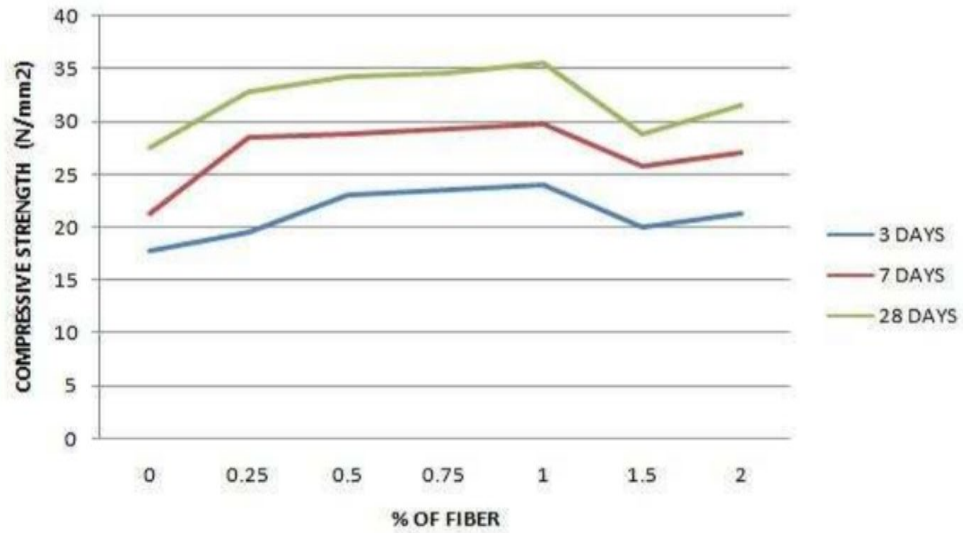


Figure 2 - 3 Variation of Compressive strength with respect to % of fiber content (Milind V. Mohod 2012)

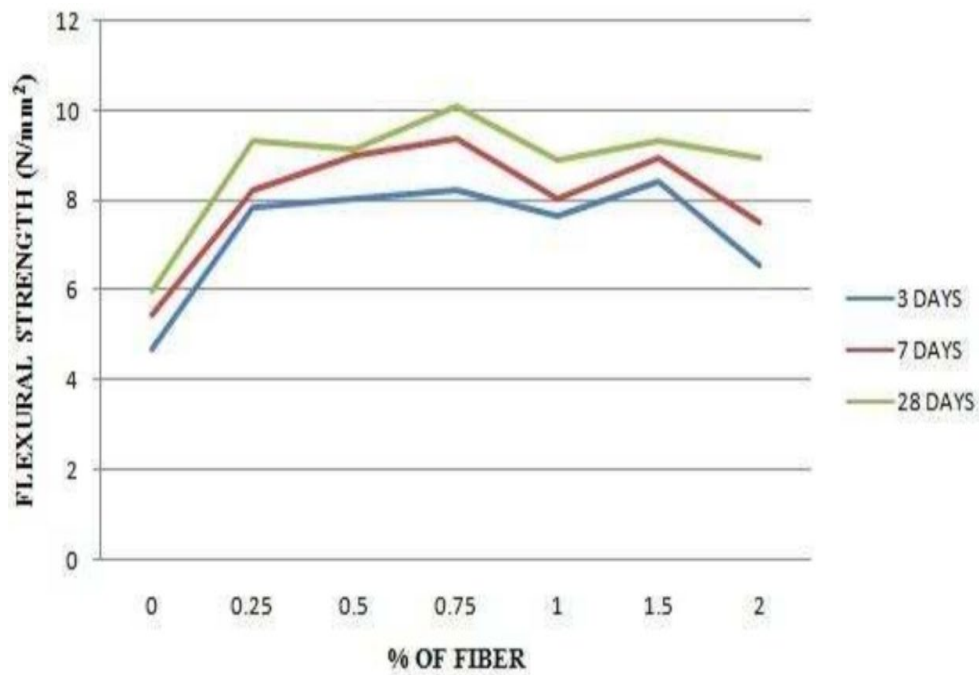


Figure 2 - 4 Variation of Flexural strength with respect to % of fiber content (Milind V. Mohod 2012)

Steel fibers were also present in precast girders. A study conducted by Dhonde, et al. in 2005 discovered that using steel fibers at the ends of prestressed girders can reduce or eliminate the cracks that often appear due to the significant stresses of steel tendons. According to the research, using steel fibers instead of traditional transverse steel reinforcement can prevent end zone cracking and enhance the ductility and crack resistance of prestressed TxDOT I-beams. The report offers design guidelines and suggestions for effectively creating, testing, and pouring steel fiber-reinforced concrete mixes in the end zones of prestressed concrete I-beams.

Fattouh et al. 2023 studied the flexural behavior of road pavement concrete slabs containing steel fiber and silica fume. The study presents that the compressive strength of the mixes that have 1% steel fiber and 10% silica fume (SFRC-SF) cured with tap water (TW) and seawater (SW) increased by 21.20% and 14.40%, respectively, compared to the control mixture (MCC) and the ultimate loads for road pavement slab that have steel fiber (RPS-MSFRC-TW) and road pavement slab that have steel fiber and silica fume cured with tap water (RPS-MSFRC-SF-TW) increased by about 24.29% and 46.95%, respectively, compared to the control road pavement slab (RPS-MCC-TW); also the ultimate loads for road pavement slab that have steel fiber (RPS-MSFRC-SW), and steel fiber with silica fume cured with seawater (RPS-MSFRC-SF-SW) increased by about 36.32% and 59.90%, respectively, when the samples were compared to the control sample (RPS-MCC-SW). therefore, adding steel fiber improved the compressive strength and the ultimate loads significantly; the experiments showed that adding steel fiber had an effective role in absorbing energy, as shown in Figure 2-5, where the area under the curves of (RPS-MSFRC) and (RPS_SFRC-SF) is greater than the area under the curve of (RPS-MCC) cured with (TW) and

(SW).

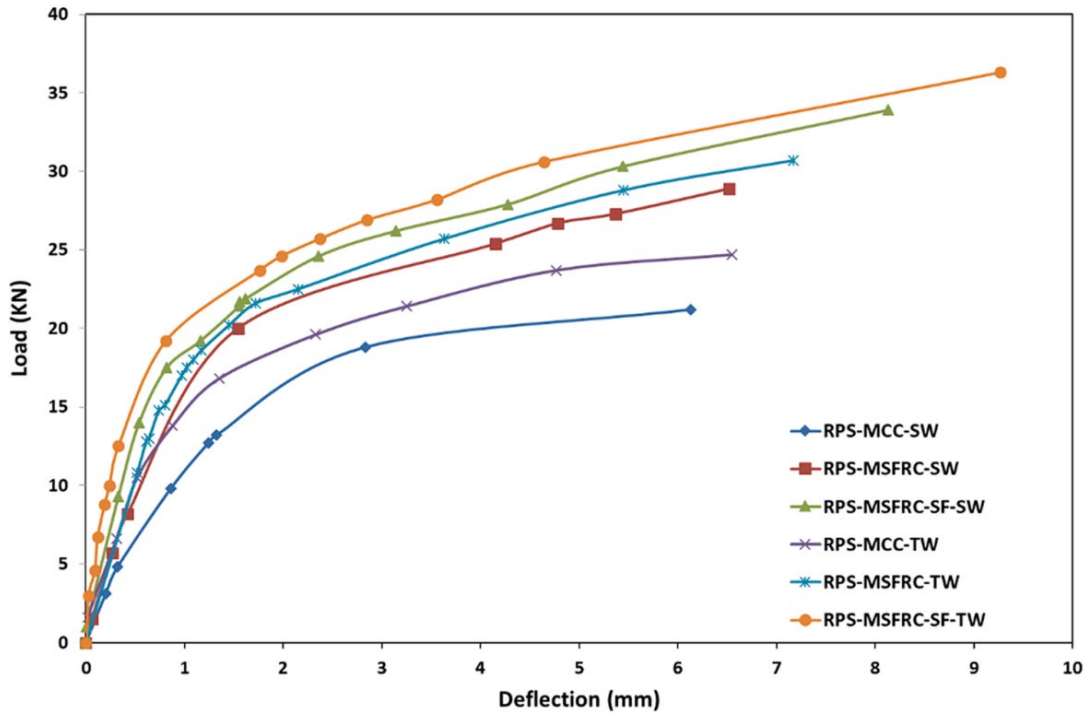


Figure 2 - 5 Load deflection curves of the tested road pavement slabs. (Fattouh et al. 2023)

Corrosion

Steel fiber-reinforced concrete (SFRC) and conventional steel bar-reinforced concrete (RC) have different characteristics when it comes to corrosion resistance. Whether SFRC is less prone to corrosion than RC depends on several factors. Corrosion in RC uses steel bars (rebar) for reinforcement. These steel bars can corrode over time when exposed to moisture and oxygen. Corrosion can weaken the steel and lead to cracking and spalling of the concrete, which can compromise the structural integrity of the concrete. In comparison, steel fiber is typically coated with a layer of zinc or other anti-corrosion materials. This coating provides a degree of corrosion resistance. However, it is essential to note that the level of corrosion resistance can vary depending on the specific type of steel fibers used and the quality of the coating.

Moreover, Steel corrosion in concrete can be caused by carbonation or chlorides. Corrosion occurs after the carbonation front or chloride ions reach the steel, which may take some time (Tuutti, 1982). The length of this period depends on the quality of the concrete, the thickness of the concrete cover, as well as environmental factors. In environments that contain chloride, such as marine settings or areas where road salt is used, the rate of corrosion of steel within the concrete can increase significantly once the corrosion has begun. The moisture condition of concrete is a crucial factor for corrosion and other deterioration mechanisms. Concrete with low moisture content has a low corrosion rate due to high resistivity, while concrete with very high moisture content has a low corrosion rate due to the slow transport of oxygen. However, for concrete with intermediate moisture content, the corrosion rate can be high due to relatively low resistivity and high transport of oxygen (Johan Ahlstrom, 2015).

A study was conducted in 2018 by Abbas and Nehdi to investigate the integrity of precast concrete tunnel lining (PCTL) segments. The study revealed that steel fiber-reinforced concrete offered crack resistance and increased durability in PCTL. The study explored the mechanical behavior of specimens extracted from full-scale PCTL segments that were made using conventional steel-rebar-reinforced concrete (RC) and steel-fiber-reinforced concrete (SFRC) for a subway tunnel in Canada. The durability of the specimens was determined through exposure to chloride ions. Test specimens were treated with chloride ion (Cl^-) solutions containing varying concentrations (3.5% and 10.0%) for up to 16 months while being subjected to weekly wetting and drying cycles. The mechanical degradation of RC and SFRC specimens was evaluated after every 4 months of chloride ion exposure. Initially, both RC and SFRC PCTL segments showed an increase in concrete mass of 0.84% and 0.35%, respectively, after 4 months of 3.5% Cl^- exposure. However, after 8 months of Cl^- exposure, a decreasing trend in mass was observed for both the RC and SFRC

specimens. The study found that conventional RC PCTL segments had weaker mechanical properties and were more susceptible to damage caused by chloride compared to SFRC PCTL segments. After 12 months of exposure to a 3.5% Cl⁻ solution, compressive and flexural strengths of RC specimens decreased by 19% and 47%, respectively. Furthermore, exposure to a 10% Cl⁻ solution caused a greater reduction in the mechanical properties of RC specimens than a 3.5% exposure. No significant decrease in compressive and flexural strengths was observed in specimens of steel fiber reinforced concrete (SFRC) due to exposure to chloride ions. Interestingly, the mechanical performance of SFRC specimens improved when subjected to chloride ions. The experimental results for both the reinforced concrete (RC) and SFRC segments suggest that SFRC has great potential as a strong contender in the construction of precast concrete tunnel linings.

Figure 2-6 and 2-7.

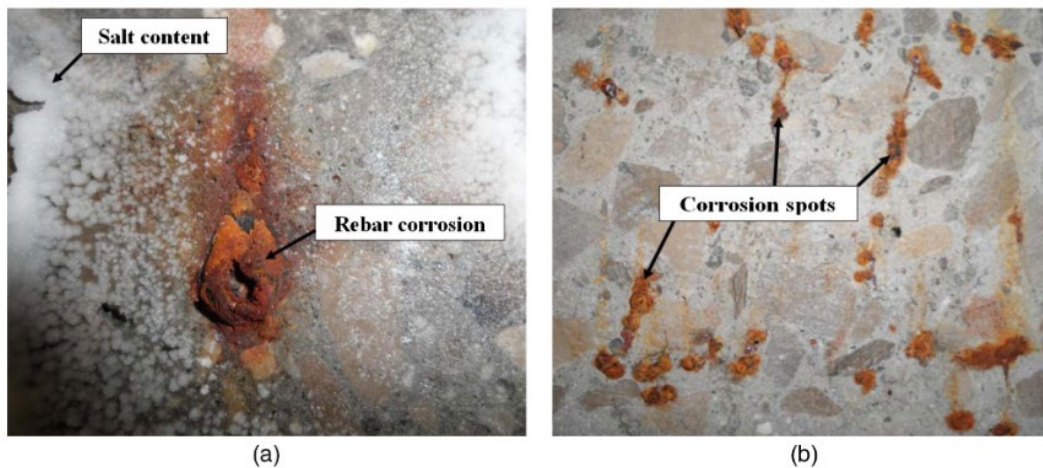


Figure 2 - 6 Visual appearance of beam specimens exposed to 10% Cl⁻solution:
(a) RC beam specimen; (b) SFRC beam specimen (Abbas and Nehdi, 2018)

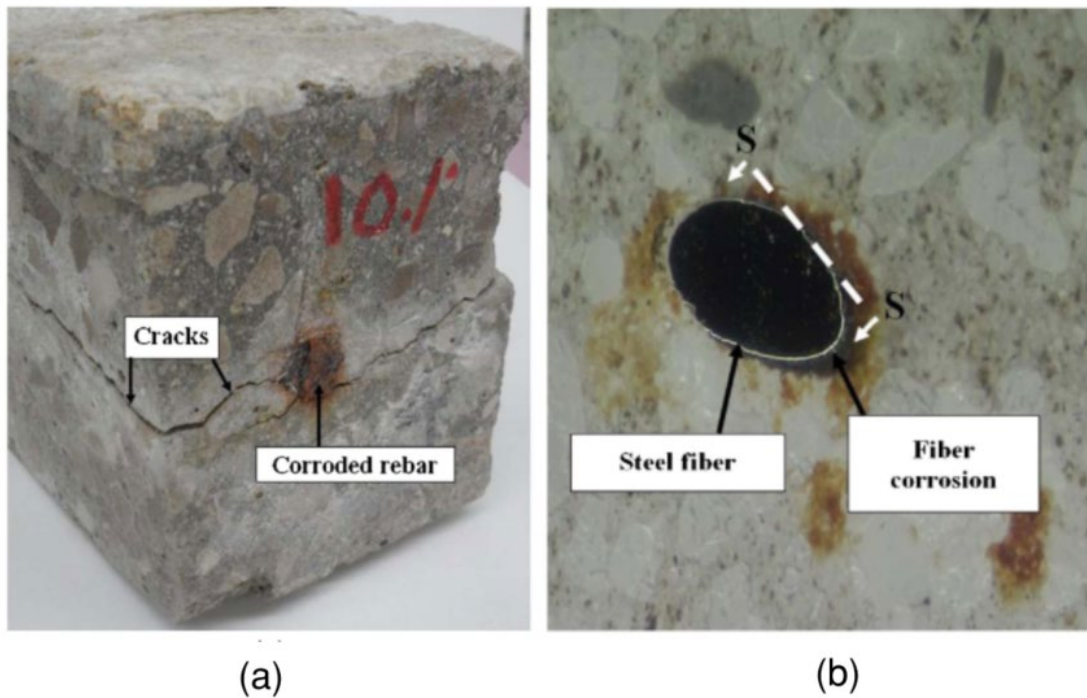


Figure 2 - 7 Cracks in specimens after exposure to 10% Cl⁻ solution:
 (a) RC beam specimen; (b) SFRC beam specimen (Abbas and Nehdi, 2018)

The orientation and distribution of steel fibers within the concrete can also affect the corrosion resistance. Properly mixed and distributed fibers can provide improved resistance to cracking and protect against the ingress of moisture and corrosive agents.

While SFRC can offer enhanced resistance to cracking and improve the durability of concrete, it may not be entirely immune to corrosion. The overall corrosion resistance will depend on the specific mix design and the environmental conditions to which the concrete is exposed. In summary, steel fiber-reinforced concrete can offer improved corrosion resistance compared to traditional reinforced concrete in some cases. However, the actual performance of SFRC in terms of corrosion resistance depends on the quality of the steel fibers, the mix design, and the environmental conditions to which the concrete is exposed. Proper construction practices and maintenance are essential for maximizing the corrosion resistance of any concrete structure

(Meson et al. 2018, Fan et al. 2019, Mangat and Gurusamy, 1988)

There is a high demand for concrete bridge decks with improved crack control performance, especially for high-durability structures (Xiang et al., 2022). This increased durability allows bridges to remain functional for more extended periods compared to decks reinforced with traditional bars. To keep traffic flowing smoothly, it is essential to make bridges more efficient. Bridge decks made of concrete are the first defense against traffic and environmental exposure. Hence, it is crucial to design them with future maintenance costs in mind throughout the life cycle of the bridge structure, as mentioned in the PCI Bridge Design Manual 2011. According to Kirkpatrick et al. (2002), the majority of the maintenance expenses for concrete bridge decks arise from fixing cracks in the deck and reinforcement corrosion. Additionally, the corrosion of reinforcing bars is the primary reason for bridge deck failure. According to the American Society of Civil Engineers ASCE Report Card 2021, more than 46,154 bridges in the US are deemed structurally deficient. The majority of these bridges have defects that are caused by steel reinforcement corrosion leading to concrete spalling, as stated in a report by Syll and Kanakubo in 2022. Rebar corrosion is a common type of corrosion that is found in most highway bridges. It happens when chloride ions migrate to concrete material like steel bars, as stated by Mangat and Gurusamy in 1988. Studies have shown that steel fibers offer a more corrosion-resistant option over conventional reinforcing bars.

Cracks

One of the most common types of defects experienced by transportation agencies is early transverse cracking of bridge decks. These cracks typically appear soon after the construction of the bridge deck and are caused by the restrained shrinkage of concrete. Frequent cracks on a bridge can lead to higher maintenance costs and a shorter lifespan of the structure. In the

past, attempts to address transverse bridge deck cracking focused on changes in concrete materials and construction methods. However, recent research has highlighted the significance of design factors in the development of transverse bridge deck cracking (Subramaniam, 2016).

Utilizing steel fibers in concrete decks reduces the cracking percentage and crack widths because steel fibers are randomly distributed in the concrete mixture and offer more crack control (ASTM C1018, 1991). (Odaa et al. 2021, Zhang et al. 2023, Mu et al. 2018, Weli et al. 2020) conducted studies showed that SFRC has offered better properties in comparison with plain concrete.

In 2005, Saadeghvaziri and Hadidi conducted a thorough finite element analysis of bridge systems, focusing on the deck and girder structures. The study involved evaluating crack patterns and stress histories and determining the impact of various design factors, such as structural stiffness, on transverse deck cracking. The study's results showcase the emergence of transverse deck cracking and underline the significance of these specific design factors. Additionally, the study recommends taking preventive measures during the design stage to decrease the likelihood of transverse deck cracking.

Olivito and Zuccarello conducted a study in 2010 to investigate the mechanical static behavior of different mixtures and their classification based on variations in fiber content and mix design. The study involved conducting several experimental tests to evaluate the uniaxial compressive strength and tensile strength. The mixtures were prepared by varying both the mix design and fiber length. The study included fiber content in volumes of 1% and 2%. The ultimate compressive strength of fiber concrete was determined through uniaxial compression tests. The first crack strength and ductility indexes were derived from four-point bending tests

on notched specimens. The tensile strength of steel fiber reinforced concrete (SFRC) was obtained by experimental procedures and analytical modeling. The experimental tests showed that SFRC behaves differently depending on the fiber content and length. Overall, the comparison between the experimental results and analytical modeling showed good agreement.

Therefore, utilizing steel fiber could be a solution for enhancing the mechanical properties of concrete.

2.3 GFRP

In civil and infrastructure engineering, structures can suffer from deterioration due to various factors, such as corrosion caused by marine environments, high chloride content in the air, and the use of deicing salts on roads. Additionally, other factors such as alkali-silica reactions, poor initial design, construction, and maintenance, as well as natural disasters like earthquakes and hurricanes can also contribute to the deterioration of structures. The cost of repairing deteriorated structures often exceeds double the original construction cost. The development of advanced materials and techniques is crucial for improving the performance of civil engineering structures, preventing their premature deterioration, and prolonging their service lives. Composite materials have proven to be successful in the aerospace, marine, transportation, and civil construction industries in recent decades. It is possible to create materials that combine the advantages and eliminate the shortcomings of each individual component through careful design. In the field of civil construction, fiber-reinforced polymer (FRP) is a promising composite material that can improve the performance of reinforced concrete structures.

FRPs are composite materials made up of high-strength fibers, usually synthetic or organic,

embedded in a resin matrix. For civil engineering structures, the most commonly used FRPs are CFRP (carbon fiber-reinforced polymer), AFRP (aramid fiber-reinforced polymer), GFRP (glass fiber-reinforced polymer), and BFRP (basalt fiber-reinforced polymer). Compared to steel, which is the traditional reinforcing material for concrete structures, FRPs have several advantages.

- Excellent corrosion resistance and electromagnetic neutrality.
- High ratio of strength to mass density.
- Excellent fatigue resistance, especially.
- Cost-effective fabrication.
- Low axial thermal expansivity.

FRPs are now widely used in concrete structures as a substitute for steel rebars due to their excellent electrochemical corrosion resistance. In 1986, Germany built the world's first highway bridge using GFRP rebars for prestressing. Since then, Europe, America, and Japan have constructed bridges using FRP-reinforced concrete. FRP reinforcing bars have been widely used in various construction projects since the 1980s. These include industrial roof decks, highway barriers, chemical and wastewater treatment plants, sea walls, floating docks, and other seafront structures. Due to their excellent dielectric properties, FRP reinforcing bars have also found applications in electrical substation reactor bases, magnetic resonance imaging facilities, airport runways, hospitals, and laboratories.

However, FRP composites have several disadvantages, including high cost, low elastic modulus, linear-elastic brittle behavior, and poor fire resistance. GFRPs, which are much cheaper than CFRPs, are commonly used in civil engineering constructions to overcome the high cost of FRP materials. Despite their higher initial material cost, cost savings arise from

various aspects such as fabrication, maintenance, retrofit, and rehabilitation of structures, which ultimately offset the high costs.

Although the GFRP reinforcement has a low modulus of elasticity and brittle behavior, adding fiber to the concrete mixture reinforced by GFRP bars will increase the ductility. In 2011, Issa et al. tested seven beams reinforced by GFRP, the tested beams were divided into four groups. The first three groups consisted of two beams each, one of normal strength and the other of high strength. The fourth group only had one normal strength beam. The reference group was the first group, and it had no internal fibers. The second group tested the effect of using internal polypropylene fibers in the concrete mix. The third group studied the effect of using internal glass fibers in the concrete mix, while the fourth group studied the effect of using internal steel fibers in the concrete mix.

According to the experimental results, using GFRP as the main reinforcement for the concrete beams achieved reasonable flexural strength. The theoretical results calculated using ACI 440 code also showed good agreement with the experimental results, with an error of about 20%. The research findings indicated that all types of fibers used improved the ductility of FRP-reinforced concrete beams. It was also observed that the span-to-experimental service load deflection ratio was relatively high when compared to the usually accepted ratio of about span/250.

According to research, supplementing concrete reinforced with GFRP bars with steel fiber is a potential solution to enhance ductility. In 2023, Kinjawadekar and colleagues conducted tests and numerical analyses to investigate the response of GFRP-reinforced flexural members in shear and bending. Over the past decade, Kinjawadekar has critically analyzed the behavior of flexural members reinforced with glass fiber-reinforced polymer (FRP) bars. This review

will aid in understanding the behavior of FRP bars as an alternate reinforcing material. However, because GFRP bars have high strength and no yield point, traditional methods of determining ductility may not be applicable. Therefore, detailed study is necessary to understand the behavior of these structures. Kinjawadekar explores various properties of GFRP-reinforced beams to appreciate the potential applications of GFRP reinforcement in flexural members.

A study conducted by A. Mufti et al. in 2014 investigated the durability of GFRP-reinforced concrete in five field structures exposed to various environmental conditions. The study used five analytical methods, namely optical microscopy (OM), scanning electron microscopy (SEM), energy dispersive x-ray (EDX), differential scanning calorimetry (DSC), and Fourier transformed infrared spectroscopy (FTIS). The analyses confirmed that exposure to alkalinity, freeze-thaw and wet-dry cycles, de-icing salts, salt water, and thermal loading for 5 to 8 years did not affect the integrity of the GFRP/concrete interface.

In 2010, Mathieu and Benmokrane conducted an experiment to study the properties of GFRP bars. The properties, including tensile, shear, flexural strengths, and flexural elastic modulus, were measured. The study found that the properties of GFRP bars increased when the temperature decreased. This phenomenon was due to the increase in stiffness of the amorphous polymer matrix at low temperatures. However, if the GFRP material contained a high level of moisture, the volume expansion of water during freezing could initiate microcracks and decrease the mechanical properties, which would compete with the increase of stiffness of the matrix. Despite this, the study observed that the shear and flexural strengths of the saturated GFRP samples subjected to low temperatures between 0°C and -60°C were unaffected. In extremely cold temperatures, like those experienced in Northern regions such as Canada where temperatures range from -40°C to 50°C,

the tensile strength and flexural modulus of elasticity of GFRP bars remained stable. This indicates that the mechanical behavior of GFRP bars is not affected by temperature within this range. While at high temperatures, near 120°C, the mechanical strength and flexural modulus dropped because of the change of state in the polymer and the reaction of degradation. At 350°C, thermal degradation of the polymer matrix caused microcracks in the polymer, resulting in decreased tensile strength and flexural modulus.

In 1996, Ehsani et al. conducted a study to test the bond strength of GFRP bars with concrete. The researchers tested a total of 102 specimens, which included 48 beam specimens, 18 pull-out specimens, and 36 hooked rebar specimens, subjected to monotonic static load. The study applied a tensile load to the rebars in gradual increments of load level until splitting of concrete, rebar pull-out failure, or rebar fracture occurred. The researchers measured the slip between the rebars and concrete at the loaded and free ends at each load level. The study considered variables such as concrete compressive strength, embedment length, clear concrete cover, rebar diameter, concrete cast depth, radius of bend, and tail length. Based on the experimental findings, the researchers established new criteria for acceptable bond performance of GFRP rebars to concrete and derived design guidelines for computing the development lengths of straight and hooked GFRP rebars to concrete. Additionally, the researchers calculated confinement factors to reflect the influence of concrete cover and casting position.

CHAPTER 3

MATERIALS AND CONCRETE STANDARD TESTS

In this chapter, the materials that are used and their specifications and properties are discussed, and the concrete standard tests are presented here.

3.1 Materials

The materials that have been used in this research are cement, coarse aggregate, fine aggregate, portable water, steel bars steel fiber, and GFRP bars as follows:

3.1.1 Cement

Ordinary Portland cement type I/II was used throughout this research for casting all standard test specimens and concrete deck specimens as shown in Figure 3-1.

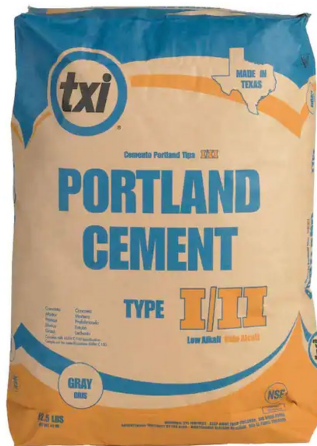


Figure 3 - 1 Type I/II Cement

3.1.2 Non-shrink Grout

A non-shrink, precision high-strength grout with compressive strength of up to 14,000 psi has been meticulously formulated to cater to a diverse range of grouting and anchoring exigencies. This specialized grouting material serves as a pivotal component in the establishment of a robust structural linkage between the bridge decks and the supporting girders, achieving this synergy by its meticulous infusion into the designated shear pockets. In this manner, the grout

not only bridges the spatial gap between these structural elements but also bolsters the overall integrity of the bridge as shown in Figure 3-2.



Figure 3 - 2 Non-Shrinkage Grout

3.1.3 Coarse aggregate

Clean crushed graded gravel was used that has a minimum diameter of 3/8- inch and a maximum diameter of 3/4-inch.

3.1.4 Fine aggregate

Clean naturally graded sand was used and weighted to the design amount for the designed mix.

3.1.5 Mixing water

Portable water was used for mixing and curing throughout the experimental work.

3.1.6 Steel bars

#3 and #4 reinforcement grade 60 were used for specimens that have steel rebar as the main reinforcement to obtain the AASHTO LRFD design method of concrete bridge decks with regular reinforcement and 0 steel fiber, and 6 x 6 x 1/4 inch of wire mesh was used for the concrete bridge decks specimens that have steel fiber as main reinforcement.

3.1.7 Steel fiber

Steel Fibers have been used in concrete for the last three decades and can be used to replace conventional reinforcement or as a supplement reinforcement. Now being produced

domestically according to ASTM A820-16 Classified Steel Fiber based on the manufacturing process. In this research, one form of Dramix 4D 65/60 BG steel fiber was used (see Figure 3-3 and 3-4), and the specifications of this steel fiber are shown in Table 3-1 (Bekaert, 2023). A dosage of 70 pounds per cubic yard of steel fiber was used as the main reinforcement in a concrete mixture of concrete decks that has steel fiber and 6 x 6 x ¼ inch wire mesh only.

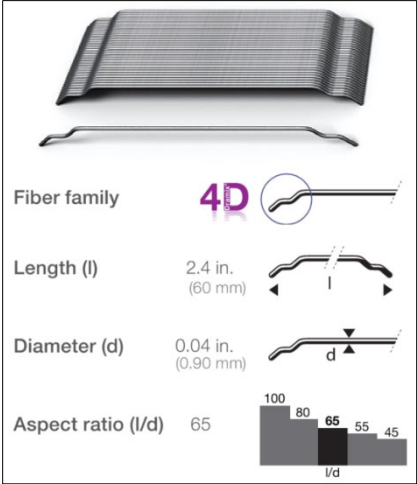


Figure 3 - 3 Hooked-end Dramix 4D Steel Fiber (Bekaert, 2023)

Table 3 - 1 Dramix 4D Steel Fiber Characteristics and Geometry

Material properties	
Nom. Tensile Strength	1600 MPa (232.060381 ksi)
Strain at ultimate strength	200000 MPa (29000 ksi)
Geometry	
Fiber Family	4D
Length (l)	60 mm (2.3622 inch)
Diameter (d)	0.9 mm (0.035433 inch)
Aspect ratio (l/d)	65



Figure 3 - 4 Hooked-end Dramix 4D Steel Fiber

3.1.8 GFRP bars

Pink #3 and #4 GFRP bars were used for reference specimens (0 steel fiber) and for specimens that have steel fiber as the main reinforcement, GFRP meets ASTM D-7957 standard and acceptance criteria for ACI 332 and ACI 440, ICC-ES AC 454. See Figure 3-5.



Figure 3 - 5 Glass Fiber Reinforced Polymer Bars (GFRP)

3.1.9 Concrete

Cement, coarse aggregate, fine aggregate, and water were mixed together in a specific amount as shown in Table 3-2 to obtain a design compressive strength of 4000 psi of plain concrete at the age of 28 days in the Civil Engineering Laboratory Building of the University of Texas at Arlington. (See Appendix A).

Table 3 - 2 Concrete Mix Design, Amounts for 1 Cubic Yard of Concrete

Material	Weight lb
Cement	600
Coarse Aggregate	1780
Fine Aggregate	1320
Water	260
Total	3960

3.2 Concrete Standard Test

Concrete standard tests allow laboratories to test and evaluate concrete mixtures to ensure their strength and safety. These standards help to identify the various properties of concrete including strength, elasticity, hardness, and workability. All casting and sampling have been done in the Civil Engineering Laboratory Building at the University of Texas at Arlington (see Figure 3-6). Two groups of test specimens were taken to check the mechanical properties of concrete at the age of 28 days with and without steel fiber as shown in Table 3-3

Table 3 - 3 Type and Number of Specimens for Standard Concrete Tests

Group	Shape	# of Specimens	Dimension of Specimens	Test
Group 1 (Plain concrete)	Cylinder	4	4-inch x 8-inch	Comprehensive Test
	Cylinder	4	6-inch x 12-inch	Tensile Test
	Cylinder	4	4-inch x 8-inch	Modulus of Elasticity Test
	Beam	4	6-inch x 6-inch x 20-inch	Flexural Test
Group 2 (70 lb/ cy steel fiber)	Cylinder	4	4-inch x 8-inch	Comprehensive Test
	Cylinder	4	6-inch x 12-inch	Tensile Test
	Cylinder	4	4-inch x 8-inch	Modulus of Elasticity Test
	Beam	4	6-inch x 6-inch x 20-inch	Flexural Test



Figure 3 - 6 Concrete Standard Specimens in The Curing Room

3.2.1 Slump Test

It was necessary to measure the slump value. The slump value gives an impression of the workability of the concrete. Slump tests were taken for plain concrete mixture with 0 steel fiber and SFRC mixture with (70 lb/cy) steel fiber. The slump of the plain concrete mixture was (5-inch) while the slump of the SFRC mixture was (3.5-inch). This means the workability has been reduced by about (30%) because of the effect of the steel fiber as shown in Figure 3-7.

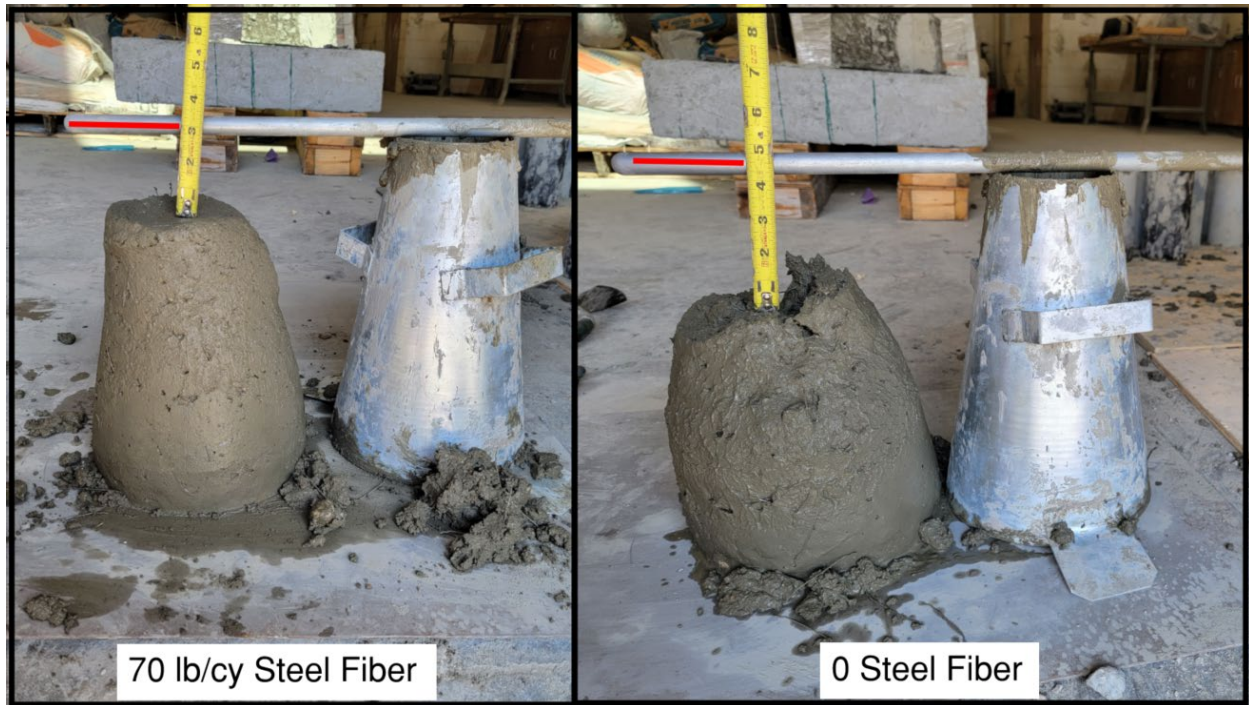


Figure 3 - 7 Slump Test for Plain Concrete and SFRC

3.2.2 Comprehensive Strength Test

Cylinders were tested under a uniaxial compression load, a 500-kip compression machine was used to perform the ASTM C39 test on 4-inch diameter by 8-inch cylinder 8 cylindrical specimens (Figure 3-8). The test results are highly dependent on a proper setup. The maximum sustained load under a constant loading rate of 400 lb/sec was recorded and used for determining the maximum compressive strength of a tested specimen. Figures 3-9 and 3-10 show the average maximum load of tested specimens of plain concrete and SFRC respectively. The average maximum load of plain concrete was (52,156 lb) while the average maximum load of SFRC was (58,115 lb).

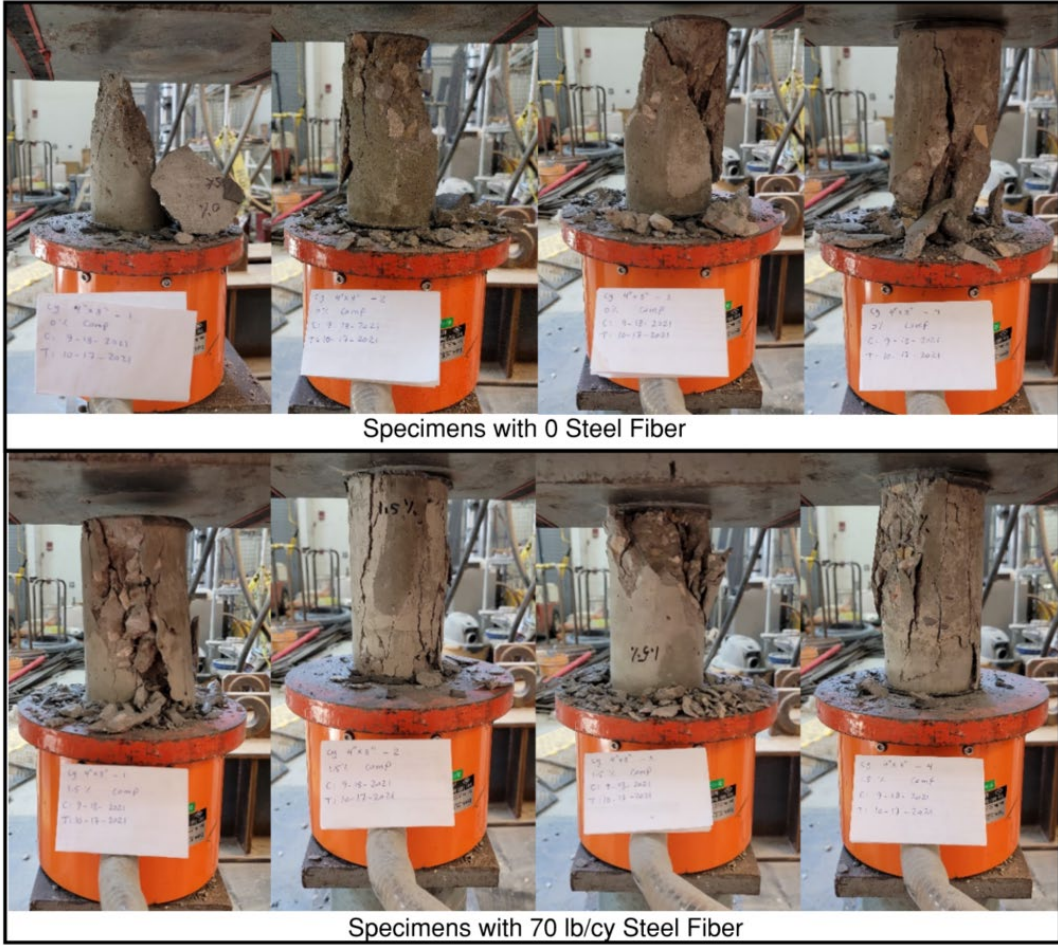


Figure 3 - 8 Compression Test for Plain Concrete and SFRC

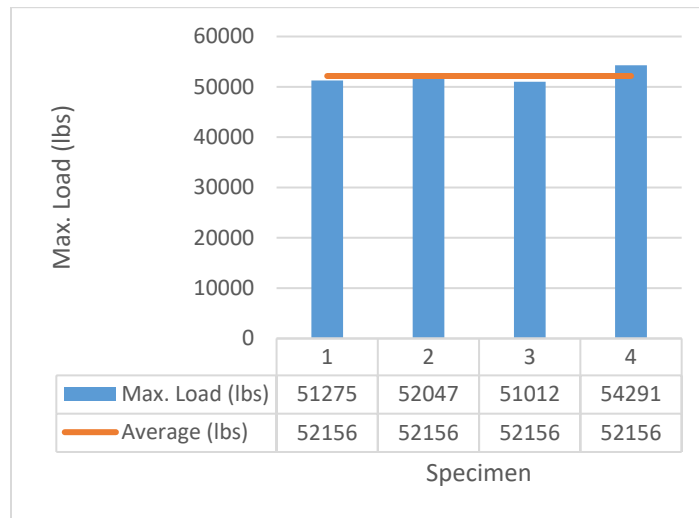


Figure 3 - 9 Ultimate Load of Compressive Test Results of Plain Concrete

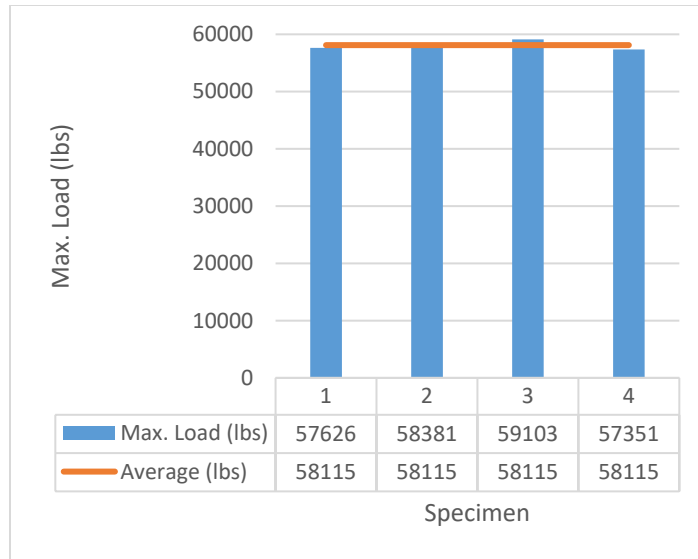


Figure 3 - 10 Ultimate Load of Compressive Test Results of SFRC

Figures 3-11 and 3-12 show the average maximum compressive strength of a tested specimen of plain concrete and SFRC respectively. The average maximum compressive strength of plain concrete and SFRC was (4150 psi) and (4625 psi) respectively, this means the concrete maximum load and maximum compressive strength increased by (11.4%) when adding steel fiber to the concrete mixture.

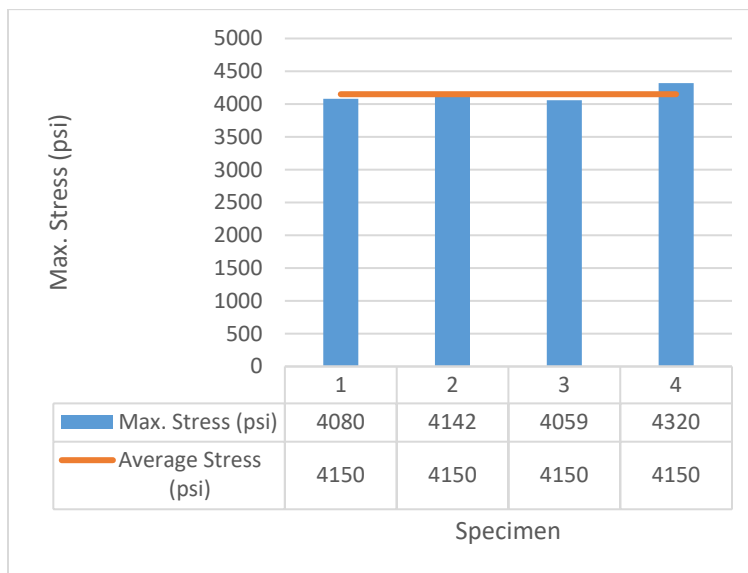


Figure 3 - 11 Ultimate Compressive Strength Test Results of Plain Concrete



Figure 3 - 12 Ultimate Compressive Strength Test Results of SFRC Concrete

3.2.3 Split Tensile Test

Eight cylinders have been tested using the 500-kip machine according to ASTM C496 as shown in Figures 3-13 and 3-14.



Figure 3 - 13 Tensile Test Machine

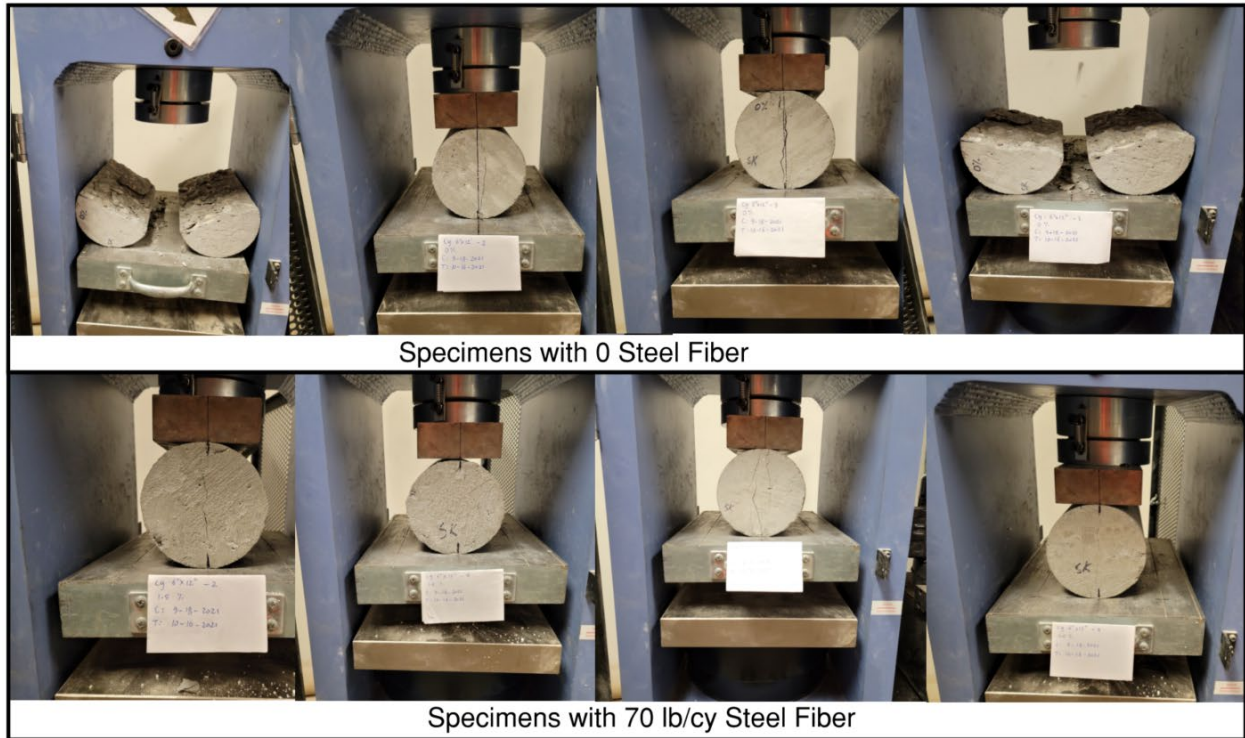


Figure 3 - 14 Tensile Test of Plain Concrete and SFRC

The results were valuable for assessing the shear strength of concrete with and without steel fiber. A 6-inch by 12-inch cylindrical specimen is placed flat on its long axis, allowing a compressive diametric force to be applied along the length of the specimen. The test is performed using a load rate of 200 psi/min until the specimen develops a tension crack along its diameter. The maximum sustained load due to the triaxle compression force is used in calculating the splitting tensile strength of the specimen. Figures 3-15 and 3-16 show the average maximum sustained load of tested specimens of plain concrete and SFRC respectively. The average maximum sustained load of plain concrete was (50,329 lb) while the average maximum sustained load of SFRC was (65,097 lb).

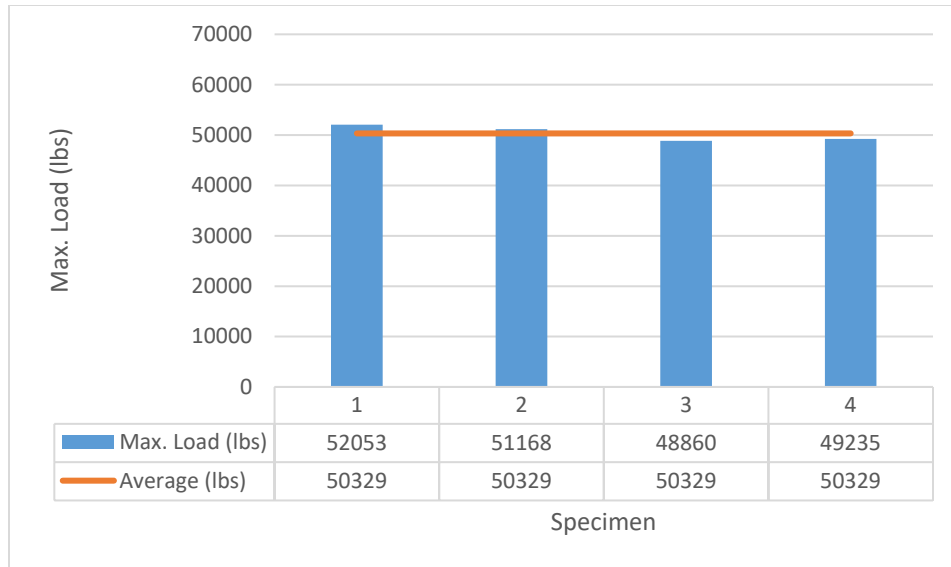


Figure 3 - 15 Ultimate Load of Tensile Test Results of Plain Concrete

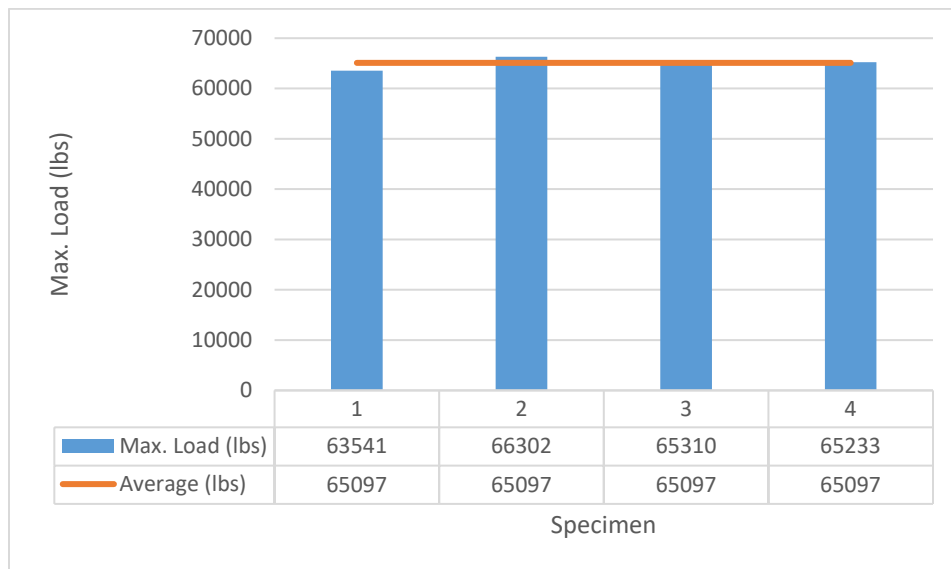


Figure 3 - 16 Ultimate Load of Tensile Test Results of SFRC

Figures 3-17 and 3-17 show the average splitting tensile strength of plain concrete and SFRC respectively. the average maximum splitting tensile strength of plain concrete was (445 psi) while the average maximum splitting tensile strength of SFRC was (576 lb), this means the concrete maximum sustained load and maximum splitting tensile strength increased by (29%) when adding steel fiber to the concrete mixture.

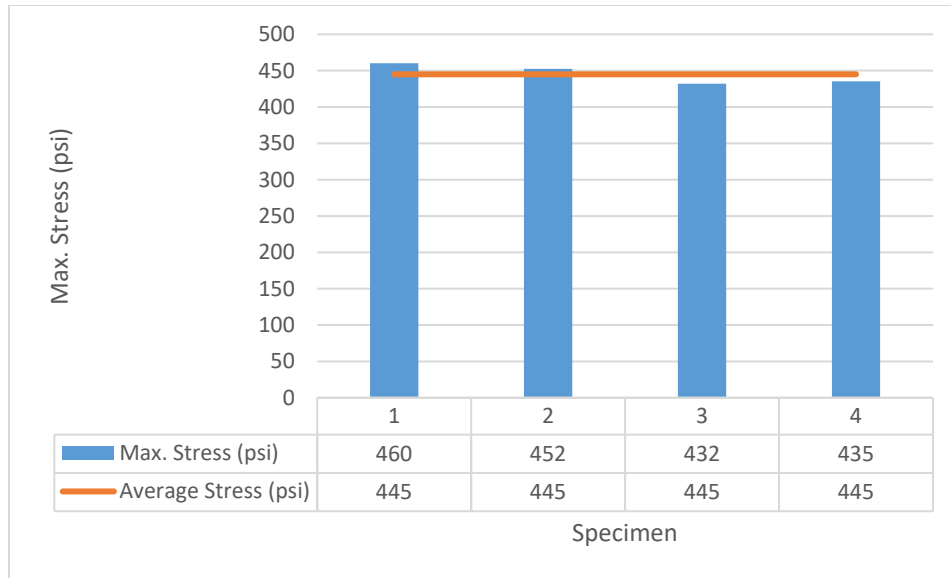


Figure 3 - 17 Ultimate Tensile Strength Test Results of Plain Concrete

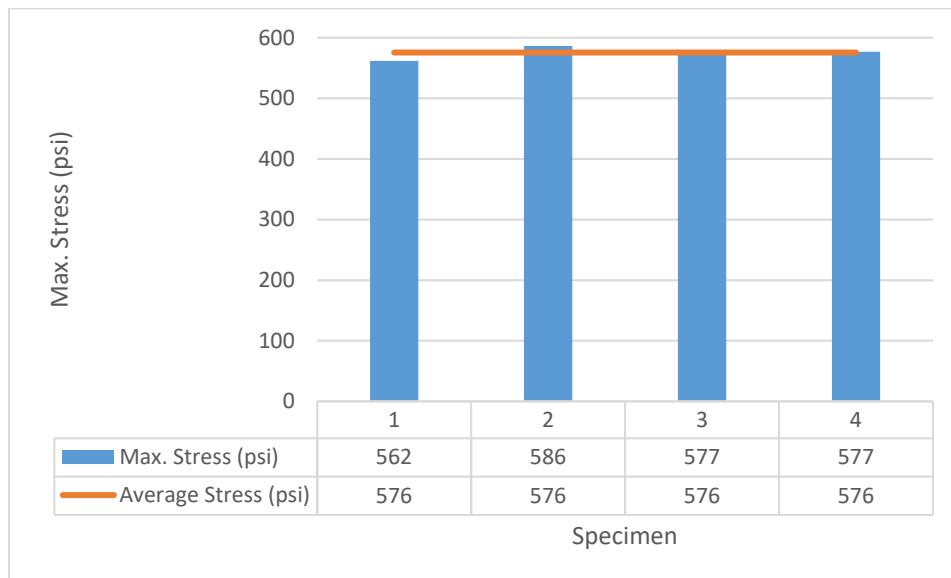


Figure 3 - 18 Ultimate Tensile Strength Test Results of SFRC

3.2.4 Flexural Test

The flexural test of a standard concrete beam is another indirect method of testing the concrete

tensile strength. Eight beams were cast and tested under flexural load at the age of 28 days. The beams had a cross-section dimension of 6-inch \times 6-inch and a length of 20-inch. The test was done according to ASTM C78 which is a 4-point bending test, the clear span was set to 18-inch and the upper bearer distance was set to 6-inch as shown in Figures 3-19 and 3-20.



Figure 3 - 19 Flexure Test Machine

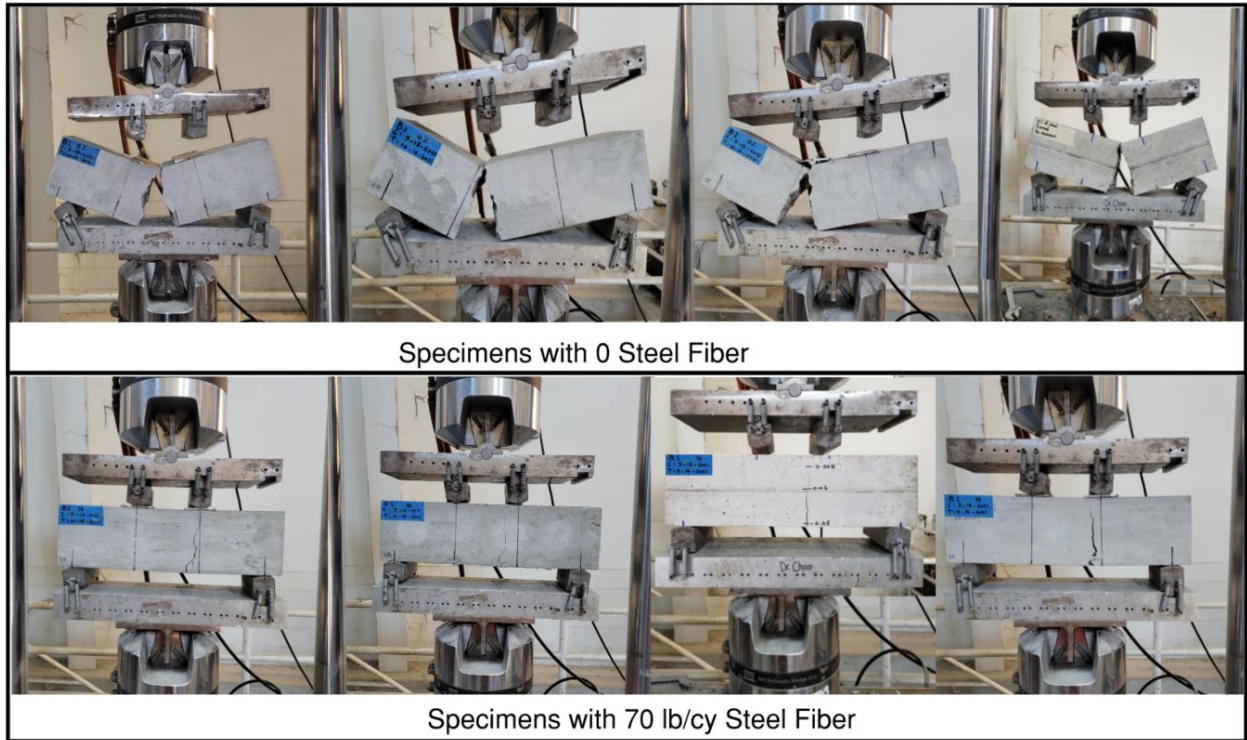


Figure 3 - 20 Flexure Test of Plain Concrete and SFRC

Figures 3-21 and 3-22 show the average maximum bending load of tested specimens of plain concrete and SFRC, respectively. The average maximum bending load of plain concrete was (6254 lb) while the average maximum bending load of SFRC was (7593 lb).

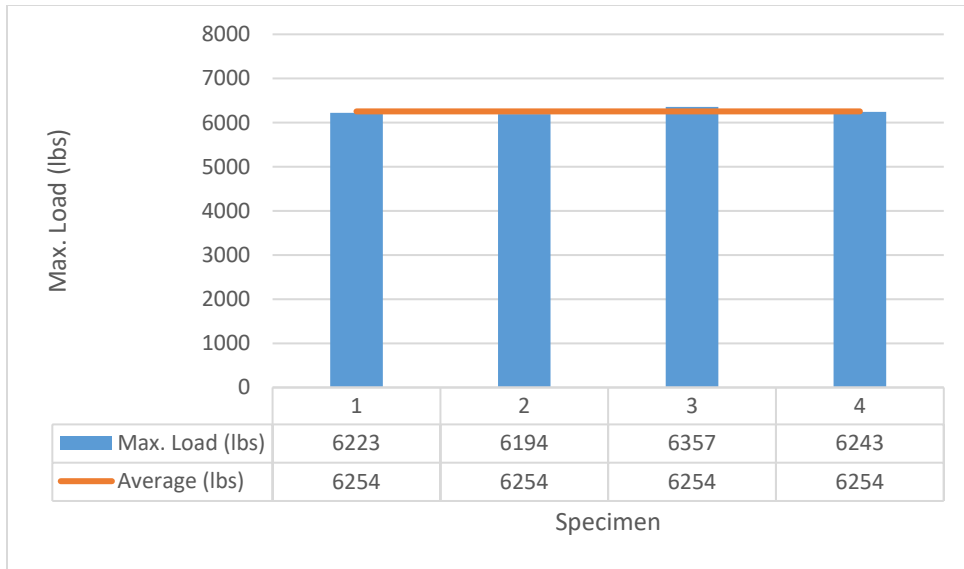


Figure 3 - 21 Ultimate Load of Flexure Test Results of Plain Concrete

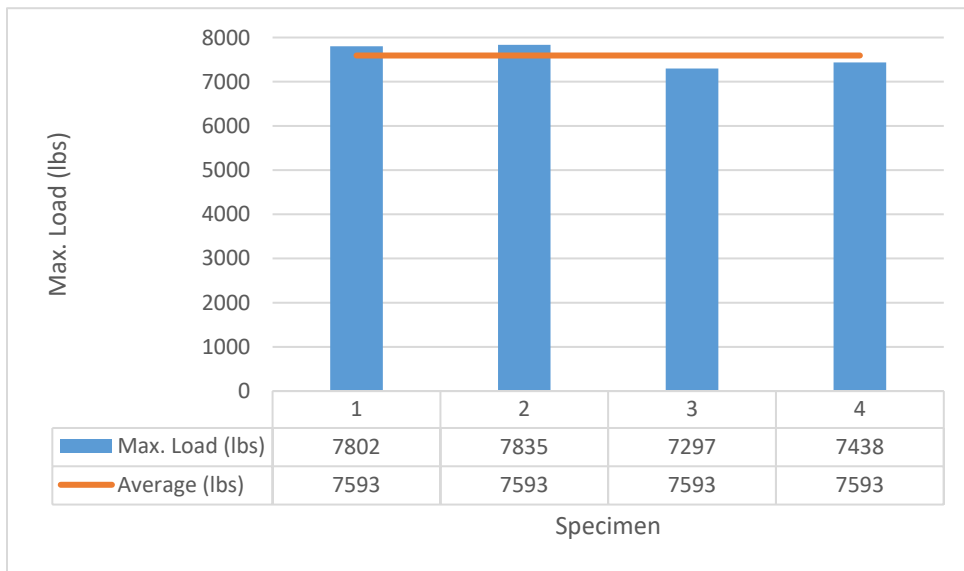


Figure 3 - 22 Ultimate Load of Flexure Test Results of SFRC

Figures 3-23 and 3-24 show the average maximum flexural stress of tested specimens of plain concrete and SFRC respectively. The average maximum flexural stress of plain concrete was (521 psi) while the average maximum flexural stress of SFRC was (633 lb). means utilizing steel fiber

in the concrete mixture increases the flexural stress by (21.5%).

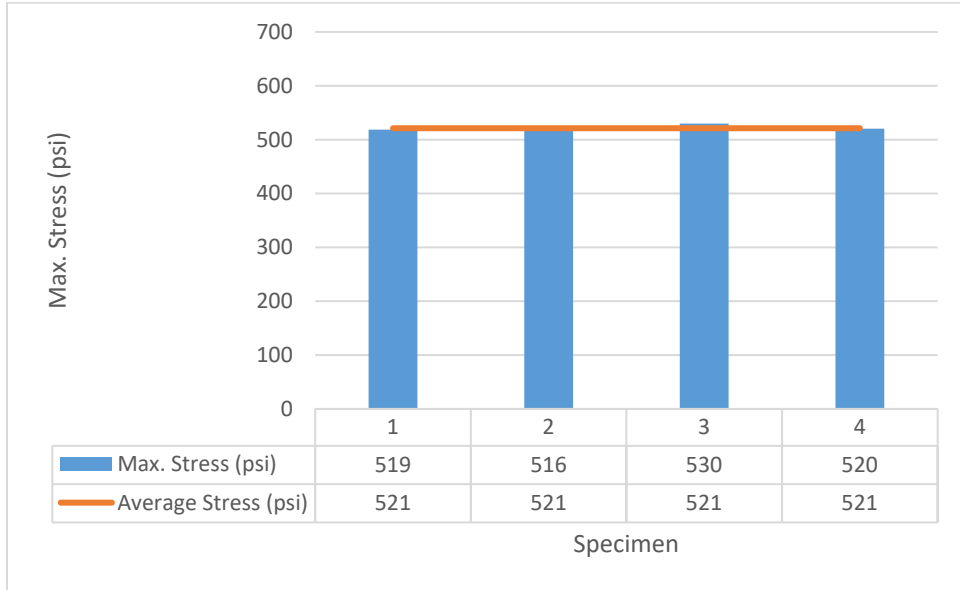


Figure 3 - 23 Ultimate Load of Flexure Test Results of SFRC

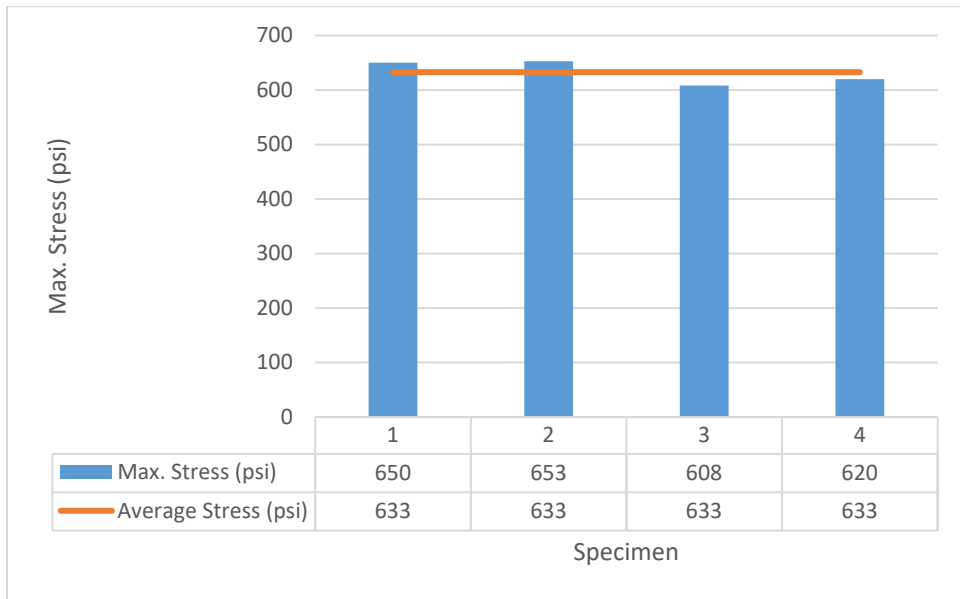


Figure 3 - 24 Ultimate Load of Flexure Test Results of SFRC

3.2.5 Modulus of Elasticity Test

The modulus of elasticity of concrete is the ratio of normal stress to the corresponding strain for compressive stresses below the proportional limit of concrete and it measures concrete stiffness or resistance to elastic deformation under stress, the higher the modulus of elasticity, the more resistant the material will give to deform within the elastic range means the higher modulus of elasticity stiffer the material is (Pauw, 1960). The approximate value of the elastic modulus of concrete can be obtained using different formulas but the accurate value can be estimated using different tests. Test according to ASTM C469 can accurately determine the modulus of elasticity of concrete as shown in Figure 3-25.



Figure 3 - 25 Modulus of Elasticity Test Machine

Eight 4-inch x 8-inch cylindrical specimens were tested at the age of 28 days, the specimen was loaded carefully to seat the gauge and observe its performance, after that, the load was

continuously applied, and stress and strain were recorded. The modulus of elasticity of concrete is computed to the nearest of 50000 psi using the following equation:

$$E_c = (S_2 - S_1) / (\epsilon_2 - 0.00005) \quad \text{Equation (3-1)}$$

where:

E_c : modulus of elasticity of concrete, psi

S_2 : stress corresponding to 40% of ultimate load.

S_1 : stress corresponding to a longitudinal strain of 50 millionths, psi

ϵ_2 : longitudinal strain produced by stress S_2 .

The modulus of elasticity of all concrete specimens was recorded as shown in Figures 3-26 and 3-27, the average modulus of elasticity of plain concrete and SFRC was (4169 ksi) and (4723 ksi) respectively.

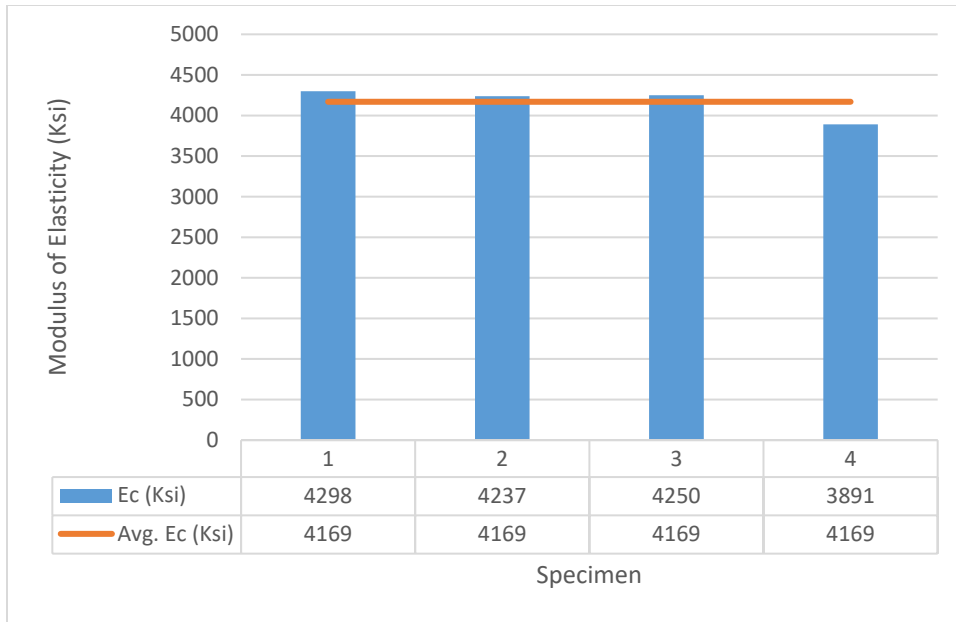


Figure 3 - 26 Modulus of Elasticity of Plain Concrete

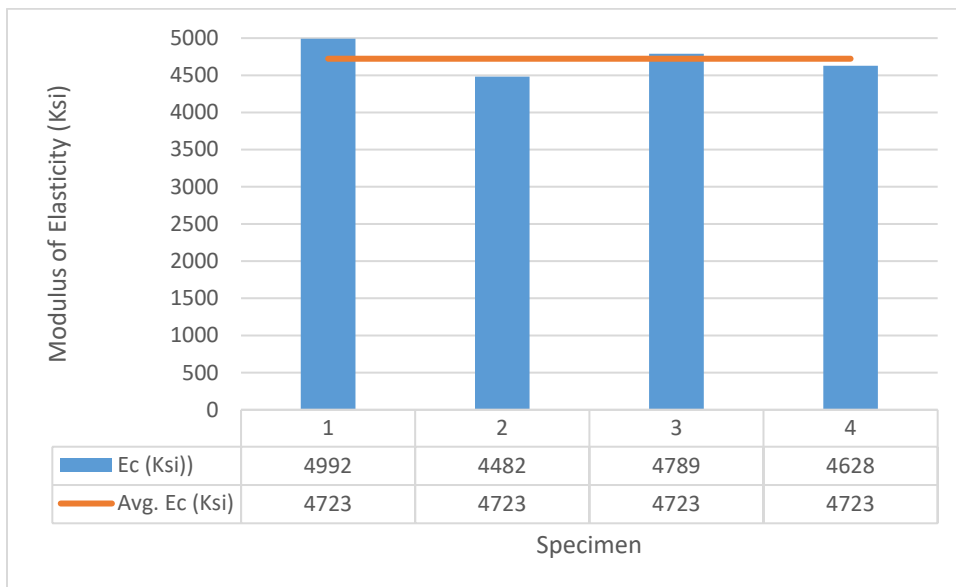


Figure 3 - 27 Modulus of Elasticity of SFRC

The stress-strain curves of plain concrete and SFRC specimens were recorded and shown in Figures 3-28 and 3-29, respectively. The area under the SFRC specimens' curve is larger than the area under the plain concrete, which means the observed energy by the SFRC is higher than the

plain concrete, and that is because of the effect of steel fiber and how it made the concrete stiffer. Additionally, the maximum concrete strain of SFRC (0.00575 in/in) was higher than that of plain concrete (0.0049 in/in) by 17%.

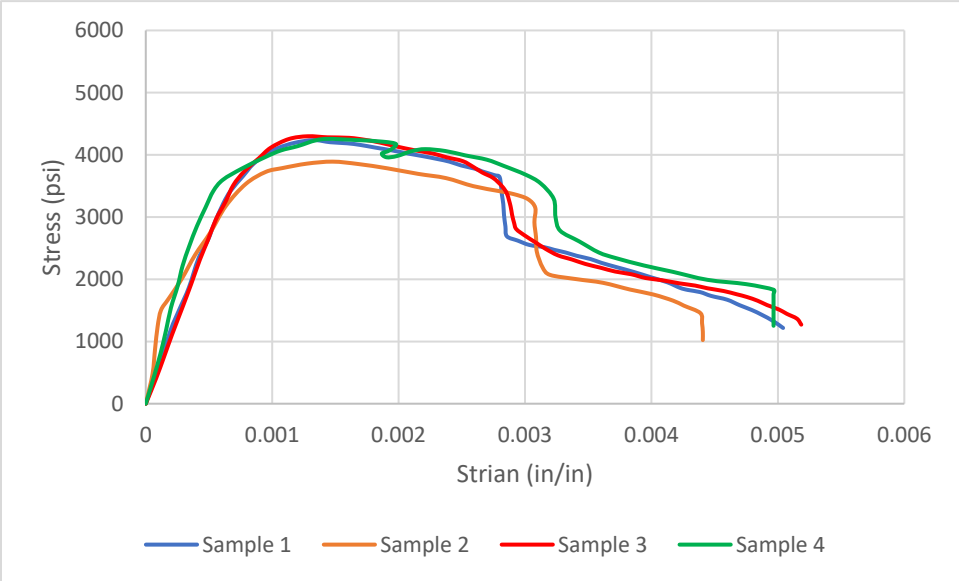


Figure 3 - 28 Stress-Strain Curves of Plain Concrete

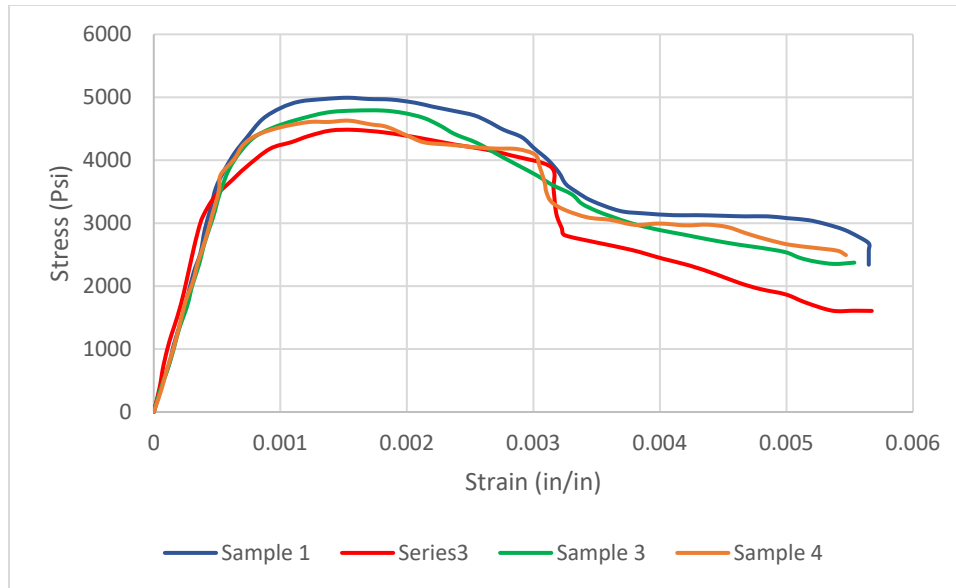


Figure 3 - 29 Stress-Strain Curves of SFRC

3.2.6 Poisson's Ratio

When a concrete specimen is subjected to axial loads, it experiences longitudinal and vertical strains due to volume reduction. Poisson's ratio of concrete is the ratio of transverse strain to longitudinal strain under these conditions, as demonstrated in Figure 3-30. The exerted loads crush small aggregate sizes, resulting in a reduction of the concrete specimen's volume. The Poisson's ratio of concrete is a constant that helps in determining the stress and deflection properties of structures like beams, plates, and shells. The value of the Poisson's ratio of concrete can vary based on different factors such as the type of specimen (dry, wet, or saturated), and loading conditions. Concrete exhibits a lower Poisson's ratio under static loads than it does under dynamic loads. Typically, the value of Poisson's ratio for concrete under dynamic loads ranges between 0.20 and 0.25. When designing concrete structures, the typical value for the Poisson's ratio is 0.2. (Wang and Li, 2007, Persson, 1999, Ferretti, 2004, Sideris et al. 2004, and Carrillo et al. 2019)

Poisson's Ratio can be expressed as

Poisson Ratio= Transverse Strain/ Axial Strain

Or

$$\nu = -\frac{d\varepsilon_{trans}}{d\varepsilon_{axial}} = -\frac{d\varepsilon_y}{d\varepsilon_x} \quad \text{Equation (3-1)}$$

Where

ν is the Poisson's ratio

ε_{axial} is the axial strain.

ε_{trans} is the transverse strain.

Strain can be expressed as

$$\varepsilon_{axial} = \frac{L_1 - L_2}{L_2} \quad \text{Equation (3-2)}$$

and

$$\varepsilon_{trans} = \frac{d_1 - d_2}{d_2} \quad \text{Equation (3-3)}$$

where

L_1 = Initial length of the specimen (ft)

L_2 = Final length of the specimen (ft)

d_1 = Initial diameter of the specimen (ft)

d_2 = Final diameter of the specimen (ft)

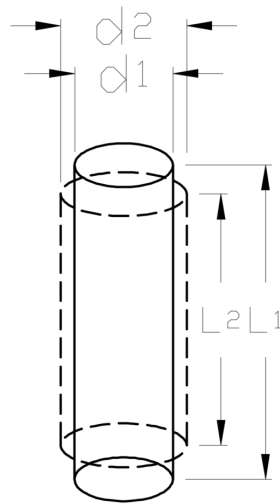


Figure 3 - 30 Initial and Final Length and Diameter of Cylinder

The standard concrete test results of four cylinders of plain concrete and four cylinders of SFRC were shown in Figures 3-31 and 3-32.

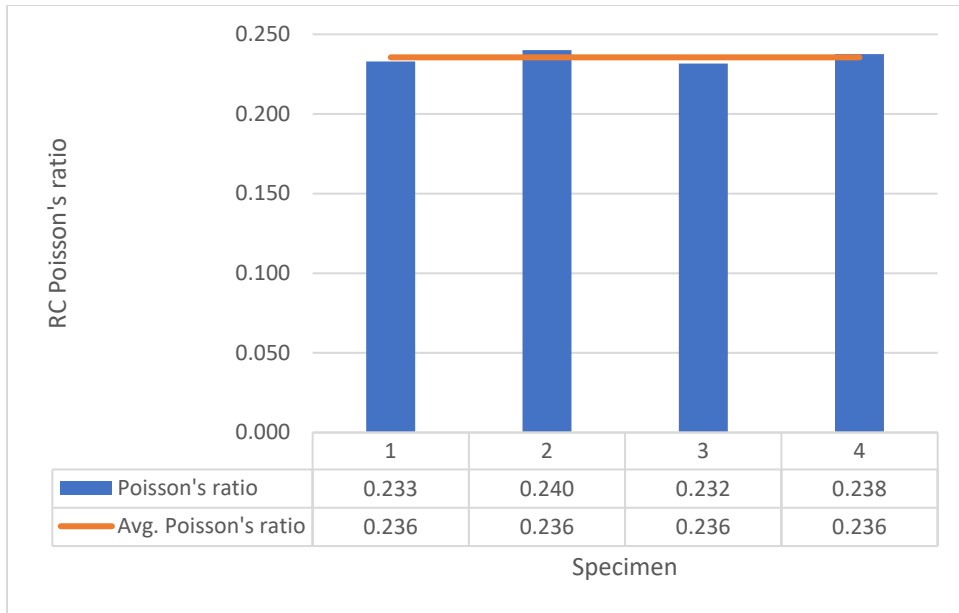


Figure 3 - 31 Poisson's Ratio Test Results of Plain Concrete

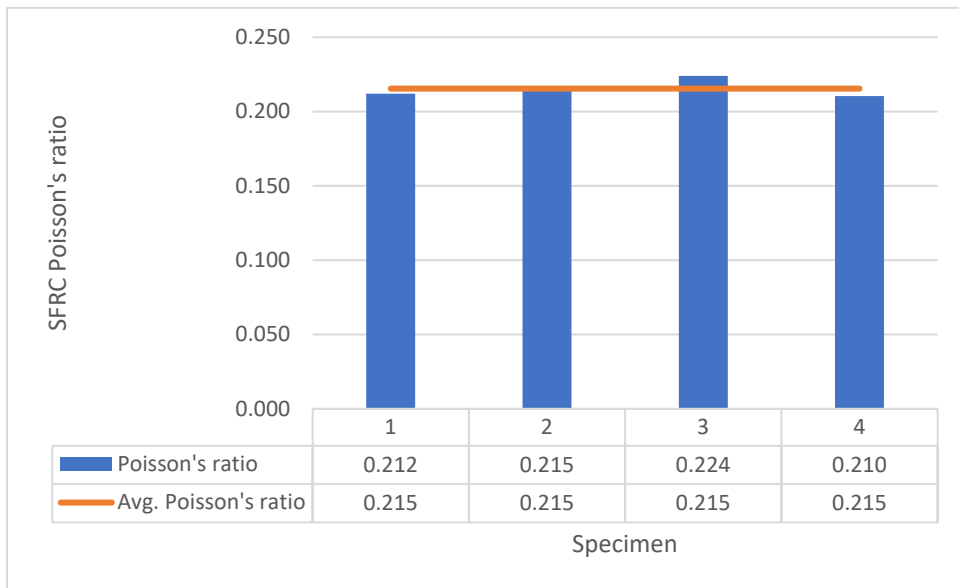


Figure 3 - 32 Poisson's Ratio Test Results of SFRC

3.3 Conclusion of concrete standard test results

Based on the results of the specimen tests, it is evident that the utilization of steel fibers had a significant impact on the mechanical properties of plain concrete. Adding 70 pounds of 4D Dramix steel fiber to the concrete mixture resulted in improved performance compared to plain concrete. Compressive strength increased by 11.4%, split tensile strength increased by 29%, flexural strength increased by 21.5%, and stiffness increased by 13%. The steel fibers were particularly effective in enhancing the tensile and flexural strength as they bridged the cracks and provided the concrete with greater capacity and energy absorption under tensile load. Adding steel fiber reduced Poisson's ratio because the fiber confined specimens and restricted transverse strain. However, it should be noted that the workability of the concrete was reduced by 30% with the addition of steel fibers, which may be undesirable.

CHAPTER 4

CONCRETE DECK SPECIMENS PREPARATION AND EXPERIMENT WORK

4.1 Overview

In this study, a concrete bridge composed of precast concrete girders and concrete decks was assumed as a case study. The girders were simply supported beams. To conduct experiments, a section of this bridge was selected, consisting of two continuous spans with three girders. This section was scaled down by half for handling and testing purposes. The specimen was designed as a reference point for comparison with other specimens of the exact dimensions but with different types of reinforcement. This chapter provides information on the specimen's dimensions, design, casting, and experimental methodology.

This study aims to analyze the behavior of concrete bridge decks under a bending load. Various types of reinforcement were utilized in concrete decks of identical dimensions. A total of twelve concrete decks were designed, prepared, and tested at the Civil Engineering Laboratory Building located at the University of Texas at Arlington. Table 4-1 shows the details of these concrete decks with various types of reinforcement.

Table 4 - 1 Concrete Decks with Various Types of Reinforcement

Specimen name	Reinforcement	Casting
RC-1	#3 and #4 steel bars	CIP (Reference)
RC-2	#3 and #4 steel bars	CIP (Reference)
SFRC-CIP-1	Steel Fiber and steel wire mesh	CIP
SFRC-CIP-2	Steel Fiber and steel wire mesh	CIP
SFRC-PC-1	Steel Fiber and steel wire mesh	PC
SFRC-PC-2	Steel Fiber and steel wire mesh	PC
GFRP-1	#3 and #4 GFRP bars	CIP (Reference)
GFRP-2	#3 and #4 GFRP bars	CIP (Reference)
SFRC-GFRP-CIP-1	Steel Fiber and GFRP mesh	CIP
SFRC-GFRP-CIP-2	Steel Fiber and GFRP mesh	CIP
SFRC-GFRP-PC-1	Steel Fiber and GFRP mesh	PC
SFRC-GFRP-PC-2	Steel Fiber and GFRP mesh	PC

4.2 Dimensions of deck case study

The assumption of this research was taking a research topic from a continuous simply supported concrete bridge girders spaced (5'-4") center to center and cast in place concrete deck of (8.5 inch) thickness. The research topic assumed a specimen consisting of three pre-cast simply supported concrete girders and two continuous spans of the cast-in-place concrete deck that has a width of (4'-8") and a length of (16'-0"), then half scale has been assumed (50% scale) for handling and testing purposes; therefore, the final dimensions of the concrete deck were (2'-8") center to center girders spacing, (4.25 inch) concrete deck thickness, (8'-0") length, and (2'-4") width, as shown in Figure 4-1.

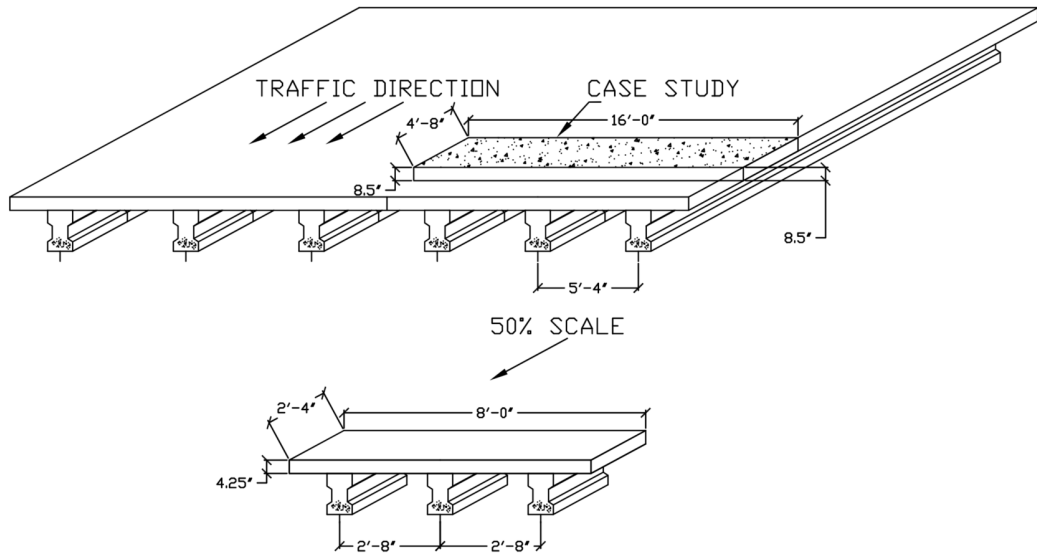


Figure 4 - 1 Case Study Details

4.2.1 Concrete Girders design

To ensure the deck would fail before the girders, 6000 psi concrete compressive strength was used for the girder concrete mixture, which is higher than the compressive strength of the decks. The girders were reinforced by #4 steel longitudinal bars and #3 stirrups. Figure 4-2 illustrates the sketch of two types of girders with identical heights and widths used in this research. Figure 4-3 shows the precast girder.

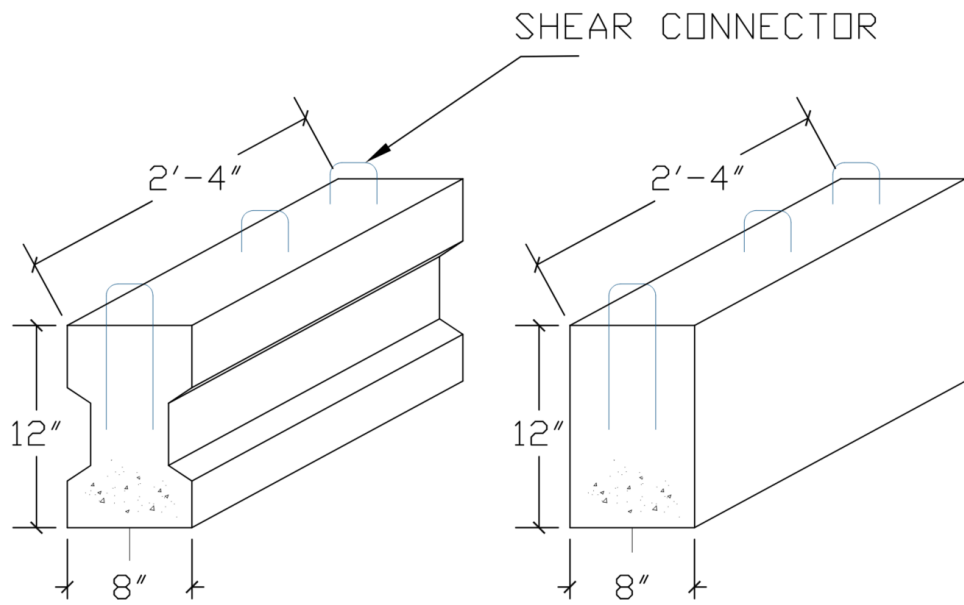


Figure 4 - 2 Sketch of Pre-Cast Concrete Girder



Figure 4 - 3 Pre-Cast Concrete Girder

4.2.2 Deck design

This study involves two groups, the first group compares concrete decks reinforced with

conventional steel bars (RC) to those reinforced with steel fiber and steel wire mesh (SFRC). The second group compares decks reinforced with GFRP bars to those reinforced with steel fiber and GFRP mesh.

1. First Group:

1.1. Conventional bars reinforced cast-in-place concrete deck (RC)

Two cast-in-place concrete deck specimens have been designed and reinforced by conventional reinforcement, designed per the AASHTO LRFD method. #3 and #4 reinforcement bars were used as primary reinforcement considering dead load, future wearing load, and HL-93 truck as live load (see Table 4-2 and Figures 4-4 and 4-5 and Appendix B).

Table 4 - 2 AASHTO LRFD Reinforcement Details of RC Decks

Moment location	Reinforcement
Positive moment reinforcement (+M)	#4 @ 9 inch
Negative moment reinforcement (-M)	#4 @ 12 inch
Distribution reinforcement	#3 @ 7 inch
Shrinkage and Temperature reinforcement	#3 @ 12 inch

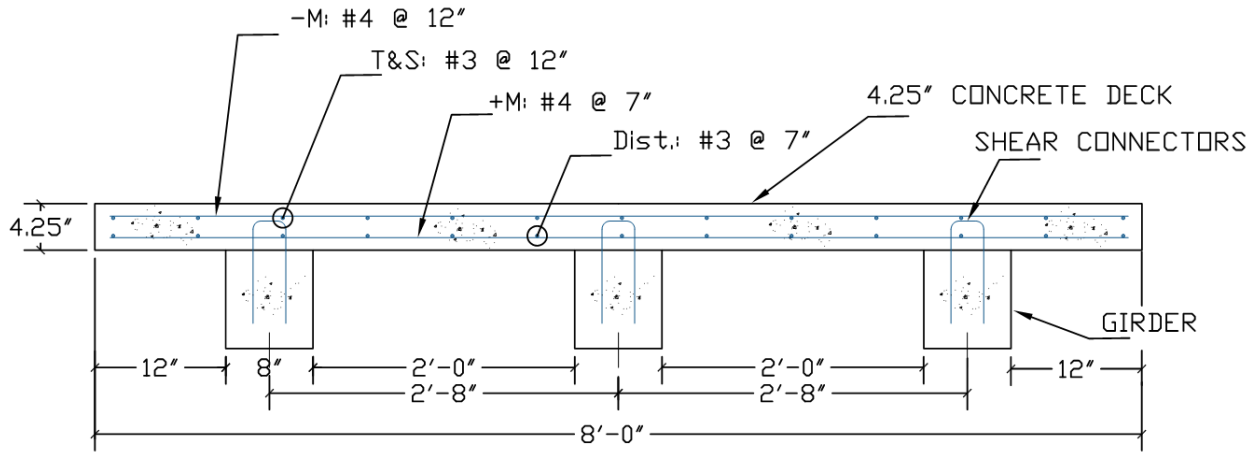


Figure 4 - 4 AASHTO LRFD Concrete Deck Design Details



Figure 4 - 5 Formworks and Bottom Layer Reinforcement of AASHTO LRFD Concrete Deck

1.2. Steel fiber reinforcement cast-in-place concrete deck (SFRC-CIP)

Two cast-in-place concrete decks were designed and reinforced with steel fiber as the primary reinforcement and steel bars wire mesh. (70 pounds per cubic yard) Dramix 4D 65/60 BG steel fiber was used in the concrete mixture as the primary reinforcement with two layers of (6-inch by 6-inch by 1/4-inch) steel bars wire mesh as a distribution reinforcement (see Figure 4-6).

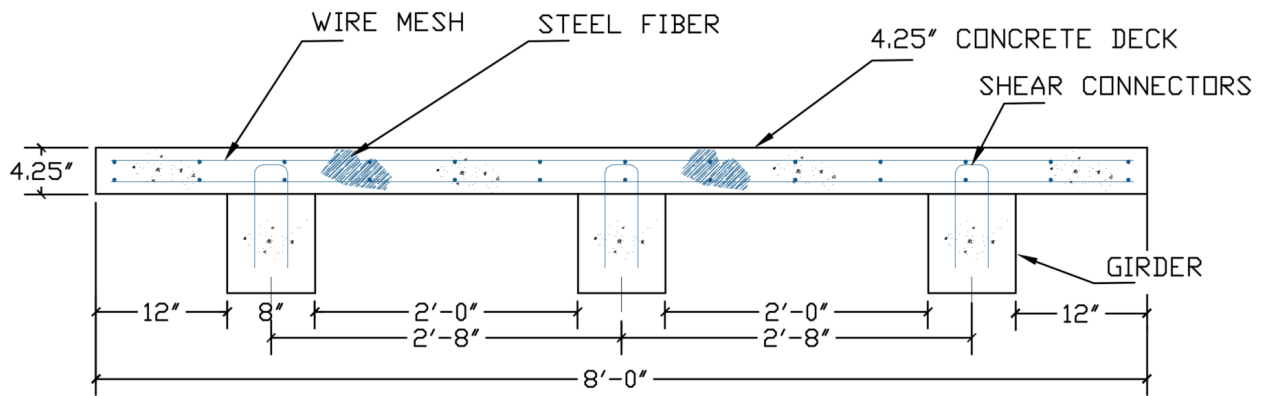


Figure 4 - 6 Steel Fiber Reinforcement Cast-In-Place Concrete Deck Details (SFRC-CIP)

1.1. Steel fiber reinforcement precast concrete deck (SFRC-PC)

Precast concrete has always been a popular choice for constructing buildings and facilities due to its ability to reduce construction time, labor, and work schedule. As such, this research aims to explore the potential of using fibers as the primary reinforcement in precast concrete decks by analyzing its behavior and comparing it to reference decks.

Figure 4-7 shows the designed precast deck with identical dimensions to the reference and cast-in-place decks. (70 pounds per cubic yard) Dramix 4D 65/60 BG steel fiber was used in the concrete mixture as the primary reinforcement with two layers of (6-inch by 6-inch by 1/4-inch) steel bars wire mesh as a distribution reinforcement it has (3-inch by 3-inch) pocket holes to be filled by concrete grout after placing the precast deck on top of the precast girders

as shown in Figures 4-8 and 4-9.

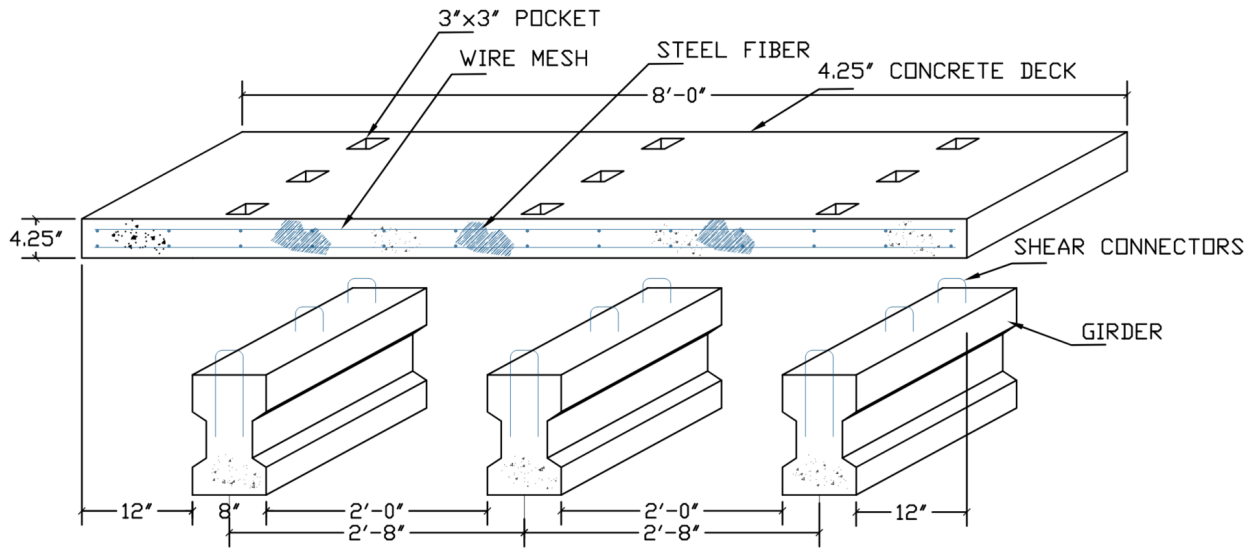


Figure 4 - 7 Steel Fiber Reinforcement Precast Concrete Deck Details (SFRC-PC)



Figure 4 - 8 Precast Deck and Girders before Grouting



Figure 4 - 9 Precast Deck and Girders After Grouting

2. Second Group:

2.1. Glass fiber bars reinforced cast-in-place concrete deck (GFRP)

Two cast-in-place concrete deck specimens have been designed and reinforced by GFRP reinforcement, designed per the AASHTO LRFD and ACI-440 codes. #3 and #4 glass fiber bars were used as primary reinforcement considering dead load, future wearing load, and HL-93 truck as live load, (see Table 4-3 and Figures 4-10 and 4-11 and Appendix B).

Table 4 - 3 Reinforcement Details of GFRP Decks

Moment location	Reinforcement
Positive moment reinforcement (+M)	#4 @ 9 inch
Negative moment reinforcement (-M)	#4 @ 10 inch
Distribution reinforcement	#3 @ 8 inch
Shrinkage and Temperature reinforcement	#3 @ 12 inch

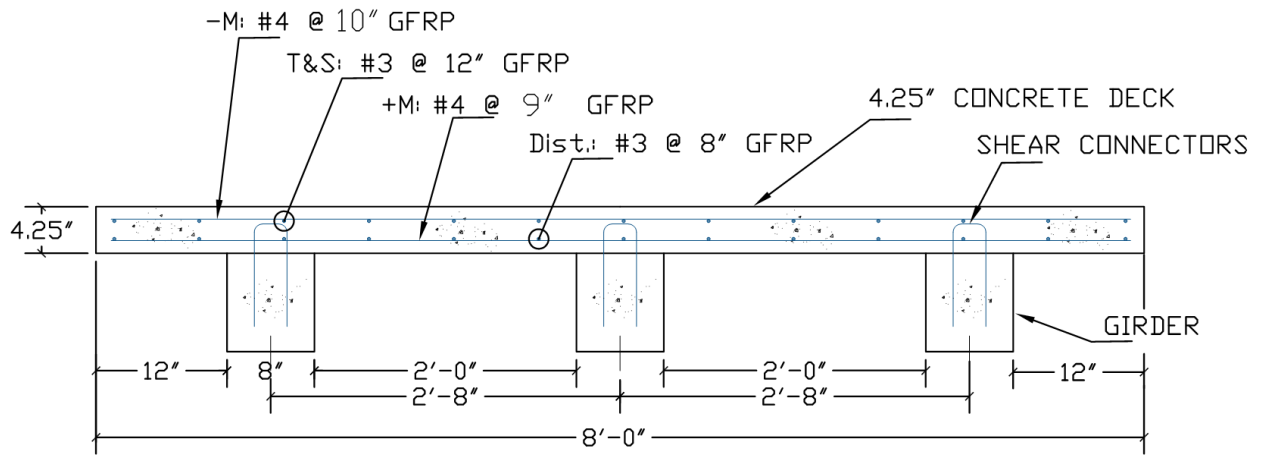


Figure 4 - 10 Reinforcement Details of GFRP Decks

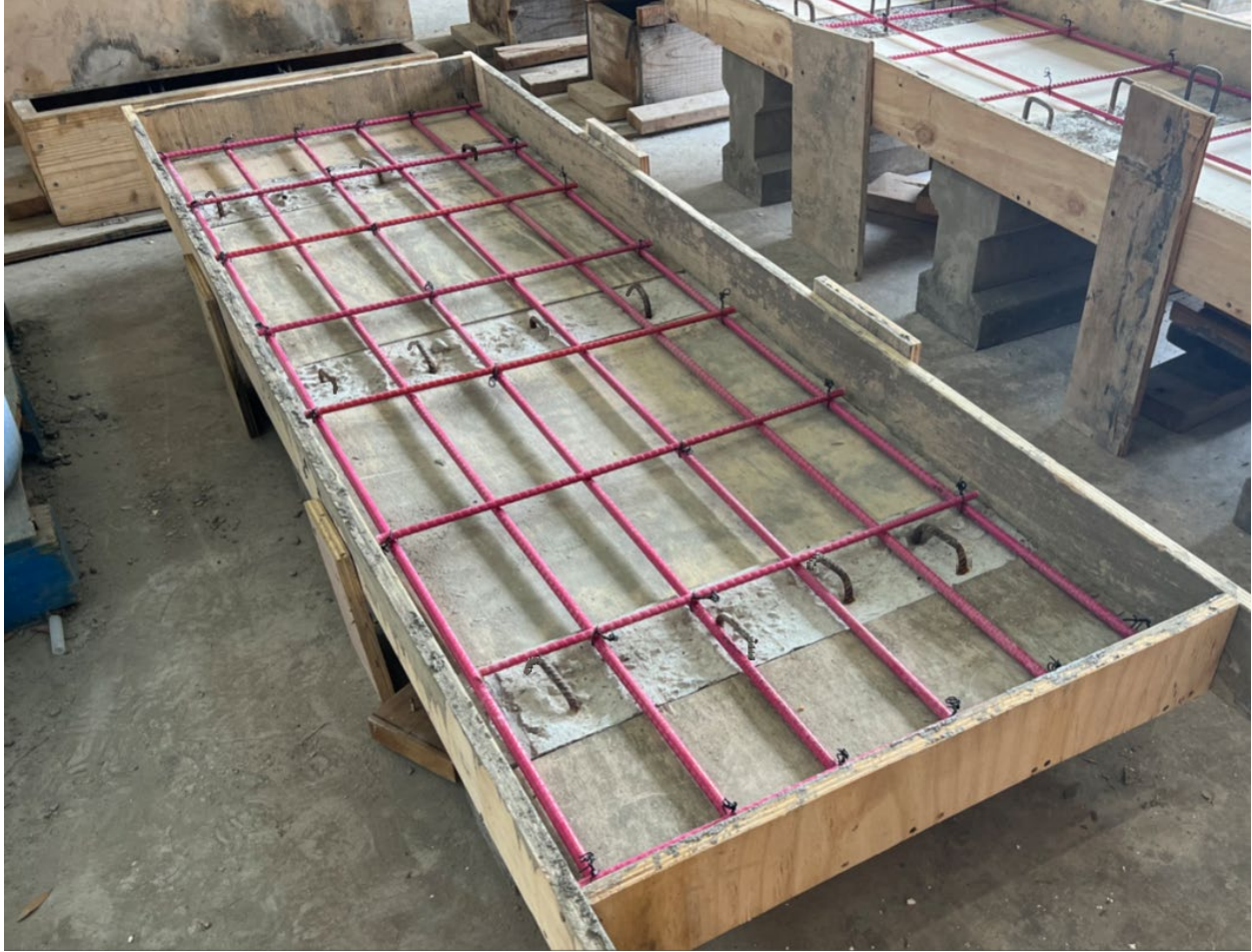


Figure 4 - 11 Formworks and Bottom Layer Reinforcement of GFRP Bars

2.2. Steel fiber with GFRP mesh reinforcement cast-in-place concrete deck (SFRC-GFRP-CIP)

In this deck, the same type and amount of steel fiber were used as the primary reinforcement as it was used before in SFRC-CIP and SFRC-PC, and two layers of GFRP mesh were supplementary reinforcement for two cast-in-place decks designed, cast, tested, and compared to reference decks as shown in Figure 4-12.

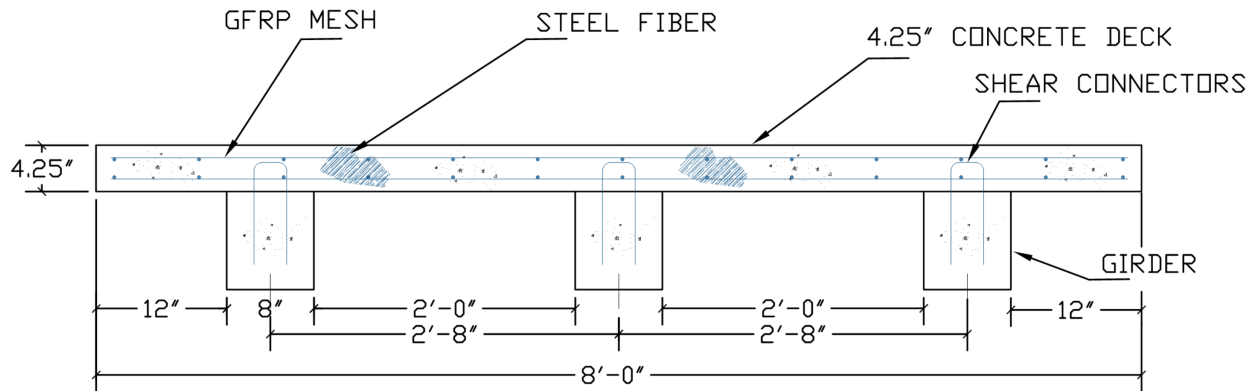


Figure 4 - 12 Reinforcement Details of SFRC-GFRP-CIP Deck

2.3. Steel fiber with GFRP mesh reinforced precast concrete deck (SFRC-GFRP-PC)

The precast decks were attached to the precast girders through shear connectors placed inside (3-inch x 3-inch) pocket holes. The same type and amount of steel fiber and two layers of GFRP reinforcement were used as it was used before in SFRC-GFRP-CIP as shown in Figure 4-13

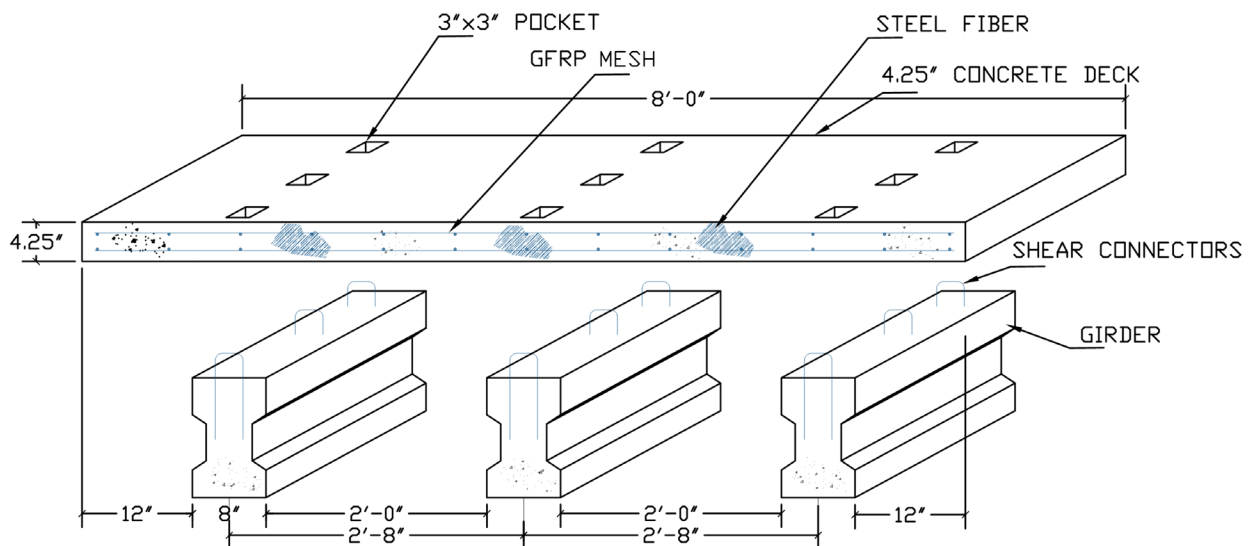


Figure 4 - 13 Reinforcement Details of SFRC-GFRP-PC Deck

4.2.3 Specimen preparation

The concrete formwork was prepared for the girders and decks, and they were prepared according to the design dimensions, as shown in Figure 4-14. A concrete strength of (6000 psi) and (4000 psi) was used for the girders and the decks respectively. Steel bars reinforcement, steel fibers, and GFRP bars were prepared, and the concrete was mixed according to the design weights shown in Table 3-2. The girders were poured first as a precast to prepare them for the concrete decks. The formwork of the decks was installed over the girders, decks were poured over it and the girder shear connectors overlapped with the concrete of the deck to give the required bond as in standard bridges.



Figure 4 - 14 Concrete Decks Formworks and Casting

4.2.4 Experimental Work

The Civil Engineering Laboratory Building houses many machines and devices to examine materials and specimens. These tools aid students and researchers in conducting scientific and engineering research. Below is a review of the machines and devices utilized in the

experiments.

1- Tensile Compression Machine

All concrete decks were tested using the MTS (400 kips) tensile compression machine as shown in Figure 4-15 below.



Figure 4 - 15 400 Kips MTS Testing Machine

2- Load Cell

The load cell manufactured by Tokyo Measuring Instruments Lab and was placed between the load base and the distribution steel beam so that the load cell started recording the load values during the experiment work. (see Figure 4-16).



Figure 4 - 16 Load Cell

3- Steel plates

(10 in x 5 in) steel plate installed between the load distribution beam and the top surface of the concrete decks represented 50% of the scale of AASHTO LRFD tire contact area (AASHTO 2014, 3.61.25) as shown in Figure 4 -17.

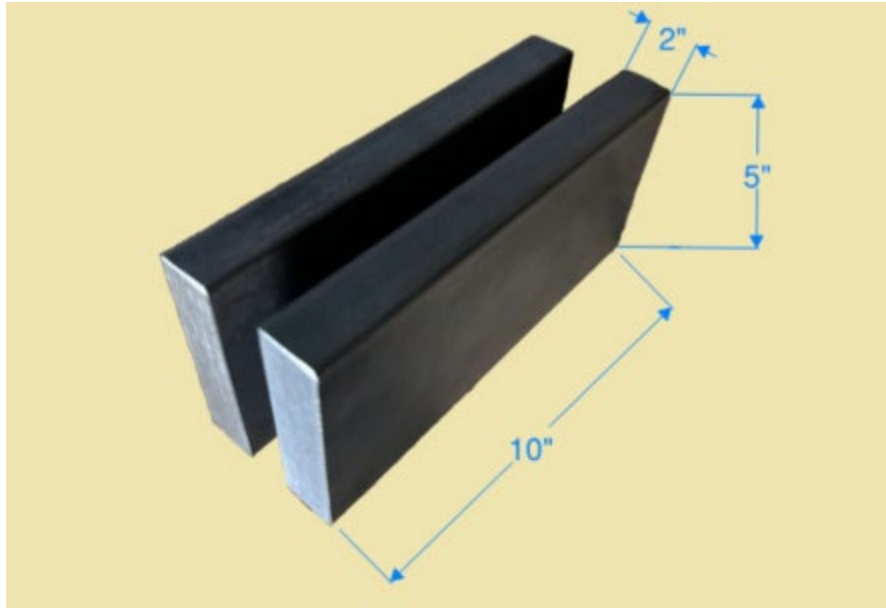


Figure 4 - 17 Steel Plate as a Tire Contact Area

4- Load Distribution Beam

The load exerted during the testing process, the applied load was transmitted from the central axis of the 400 kips MTS testing machine to the midpoints of the concrete decks' spans via a steel beam that was reinforced with stiffeners as shown in Figure 4-18.

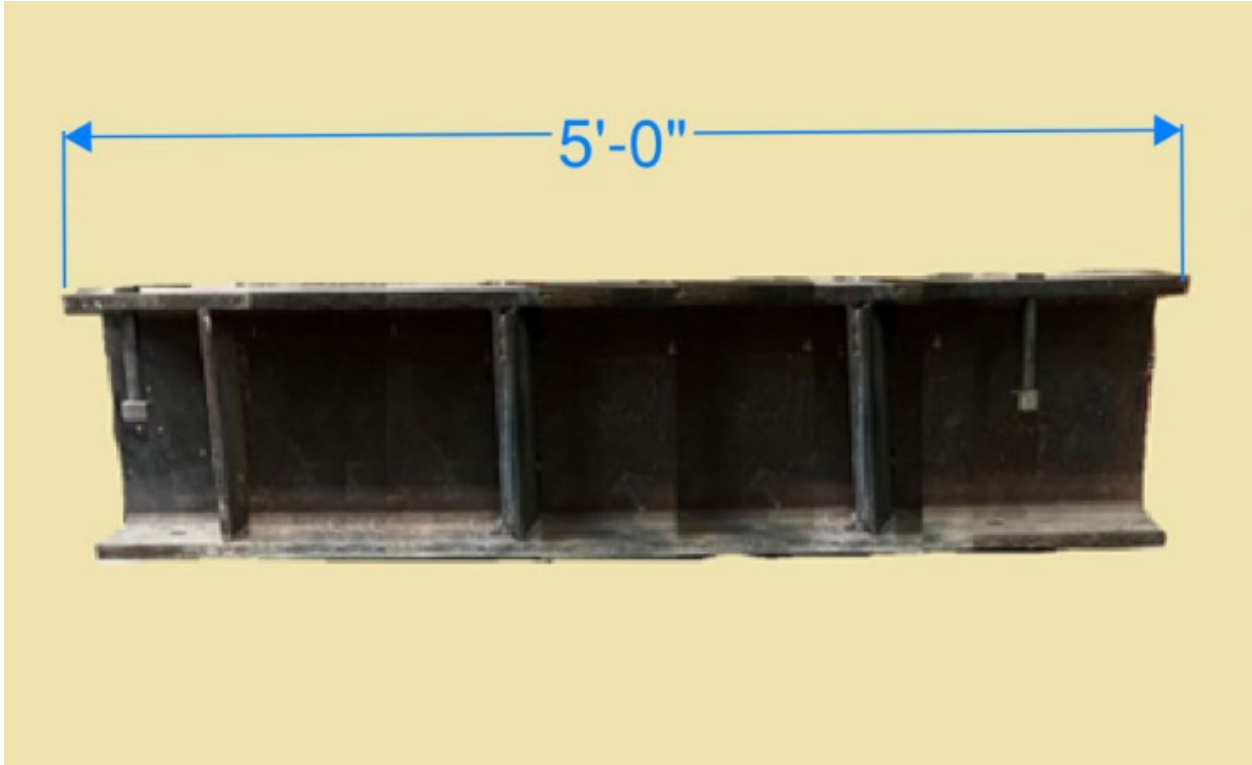


Figure 4 - 18 Load Distribution Steel Beam

5- Linear Variable Differential Transformer (LVDT)

The SDP-200D displacement transducer is an axial-type transducer manufactured by Tokyo Measuring Instruments Lab. It measures 200 mm and is installed at the bottom of mid span of each deck. The strain gauge-type design makes this transducer free of the noise generated by sliding electrical contact points. Taking advantage of the stroke of the axial part, it can measure a large amount of displacement and make stable measurements over a long period of time. As it is provided with graduations, alignment work can be done easily as shown in Figure 4-19.



Figure 4 - 19 Linear Variable Differential Transformer Sensor

6- Strain Gauge

During load application, a strain gauge of the PL-60-11-5LJC-F type with three wires was used to measure the concrete strain. This strain gauge was manufactured by Tokyo Measuring Instruments Lab and was installed at the mid-span bottom of the concrete deck. The strain gauge was attached to the concrete surface according to the provided instructions for gluing, as shown in Figure 4-20.



Figure 4 - 20 Strain Gauges

7- Multi-channel data acquisition system

Cable-connecting up to 20 units with 50 channels per unit, which enables simultaneous sampling measurement of up to 1000 channels. It can measure 100-Hz occurrences at the fastest sampling rate of 1 kHz. The cable can connect devices up to 100 meters apart, allowing

for wide-area, multi-channel dynamic strain measurement that is not possible with conventional instruments for measuring dynamic strain. Type S-4100 data acquisition system manufactured by Tokyo Measuring Instruments Lab was used to record all the data recorded by load cell, LVDTs, and strain gauges. As shown in Figure 4-21

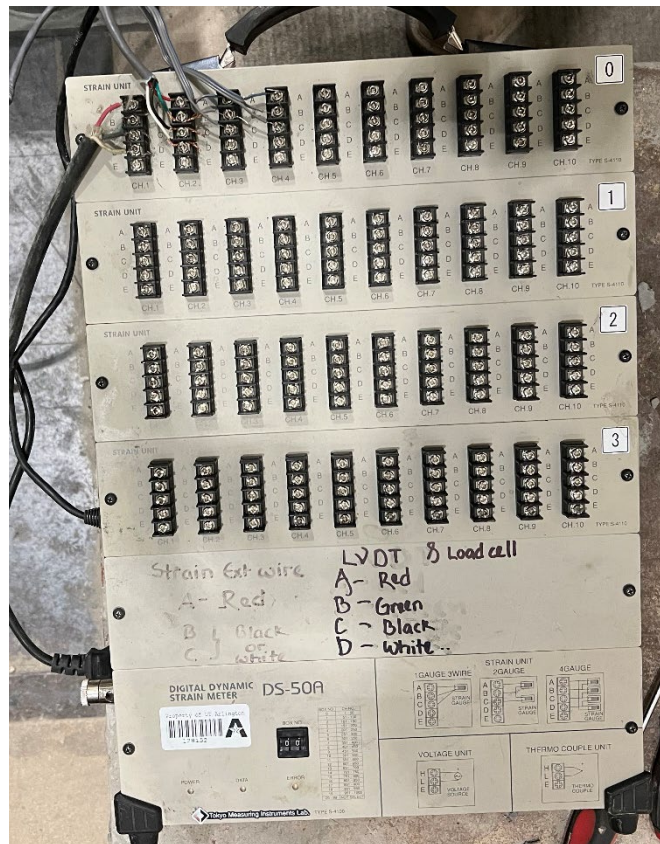


Figure 4 - 21 Data Acquisition System

4.2.5 Specimen testing

All twelve specimens were tested at the age of 28 days in the Civil Engineering Laboratory Building at the University of Texas at Arlington. Specimens were placed under the (400 kips) compression machine to apply the load. The load was applied to the center of the concrete deck and then distributed to the middle of each span through a load-distribution steel beam as

a concentrated load. (2-inch) the thickness of steel plates has been provided between the load distribution beam and the top surface of the deck. This plate has dimensions of (10-inch) length (perpendicular to the direction of travel) by (5-inch) width. The dimensions of the plate represented 50% of the scale of AASHTO LRFD tire contact area (AASHTO 2014, 3.61.25). The load cell was applied between the load-distribution steel beam and the (400 kips) compression machine. Linear Variable Differential Transformers (LVDT) have been set up in the middle of each span to measure the change in deflection with the increase of loads. Strain gauges have also been installed in the middle of each span at the bottom surface of the deck to measure the strain with the applied stress. All strain gauges, LVDTs, and load cell are connected to the Data Acquisition System (DAS) to collect the readings during the load test experiment as shown in Figure 4-22 and Figure 4-23.

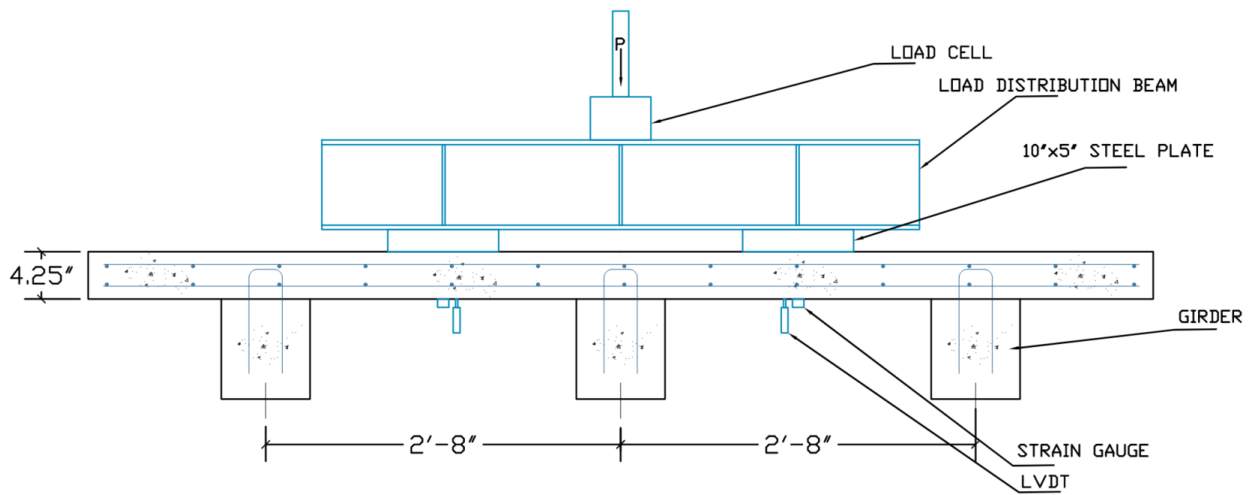


Figure 4 - 22 Schematic Testing Setup

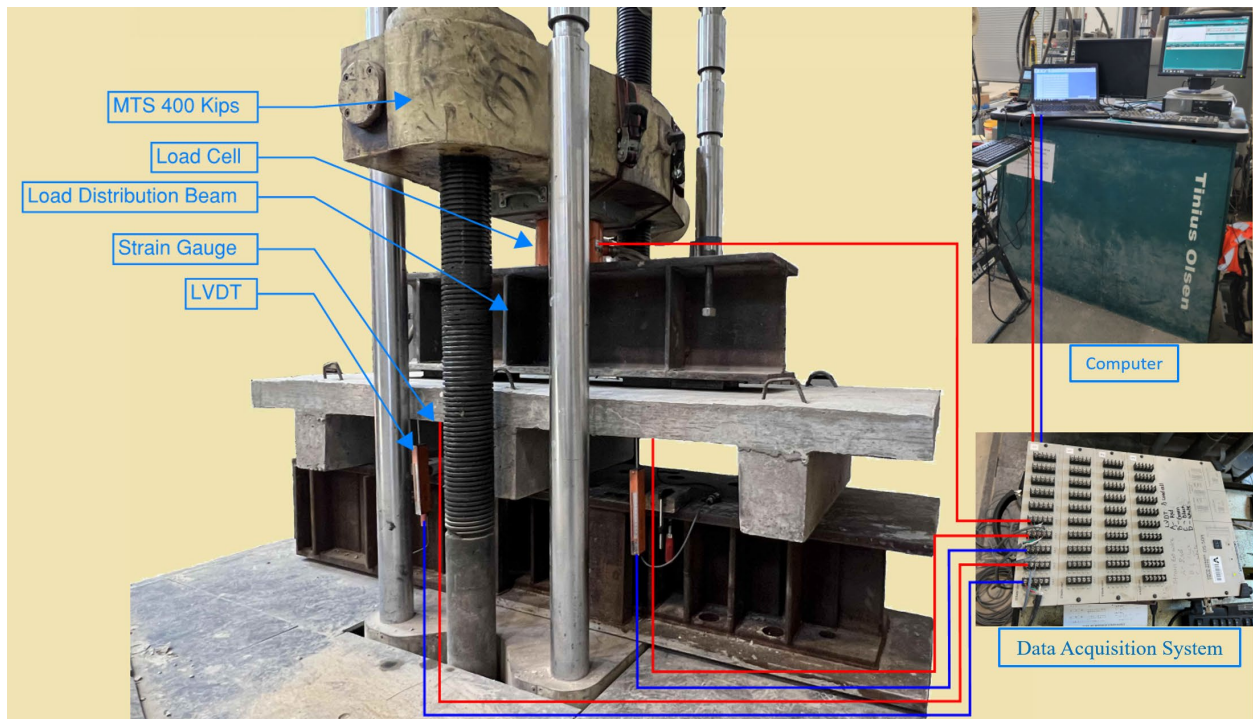


Figure 4 - 23 400 Kips MTS Testing Machine and Test Configuration

Each sample was installed, as shown in the figure above, representing a bridge section subjected to the compression load of car tires on each span. The load was applied by the (400 ksi) compression machine with a load rate of (500 lb/min), and the applied load was recorded through a load cell.

CHAPTER 5

FINITE ELEMENT MODELING (FEM)

5.1 Overview

Chapter 5 only covered the initial and developed FE model of the concrete decks but included modeling all the structural elements, concrete, steel plates, steel reinforcement, GFRP reinforcement, steel fiber reinforced concrete, and loading conditions. Chapter 5 also involved the initial material properties and all the assumptions made to model each element in FE.

5.1.1 Initial Numerical Modeling

Numerical simulations were conducted on reinforced concrete decks using the ABAQUS (2020) software. The modeling of specimens involved detailed discussions on concrete material models, boundary conditions, as well as various material and geometric parameters. The concrete material was modeled as a homogeneous 3D solid section. FRP-confined concrete was numerically simulated using the Drucker-Prager plasticity model (Mirmiran et al., 2000; Rousakis et al., 2008; Karabinis et al., 2008). Generally, a numerical model was detailed enough to capture all critical and essential phenomena but was not so complex that it significantly increased the analysis time of the computer. In order to achieve better results than previous experimental findings, the geometry of the control model was simulated and calibrated for various factors such as dilation angle, stress ratio, shape factor, plastic potential eccentricity, and viscosity parameter of the concrete damaged plasticity (CDP) model. This was done by considering different element types and mesh sizes. Figure 5-1 shows the model view of the targeted deck. The model employed 8-node linear brick elements (C3D8) for the concrete and 2-node linear truss elements (B21) for the reinforcements, as these can carry only tensile forces. Moreover, a simple support boundary condition was assumed for all the

girders. The reinforcements were then embedded in the concrete using the embedded region constraint option. The reinforcements were the embedded elements, and the girders and the concrete deck were the host elements. The interactions between the girders and the concrete deck were initially simulated using a tie constraint option. The #3 and #4 reinforcements are modeled in FE, so the total deck thickness above the girder flange is 4.25 inches.

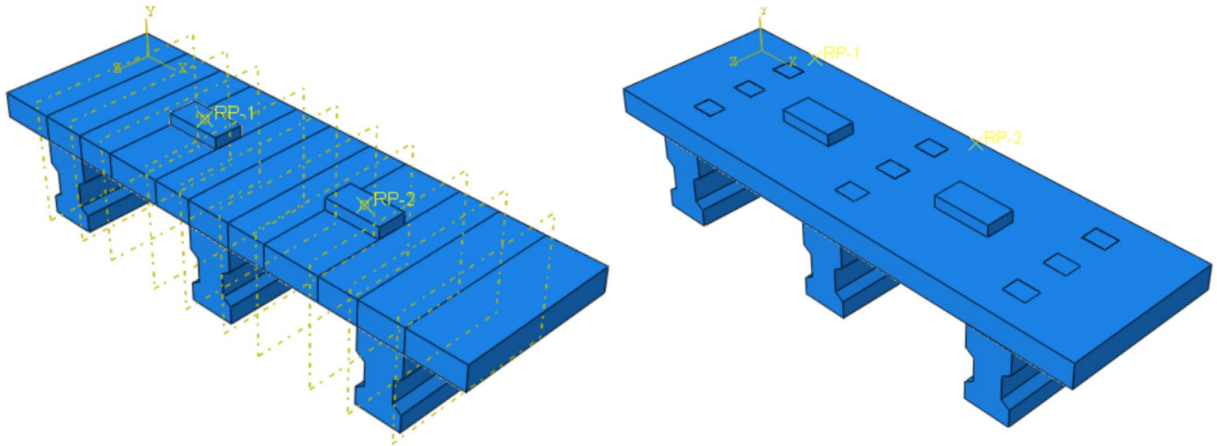


Figure 5 - 1 Model View of the Concrete Decks

5.1.2 Precast Girders

Each specimen has three precast girders with a length of 28 inches and a height of 12 inches. These girders were modeled in FE with a #4 embedded reinforcement. The material properties for the girders were provided to the FE model as concrete compressive strength (f_c') (5000 psi). Each girder has three shear connectors spaced 8 inches center to center with a projection of 3 inches. Figures 5-2 show the model view of longitudinal reinforcement in FE for each girder, represented by small white dots, and the shear connectors, represented by red color bars.

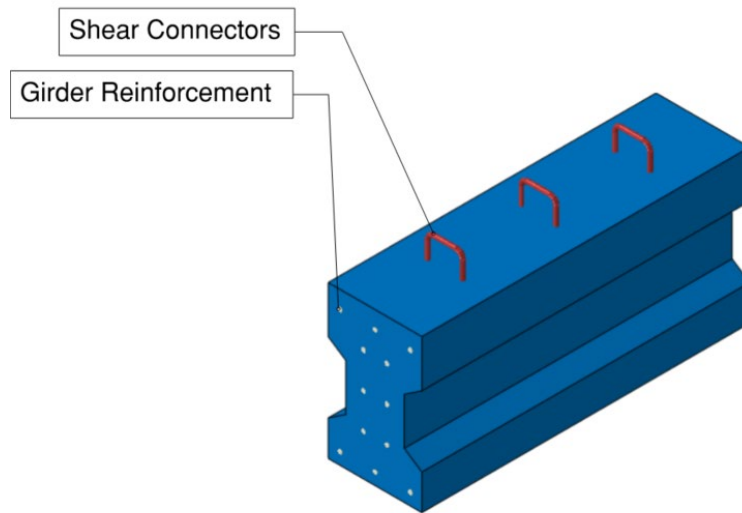


Figure 5 - 2 FE Model of Girders

5.1.3 Concrete Decks

Six types of concrete decks have been modeled in the FE based on the type of reinforcement and type of casting. All decks have a compressive strength, f_c' , determined by standard concrete tests and dimensions of 8 feet long by 28 inches wide and 4.25 inches thick. The cast-in-place decks were cast on top of the precast girders, while the precast decks were precast with nine shear pockets (3 in x 3 in), as shown in Figure 5-4. These six types of decks are as follows:

5.1.3.1. RC decks

This type of deck was modeled in FE using #3 and #4 steel bars as the main reinforcement, as mentioned in Table 4-2. These bars were embedded in the concrete deck, and the shear connectors were also embedded in the girders and the concrete deck. Fully composite action was assumed between the top flange of the girders and the deck as the deck was cast in place

as shown in Figure 5-3.

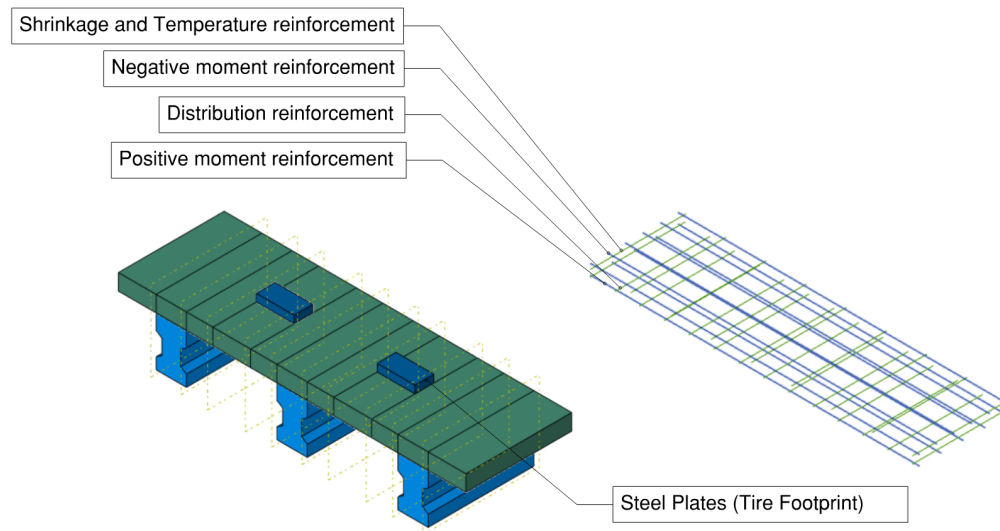


Figure 5 - 3 FE Model of RC Decks

5.1.3.2. SFRC-CIP

In this deck, (70 lb/cy) of 4D Dramix steel fiber has been used as the main reinforcement. Therefore, the concrete elasticity is different than RC. (6-inch by 6-inch by 1/4-inch) steel bars wire mesh as the supplementary reinforcement were embedded in the concrete deck. Additionally, fully composite action was assumed between the top flange of the girders and the deck as the deck was cast in place.

5.1.3.3. SFRC-PC

In this concrete deck, the exact dosage of steel fiber and wire mesh were assumed to be used, and nine shear pockets (3 in x 3 in) were modeled to connect the girders and the deck. Partially composite action was assumed between the top flange of the girders and the deck since the deck was precast as shown in Figure 5-4.

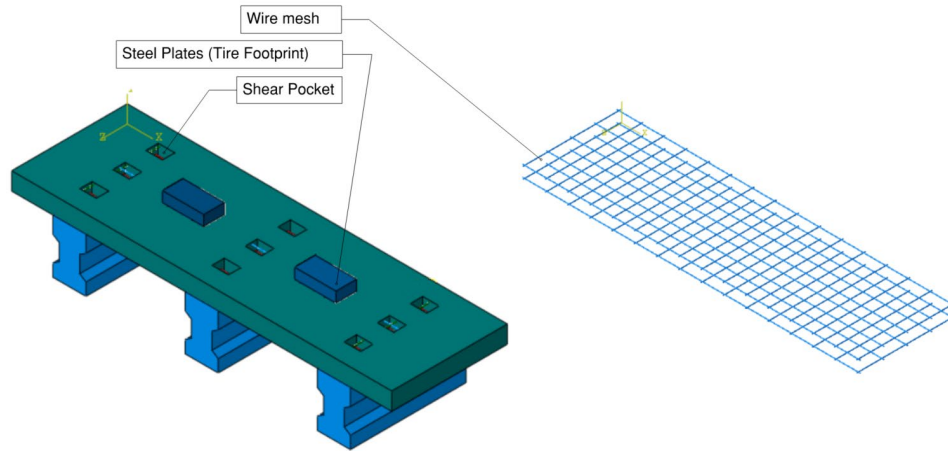


Figure 5 - 4 FE Model of SFRC-PC

5.1.3.4. GFRP

This type of deck was modeled in FE using #3 and #4 GFRP pink bars as the main reinforcement, as mentioned in Table 4-3. These bars were embedded in the concrete deck, and the shear connectors were also embedded in the girders and the concrete deck. Fully composite action was assumed between the top flange of the girders and the deck as the deck was cast in place as shown in Figure 5-5.

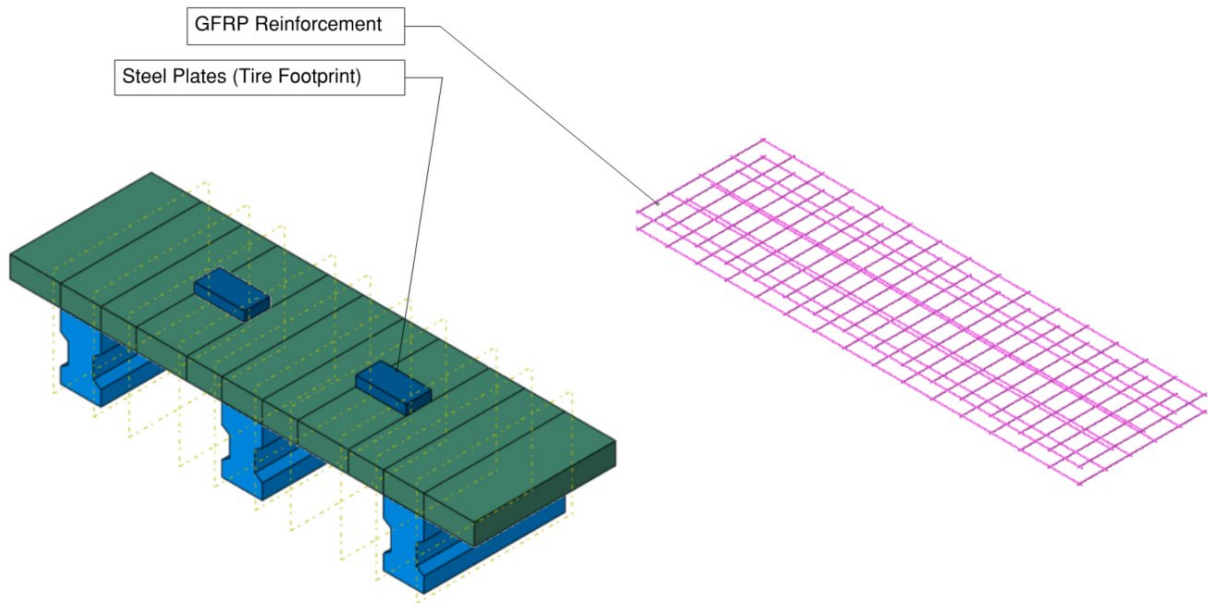


Figure 5 - 5 FE Model of GFRP

5.1.3.5. SFRC-GFRP-CIP

In this deck, (70 lb/cy) of 4D Dramix steel fiber has been used as the main reinforcement. Therefore, (#3 bar, 12-inch by 12-inch) GFRP bars mesh as a distribution reinforcement were embedded in the concrete deck as the supplementary reinforcement. Additionally, fully composite action was assumed between the top flange of the girders and the deck as the deck was cast in place.

5.1.3.6. SFRC-GFRP-PC

In this concrete deck, the exact dosage of steel fiber and GFRP mesh were assumed to be used, and nine shear pockets (3 in x 3 in) were modeled to connect the girders and the deck. Partially composite action was assumed between the top flange of the girders and the deck since the deck was precast as shown in Figure 5-6.

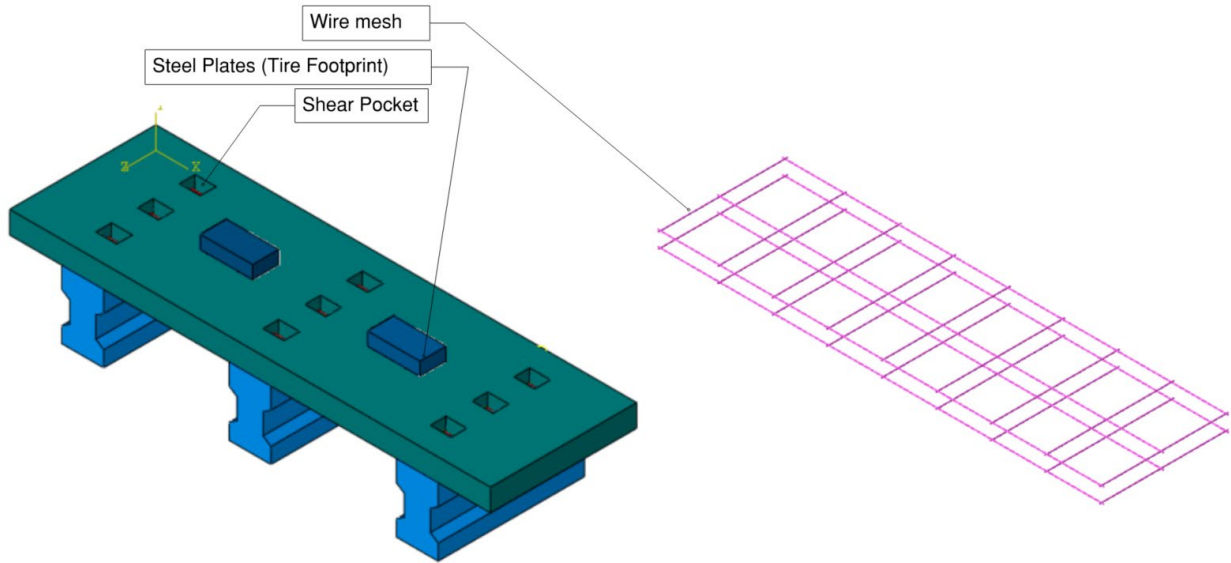


Figure 5 - 6 FE Model of SFRC-GFRP-PC

5.1.4 Concrete and Steel Properties

The concrete standard test is used to determine the compressive strength (f_c') of concrete. This strength is typically classified at 28 days, by which time the desired strength is usually achieved. However, concrete continues to gain strength over time, resulting in improved mechanical characteristics such as tensile strength and modulus of elasticity. Therefore, it is crucial to consider the change in concrete strength in Finite Element (FE) analysis. The AASHTO LRFD (2020) standards do not address these increments, as stated by John Corven in 2016. On the other hand, the Comité euro-international du béton/Federation International La précontrainte (CEB-FIP) Model Code (1990) (FHWA, 2016) provides a relationship that describes the variation in concrete compressive strength over time.

5.2 Material properties

Material properties were fed in the ABAQUS software through entering these properties in the material manager menu for each material, such as plain concrete, SFRC, steel rebar, and GFRP rebar. These materials include density of each material and elasticity like Young's

Modulus and Poisson's Ratio, and plasticity properties.

- Density: each material has its density in lb/ft^3 units as shown in Figure 5-7. According to the lab tests, the density of plain and SFRC concrete were 146.5 lb/ft^3 and 147.8 lb/ft^3 respectively. The steel bars and GFRP bars density were taken as 490 lb/ft^3 and 118 lb/ft^3 respectively.

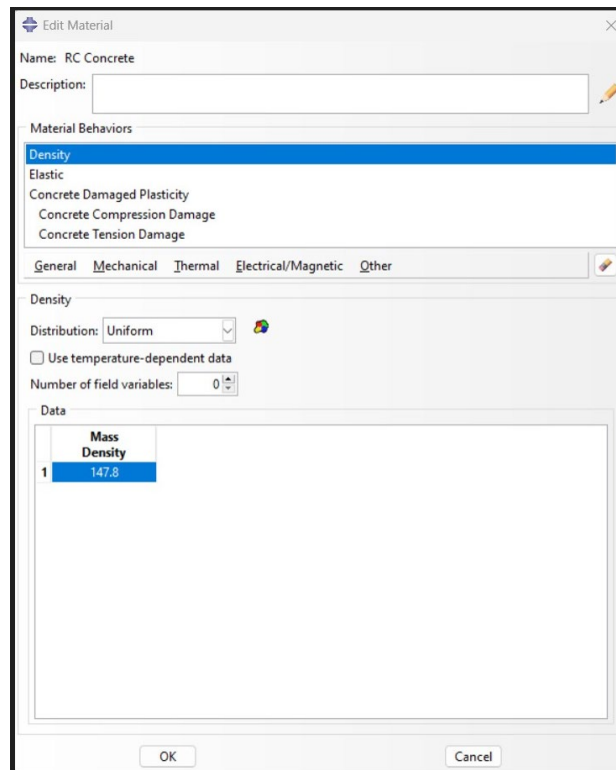


Figure 5 - 7 Menu of Material Density

- Elasticity: when the materials are still in the elastic zone during the applied load. The elasticity of concrete was based on the lab test results listed in Table 5-1. The differences in modulus of elasticity and Poisson's ratio for each material caused the differences in the behavior of the materials in the software as shown in Figure 5-8.

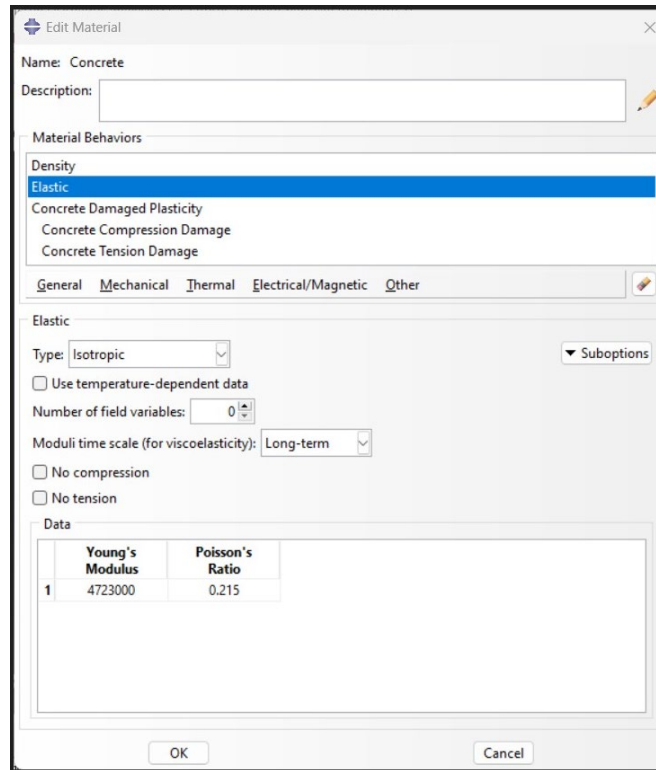


Figure 5 - 8 Menu of Material Elastic Properties

Table 5 - 1 Modulus of Elasticity and Poisson's Ratio of Concrete Decks

Material Type	Modulus of Elasticity (E) (ksi)	Poisson's Ratio (ν)
Plain Concrete	4,169	0.236
SFRC	4,723	0.215
Steel Reinforcement	29,000	0.28
GFRP Reinforcement	6,250	0.33

- Plasticity: when the materials move from the elasticity to the plasticity zone. Different plasticity properties of different types of concrete also entered in the concrete damage plasticity menu, such as concrete dilation angle, eccentricity, the equi-biaxial compressive strength of concrete (f_{b0}) to the uniaxial compressive strength (f_{c0}), the stress intensity factor, and viscosity parameter as shown in Figure 5-9.

- Concrete dilation angle: 30~40
- Eccentricity: 0.1
- f_{b0} / f_{c0} : 1.16
- K : 2/3
- Viscosity parameter: 0.0

Based on the lab compression and tension test results, the concrete compression and tension behavior including the yield stress and the inelastic strain were entered in the compression and tension behavior menu as shown in Figure 5-10 and 5-11. In addition to that, the damage parameter (Equation 5-1) and the inelastic strain for both concrete compression and tension damage also fed in the menu as shown in Figure 5-12 and 5-13.

$$d = 1 - \frac{E_i}{E_0} \quad \text{OR} \quad d = 1 - \frac{\sigma_i}{\sigma_u} \quad \text{Equation 5-1}$$

Where:

d is the damage factor (compression or tension).

E_i is the modulus of elasticity.

E_0 is the unloading stiffness at any strain.

σ_i is the strength at any point.

σ_u is the ultimate strength (compression or tension).

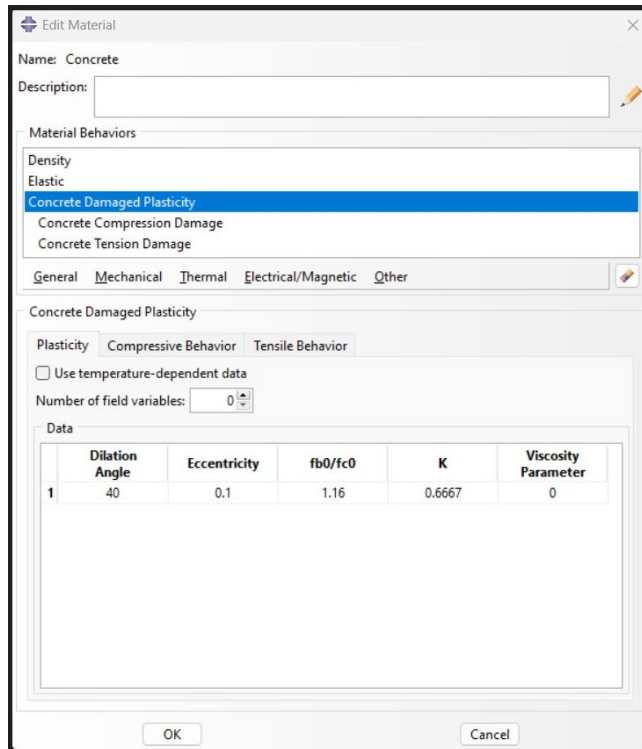


Figure 5 - 9 Concrete Damage Plasticity Menu

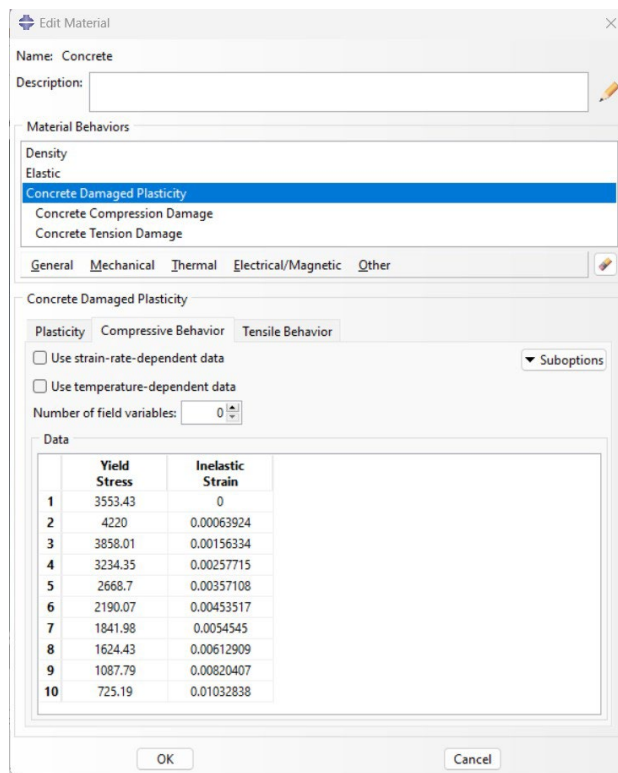


Figure 5 - 10 Compressive Behavior Menu

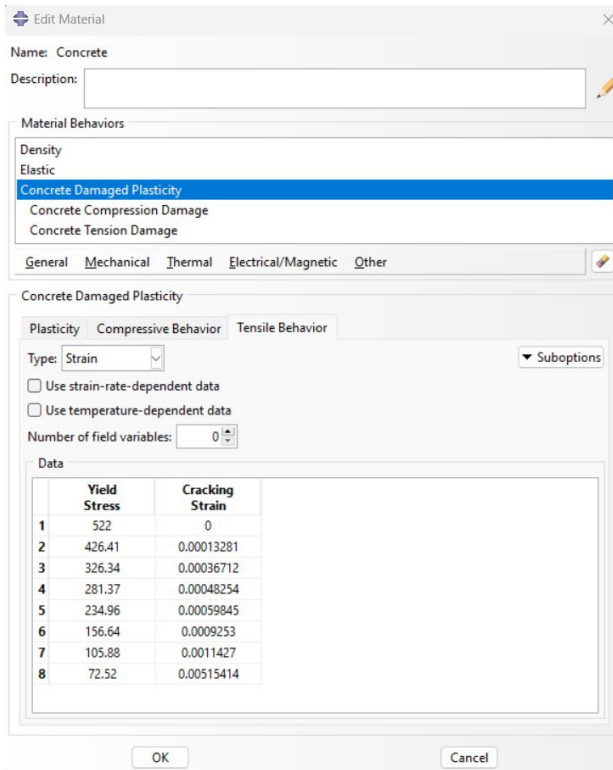


Figure 5 - 11 Tensile Behavior Menu

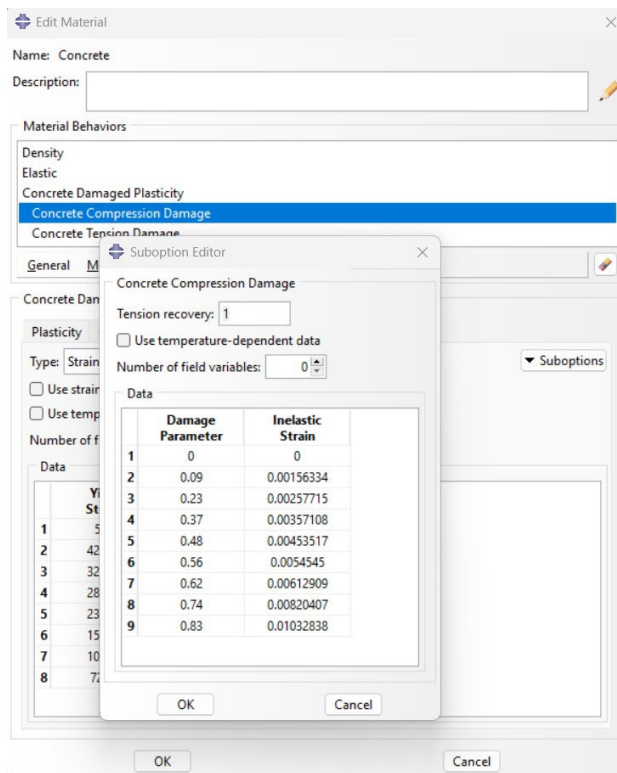


Figure 5 - 12 Concrete Compression Damage Menu

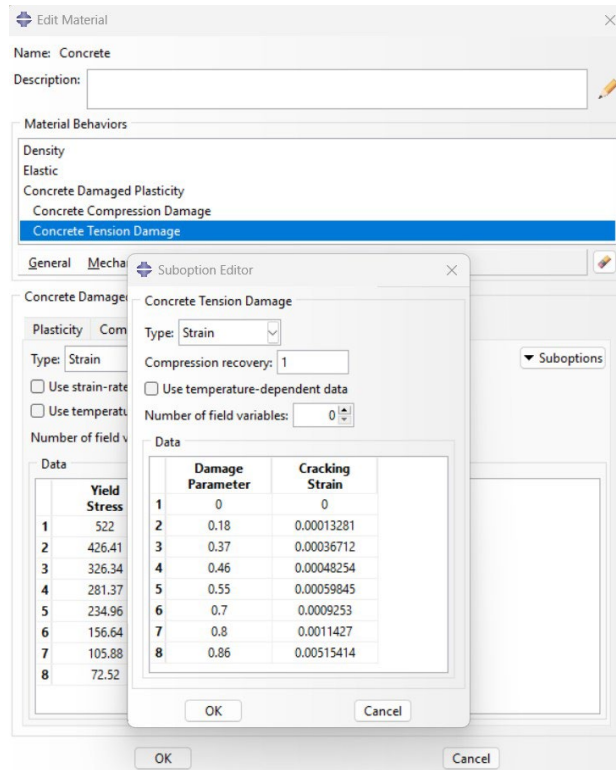


Figure 5 - 13 Concrete Tension Damage Menu

5.3 Boundary Conditions

Boundary conditions are crucial in the FEM analysis of concrete deck models, as illustrated in Figure 5-14. Specifically, the deck, girders, and loading plates are all subject to location-based boundary conditions. To prevent movement in the x, y, and z directions, the girders are considered fixed, and no rotations are allowed in these directions. The composite action between the deck and the girders is considered, with 100% for cast-in-place decks and 80% for precast decks.

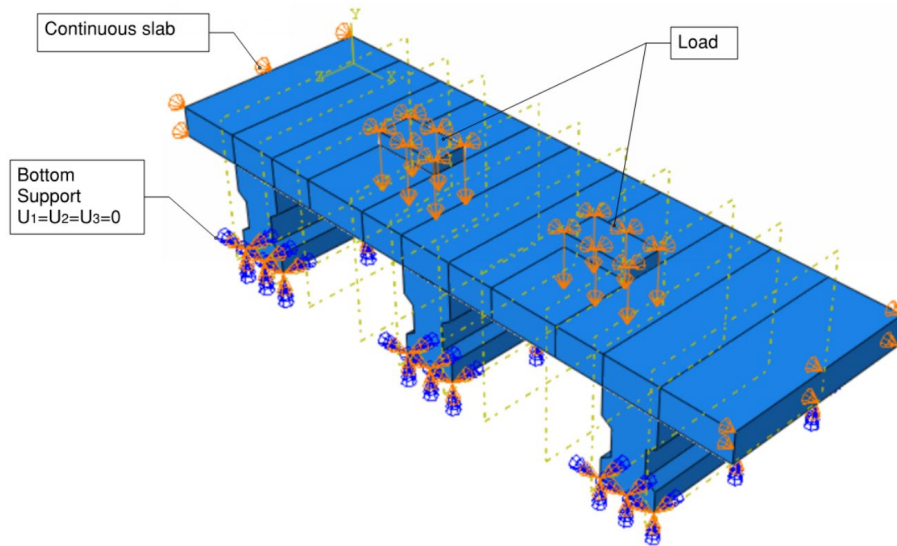


Figure 5 - 14 Boundary conditions of numerical simulation

5.4 Interaction

The process of interaction serves to establish how various components work together, including factors such as friction between loading plates and the concrete deck's surface, composite action between the precast girders and the deck, bonding between the reinforcement and the concrete, and composite action between the shear connectors and the deck. This enables the model to learn how to effectively manage these surfaces.

Once all the necessary information has been inputted into the model, the simulation can proceed to run the job and analyze the results. These results include the deflection, stress components, plastic strain component, compressive damage, tensile damage, and other relevant components, as depicted in Figures 5-15 and 5-16. The results provided represent the current model, which includes dimensions, material properties, interactions between parts, and boundary conditions. Furthermore, the results were highly accurate, closely resembling the experiment results, which indicates that the simulation of the model was almost identical

to the real-life specimens.

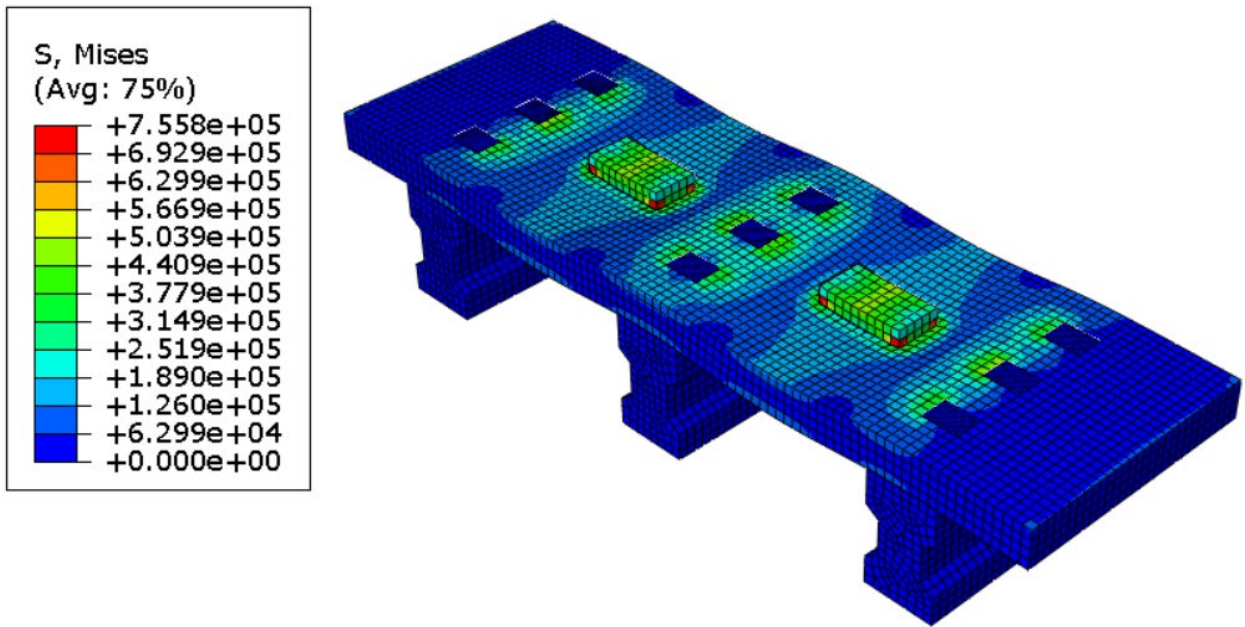


Figure 5 - 15 Stresses shape / location

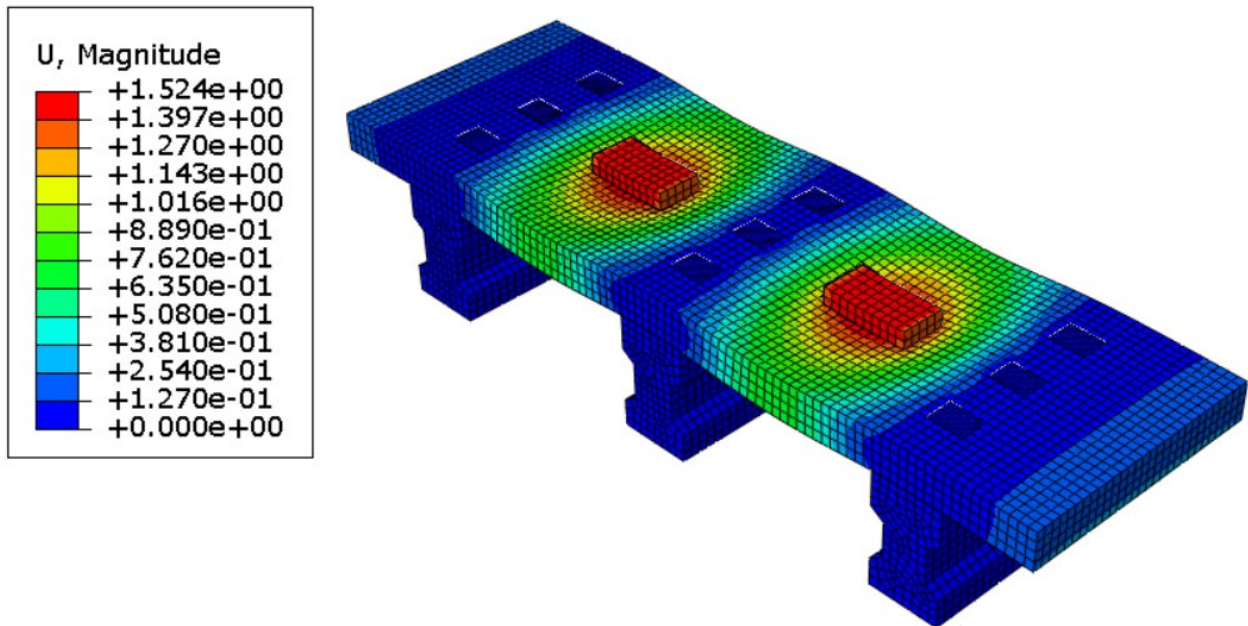


Figure 5 - 16 Deflection shape / location

5.5 Results

After building and verifying the accuracy of the model, the next step is to create curves for all the components. To do this, XY Data can be created to generate a stress-strain curve or any other curves for any node in the model by selecting the desired output field such as stress, strain, load, deflection, etc. Once the required fields have been selected, the plot of the XY curve can be generated as demonstrated in Figure 5-17.

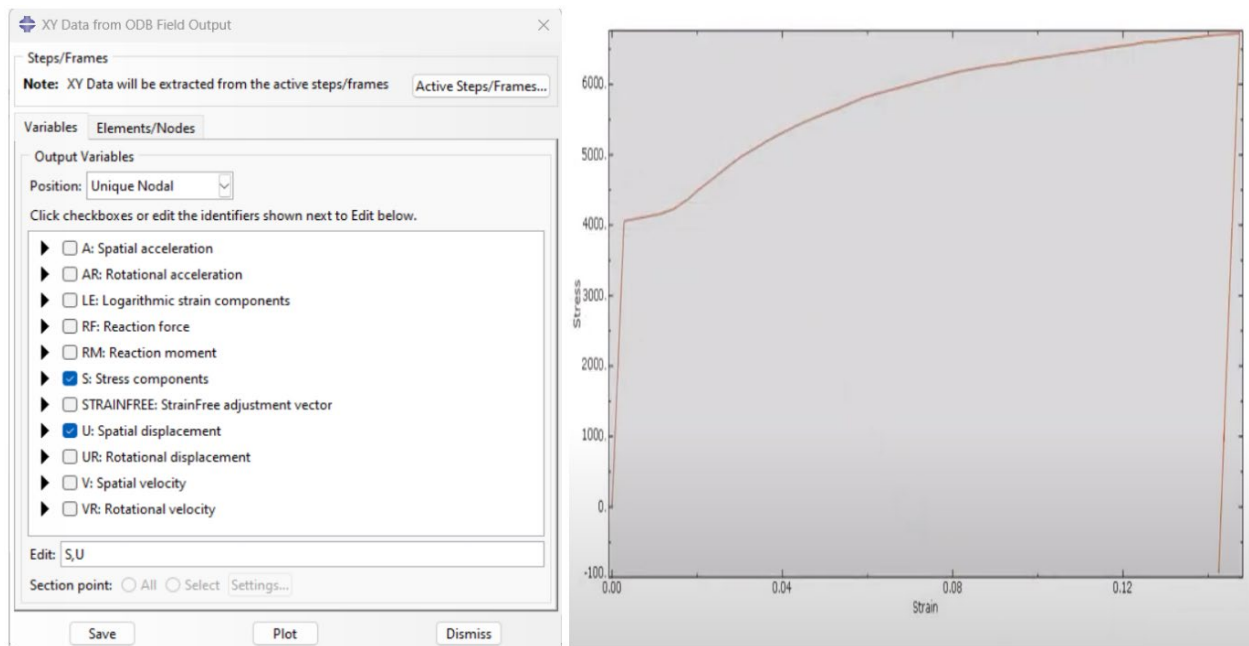


Figure 5 - 17 XY Data Field Output and S-S Curve

5.6 Conclusions of the FE Modeling

FE models are valuable tools for analyzing samples and predicting results for different shapes or dimensions. For example, in a bending study or any other concrete properties study, properties such as modulus of elasticity, Poisson's ratio, concrete damage plasticity, concrete compressive damage, and concrete tensile damage must be conducted. Additionally, different types of reinforcement can be used, taking into consideration the properties of the reinforcement, diameter,

and interaction between the reinforcement and the concrete. In other words, the FE model can predict the results as long as the properties are input correctly and all other required boundaries, meshing, and interactions are input correctly as well.

CHAPTER 6

RESULTS AND DISCUSSIONS OF SFRC-CIP & SFRC-PC VS. RC

6.1 Results Presentation

The test recorded all the outcomes, including the values of load-displacement data ($P-\Delta$), maximum loads, stresses, strains, initial cracks, and crack width. The results were collected from six concrete decks, with each pair of decks being reinforced with different types of reinforcement, as illustrated in Table 4-1.

Service and ultimate load were recorded. In order to record the service load, a concrete structure must remain functional and serve its intended purpose for its entire lifespan. Any excessive deflection should not hinder the structure's function or be aesthetically unappealing. Additionally, cracks should neither be unsightly nor wide enough to cause durability issues. In designing for serviceability limit states, it is crucial to predict the instantaneous and time-dependent deformation of the structure accurately. However, concrete's non-linear behavior caused by cracking, tension stiffening, creep, and shrinkage makes this task complicated. (Eurocode 2004; Motter 2009, and Gilbert 2011).

The results analysis was divided into two groups. The first group discusses the results of the concrete decks that were reinforced with steel fiber as the main reinforcement and steel wire mesh as supplementary reinforcement, in comparison with reference concrete decks that were reinforced with steel bars according to the AASHTO LRFD. The second group discusses the results of concrete decks that were reinforced with steel fiber as the main reinforcement and GFRP mesh as supplementary reinforcement, in comparison with reference concrete decks that were reinforced with GFRP bars. This chapter discusses the results outcome of the first group which are SFRC-CIP and SFRC-PC decks to be compared to RC decks.

6.1.1 Reference RC Concrete Decks

Two concrete decks were cast-in-place on top of three precast concrete girders. Decks designed per the AASHTO LRFD method. #3 and #4 reinforcement bars were used as the main and distribution reinforcement. Concrete decks were tested to be the reference for comparison with the other concrete decks. As shown in Figures 4-4 and 4-5.

1- Load – Displacement Curves

Load-displacement ($P-\Delta$) values were measured in this study for all specimens using load cells and LVDT devices. The load cell recorded the applied load in kips, while the deflection was recorded in inches at the mid-span of each spacing between girders of all decks. In this study, load-displacement ($P-\Delta$) values were measured for all specimens using load cells and LVDT devices. The load cell accurately recorded the applied load in kips, while the deflection was recorded in inches at the mid-span of each spacing between girders of all decks. The RC decks' first crack was recorded at an average service load of 41 kips with a deflection of (0.037 in), while the average ultimate load was (51 kips) with a deflection of (0.052) in. The maximum deflection at the failure was (0.35 in). Moreover, the area under the average load-deflection curve equals (10.5 area units). Figures 6-1 and 6-2 show the load-deflection curves of RC-1 and RC-2 specimens, respectively.

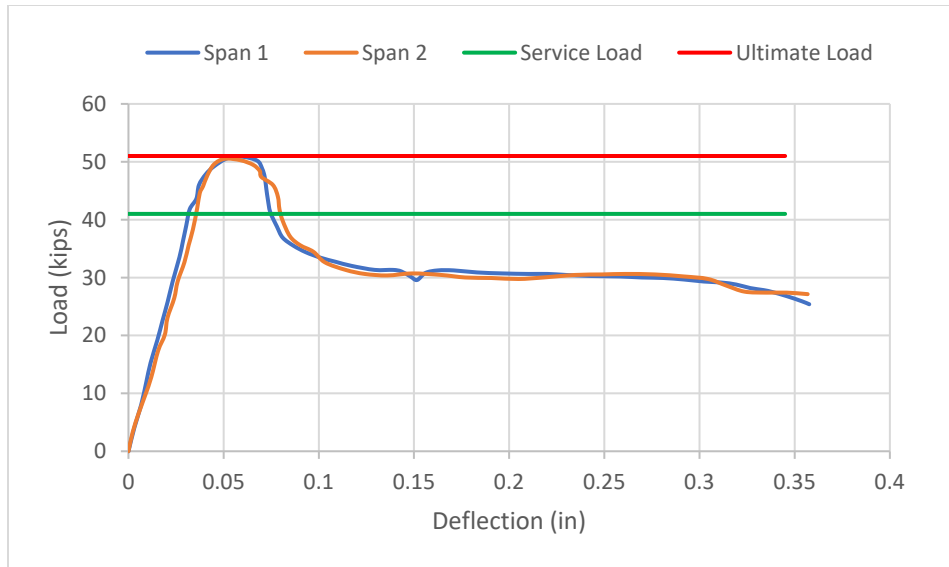


Figure 6 - 1 Load-Displacement Curve of RC-1 Deck

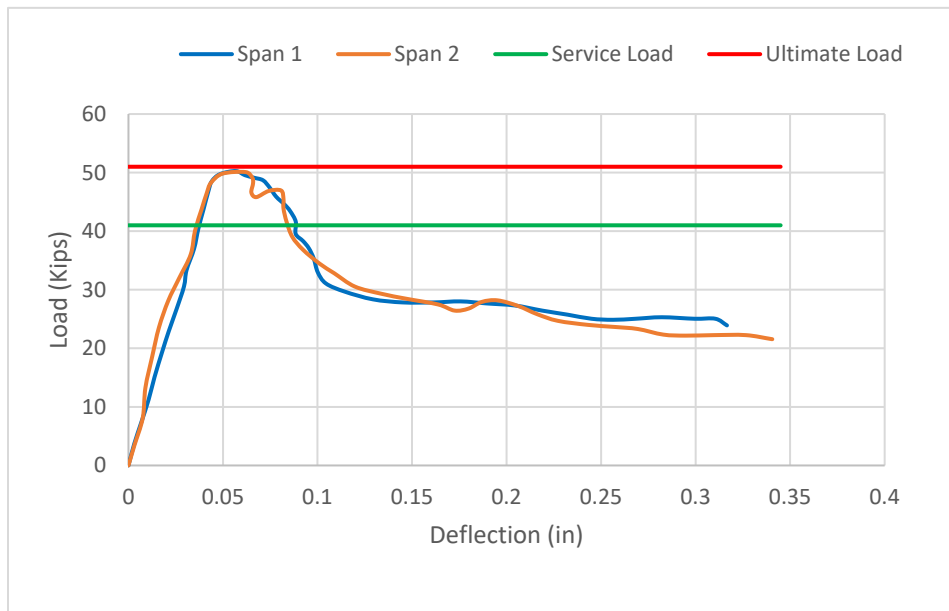


Figure 6 - 2 Load-Displacement Curve of RC-2 Deck

2- Stress-Strain Curves

Load cells and concrete strain gauges were used to measure stress-strain values. Strain gauges were installed at the bottom of the mid-span spacing between the girders of all decks. At a service stress of (3389 psi), the average strain was (0.0009 in/in), while at an ultimate stress

of (4011 psi), the average strain was (0.0016 in/in). The maximum strain before failure was recorded at (0.0032 in/in). Additionally, the area under the average stress-strain curve is equal to (9.7 area units). Figures 6-3 and 6-4 show the stress-strain curves of RC-1 and RC-2 specimens, respectively. Figure 6-5 shows the failure shape of the RC specimen.

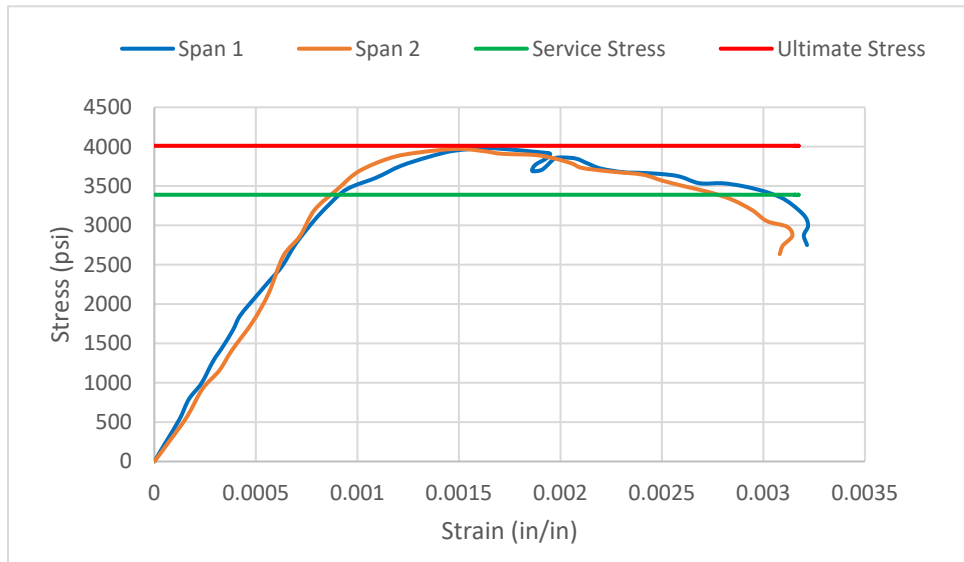


Figure 6 - 3 Stress-Strain Curve of RC-1 Deck

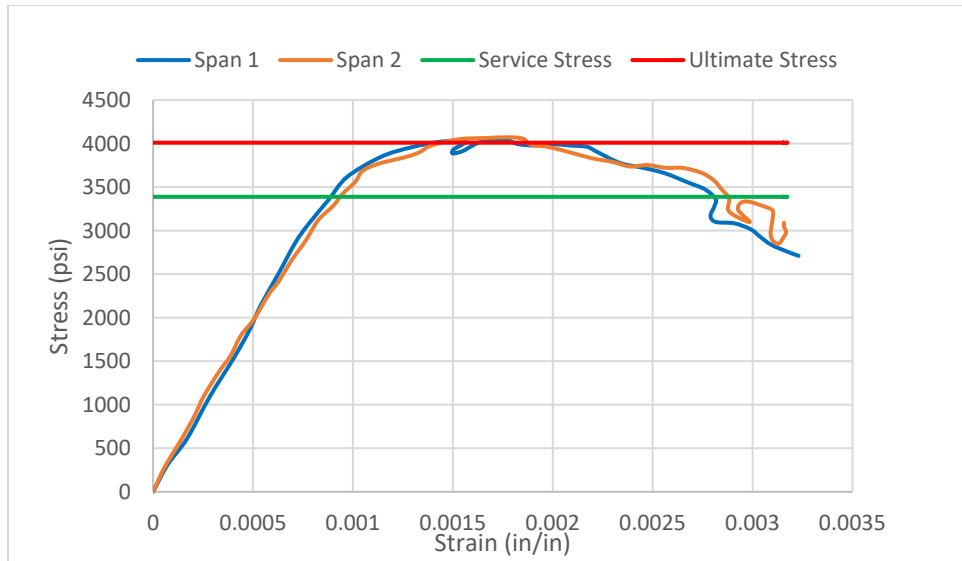


Figure 6 - 4 Stress-Strain Curve of RC-2 Deck



Figure 6 - 5 RC Concrete Deck Specimen

6.1.2 SFRC-CIP Concrete Decks

Two concrete decks were cast-in-place on top of three precast concrete girders. (70 lb/cy) steel fiber was the main reinforcement of these specimens and (6 x 6 x ¼ in) wire mesh supplementary reinforcement.

1- Load – Displacement Curves

The SFRC-CIP decks were tested, and the first crack appeared at an average service load of (47 kips), with a deflection of (0.039 in). The average ultimate load was (57 kips), with a deflection of (0.075 in). The maximum deflection at the failure was (0.42 in). The area under the average load-deflection curve was (17.0 area units). Figures 6-6 and 6-7 show the load-deflection curves of SFRC-CIP-1 and SFRC-CIP-2 specimens, respectively.

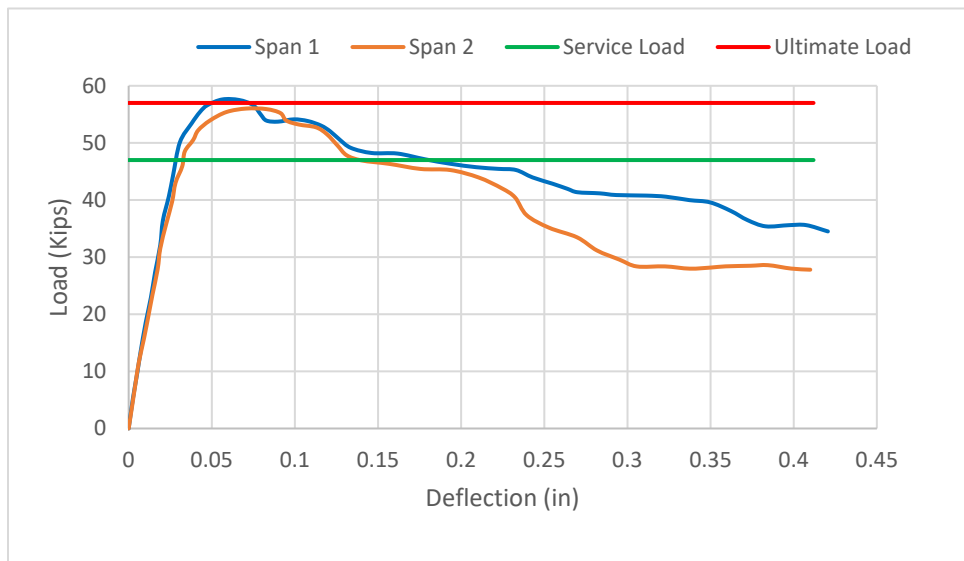


Figure 6 - 6 Load-Displacement Curve of SFRC-CIP-1 Deck

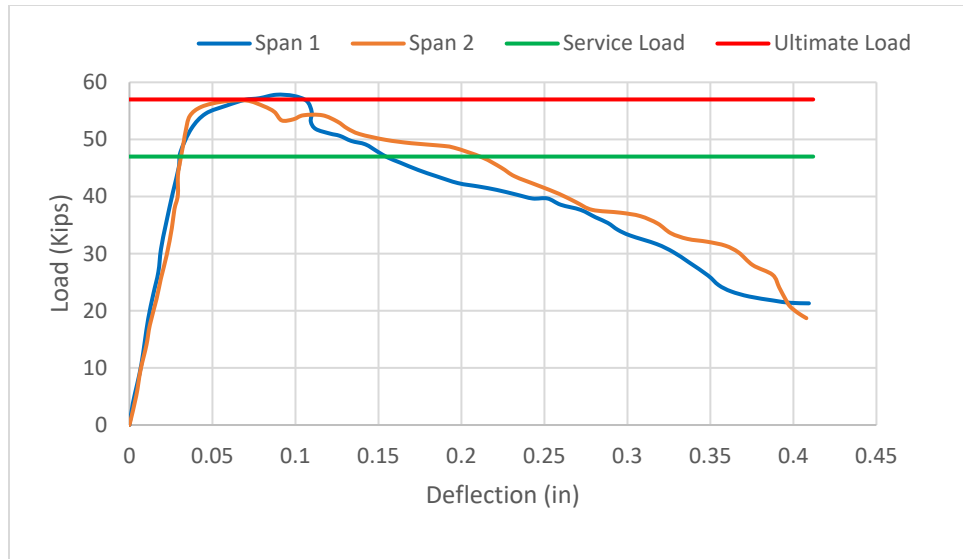


Figure 6 - 7 Load-Displacement Curve of SFRC-CIP-2 Deck

2- Stress-Strain Curves

At a service stress of (3646 psi), the average strain was (0.0008 in/in), while at an ultimate stress of (4631 psi), the average strain was (0.0018 in/in). The maximum strain before failure was recorded at (0.0044in/in). Additionally, the area under the average stress-strain curve equals (16.9 area units). Figures 6-8 and 6-9 show the stress-strain curves of SFRC-CIP-1 and SFRC-CIP-2 specimens, respectively. Figure 6-10 shows the failure shape of the SFRC-CIP specimen.

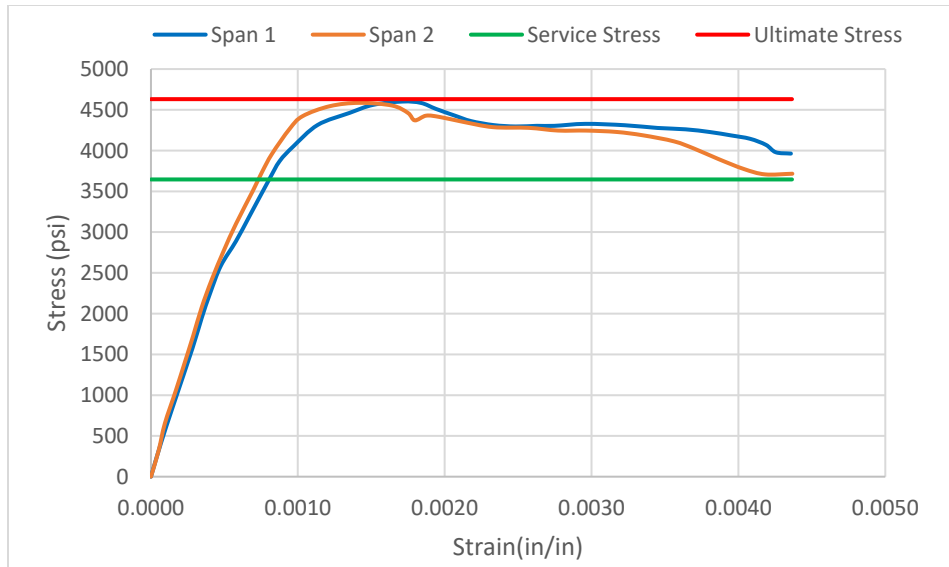


Figure 6 - 8 Stress-Strain Curve of SFRC-CIP-1 Deck

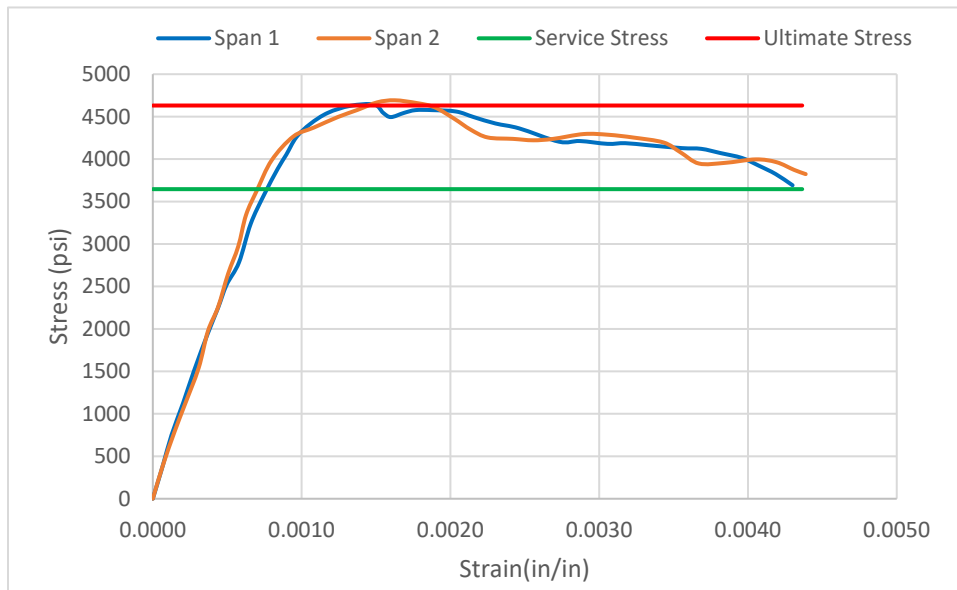


Figure 6 - 9 Stress-Strain Curve of SFRC-CIP-2 Deck



Figure 6 - 10 SFRC-CIP Concrete Deck Specimen

6.1.3 SFRC-PC Concrete Decks

Two precast concrete decks were joined by three precast concrete girders in the shear pocket and connectors. These specimens were primarily reinforced with (70 lb/cy) of steel fiber and supplemented with wire mesh measuring (6 x 6 x ¼ in).

1- Load – Displacement Curves

Through testing, it was determined that at an average service load of (46 kips), the SFRC-PC decks showed the first sign of cracking, with a deflection of (0.038 in). The average ultimate load was (57 kips), with a deflection of (0.080 in). At the point of failure, the maximum deflection was (0.43 in). Additionally, the area under the average load-deflection curve was measured to be (17.3 area units). Figures 6-11 and 6-12 depict the load-deflection curves of SFRC-PC-1 and SFRC-PC-2 specimens, respectively.

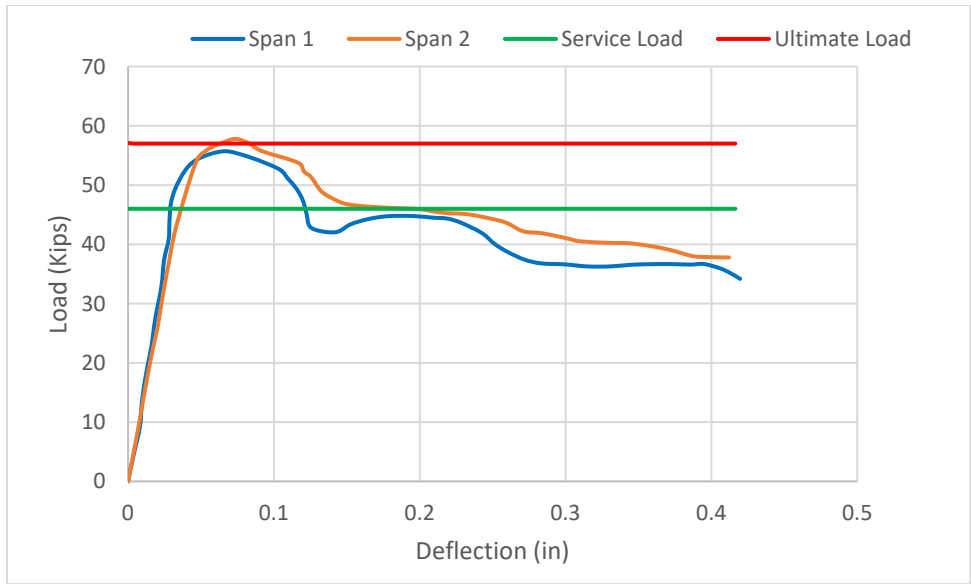


Figure 6 - 11 Load-Displacement Curve of SFRC-PC-1 Deck

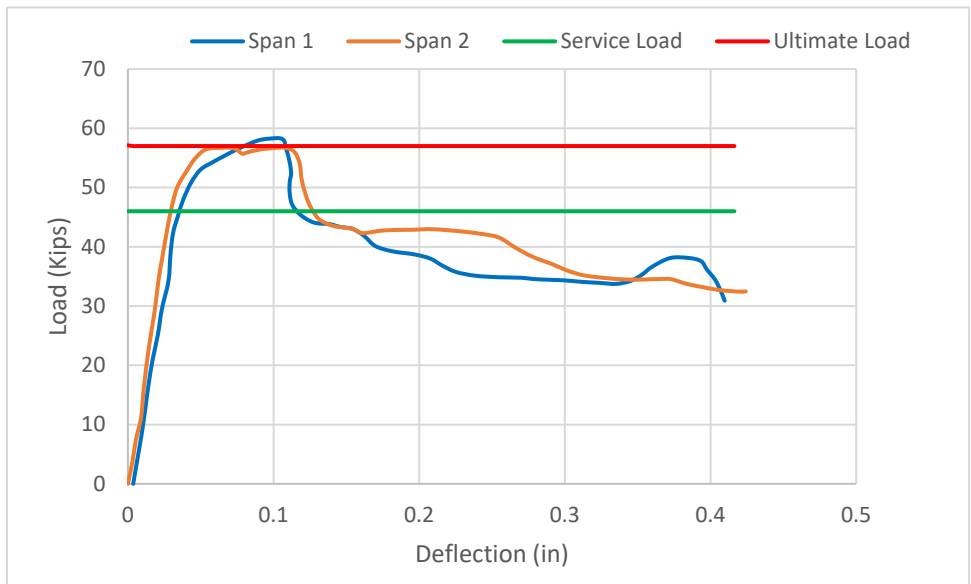


Figure 6 - 12 Load-Displacement Curve of SFRC-PC-2 Deck

2- Stress-Strain Curves

When subjected to a service stress of (3560 psi), the specimens exhibited an average strain of (0.0008 in/in). As the stress increased to an ultimate stress of (4674 psi), the average strain also increased to (0.0018 in/in). The maximum strain observed before failure occurred at (0.0044in/in). Moreover, the area under the average stress-strain curve was calculated to be (16.1 area units). Figures 6-13 and 6-14 depict the stress-strain curves of SFRC-PC-1 and SFRC-PC-2 specimens, respectively. Figure 6-15 shows the failure shape of the SFRC-PC specimen.

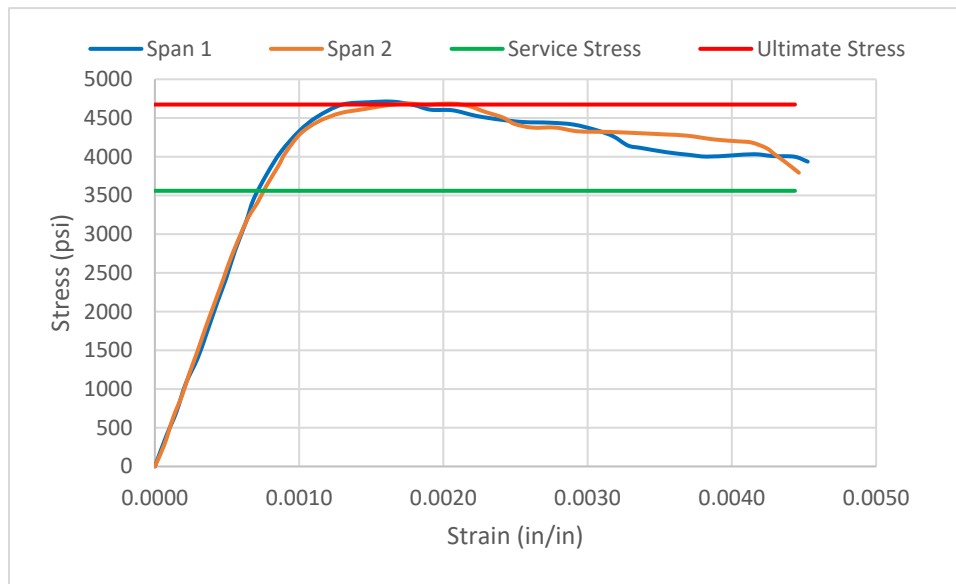


Figure 6 - 13 Stress-Strain Curve of SFRC-PC-1 Deck

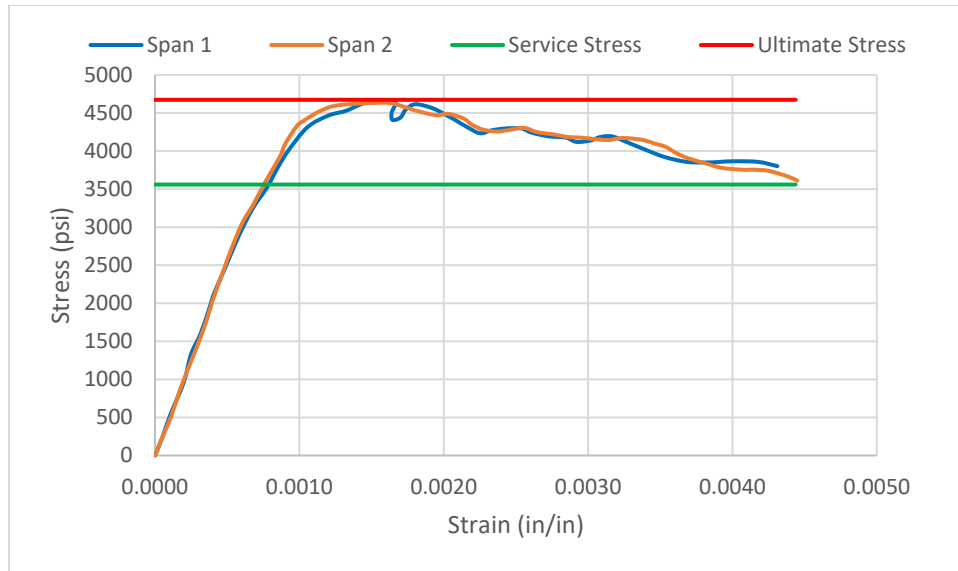


Figure 6 - 14 Stress-Strain Curve of SFRC-PC-2 Deck



Figure 6 - 15 SFRC-PC Concrete Deck Specimen

6.2 Results Comparison

In order to find out the increases in load capacity, stiffness, stress, energy, etc., the comparison measured (% increasing rate) was estimated by Equation 1.

$$\% \text{ Increasing} = \frac{X_S - X_r}{X_r} * 100$$

Equation (6-1)

Where:

X_r is the value of load capacity, stiffness, stress, energy, etc., of the reference specimens.

X_s is the value of load capacity, stiffness, stress, energy, etc., of the SFRC or GFRP specimens.

There are some different ways to calculate the ductility index, (Spadea et al. 1997) suggested an equation (Equation 6-2) to compute the energy ratio (ductility index μ_E) for the concrete decks, as shown in Figure 6-16.

$$\mu_E = \frac{E_{tot}}{E_{75\% P_{Ult}}} \quad \text{Equation (6-2)}$$

where:

μ_E is the ductility index

E_{tot} is the energy at ultimate load.

$E_{75\% P_{Ult}}$ is the energy at 75% of the ultimate load.

The ductility index was calculated from the load-displacement curves by applying Spadea's equation. The (μ_E) values of SFRC-CIP and SFRC-PC decks were measured and compared with RC decks, and the same for SFRC-GFRP-CIP and SFRC-GFRP-PC were compared with the GFRP reference decks.

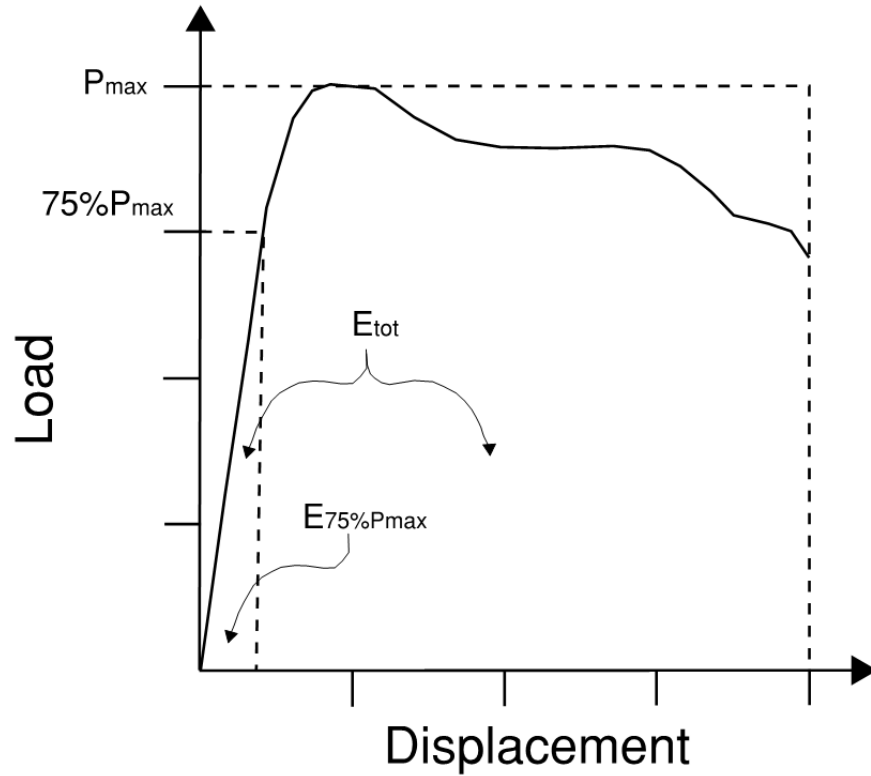


Figure 6 - 16 Definition of the Ductility Index Estimation Curve

6.2.1 Load – Displacement Characteristics

Adding steel fiber as the main reinforcement in concrete had a noticeable impact on its strength and deflection. Data shows that RC decks had an average service load of (41 kips), whereas SFRC-CIP and SFRC-PC decks had an average service load of (47 kips) and (46 kips) respectively. Similarly, the average ultimate load for RC decks was (51 kips), while the SFRC-CIP and SFRC-PC decks had an average ultimate load of (57 kips). These numbers demonstrate a (14.6%) and (12.2%) increase in the service load capacity and a (11.8%) increase in the ultimate load capacity for both SFRC-CIP and SFRC-PC decks. In addition, the deflection at service load remains consistent across all decks, but there is a notable increase

in deflection at ultimate load when applied to RC, SFRC-CIP, and SFRC-PC decks, ranging from (0.052 in), (0.075 in), to (0.080 in). Interestingly, the maximum deflection prior to failure for SFRC-CIP and SFRC-PC decks was (0.42 in) and (0.43 in) respectively, exceeding the (0.35 in) deflection of RC decks. This indicates that the steel fiber influences increasing the deflection prior to failure. Table 6-1 shows the RC, SFRC-CIP, and SFRC-PC decks load-displacement values.

Table 6 - 1 Load-Displacements of RC, SFRC-CIP, and SFRC-PC Decks

Deck ID	P _{service} kips	%P _{service} Increases	P _{Ult} kips	%P _{Ult} Increase	Δ at P _{service} in	Δ at P _{Ult} in	Δ _{Max} in
RC	41	14.6	51	11.8	0.037	0.052	0.35
SFRC-CIP	47		57		0.039	0.075	0.42
SFRC-PC	46	12.2	57	11.8	0.038	0.080	0.43

6.2.2 Ductility Index

The ductility index was calculated from the load-displacement curves by applying Spadea’s equation (Equation 6-2). Table 6-2 provides values for the total energy at the ultimate load and at (75%) of the ultimate load. The results indicate that the ductility index of the SFRC-CIP and SFRC-PC decks exceeded that of the RC decks by (56.6%) and (33.3%) respectively. This suggests that incorporating steel fiber reinforcement as the main reinforcement in the concrete decks significantly improved the concrete ductility. This was evident in the load-deflection curves, where a larger area under the curve indicates that the specimens absorbed more energy during testing.

Table 6 – 2 Energy Absorbed, and Ductility Index of RC, SFRC-CIP, and SFRC-PC Decks

Deck ID	P_{Ult} kips	E_{tot} Kip-in	$E_{75\%P_{Ult}}$ Kip-in	$\%E_{tot}$ Increasing	μ_E	$\% \mu_E$ Increasing
RC	51	10.5	0.82	61.9 64.8	12.9	56.6 33.3
SFRC-CIP	57	17.0	0.84		20.2	
SFRC-PC	57	17.3	1.0		17.2	

6.2.3 Stress-Strain Characteristics

It was observed that utilizing steel fibers improved the strength of concrete, including its resistance to cracking, compressive strength, and tensile strength. The use of hooked-end steel fibers improved the strength compared to conventional reinforcement. The average service stress of reinforced concrete RC decks was (3389 psi) while the average service stress of the SFRC-CIP and SFRC-PC decks was (3646 psi) and (3560 psi), that is a (7.6%) and (5.1%) increases in service strength, respectively. Similarly, the average ultimate stress of RC decks was (4011 psi) while that of SFRC-CIP and SFRC-PC decks was (4631 psi) and (4674 psi) meaning the improvement in ultimate strength are (15.5%) and (16.5%), respectively. Moreover, the area under the SFRC-CIP and SFRC-PC curves is larger than the area of the RC curve by (74.2%) and (65.9%), respectively (Table 6-3). This means the energy has been absorbed and carried by the decks since the SFRC-CIP and SFRC-PC decks behaved as more ductile material. It was able to deflect and absorb more energy before failure.

Table 6 - 3 Stress-Strain of RC, SFRC-CIP, and SFRC-PC Decks

Deck ID	Stress _{service} psi	$\%Stress_{service}$ Increases	Stress _{ult} psi	$\% Stress_{ult}$ Increases	Strain at Stress _{service}	Strain at Stress _{ult}	Area Under the Curve	$\%Area$ increases
RC	3389	7.6 5.1	4011	15.5 16.5	0.0009	0.0016	9.7	74.2 65.9
SFRC-CIP	3646		4631		0.0008	0.0018	16.9	
SFRC-PC	3560		4674		0.0008	0.0018	16.1	

6.2.4 Crack Width

It was also noticed that SFRC-CIP and SFRC-PC decks exhibited more ductile behavior than

the RC decks. Thus, the main first cracks in SFRC-CIP and SFRC-PC decks have arisen after the RC decks. During loading, crack progress was recorded for all loading steps' a specific crack was identified, and its width was measured in all specimens. The main cracks were located at the bottom of the mid spans of each deck (for the positive moment) and at the top of the deck near the edge of the girders (for the negative moment) (load vs. crack width curve shown in Figure 6-17), Furthermore, as loading continued, the crack started appearing at a load of (35 kips) and (37 kips) for SFRC-CIP and SFRC-PC decks, respectively, while it started appearing at a load of (29 kips) for RC decks. Moreover, the crack width in SFRC-CIP decks reached a maximum of (0.19 in) and (0.20 in) for SFRC-PC, with the maximum crack width being (0.22 inch) on the RC decks. Based on the experimental work results of this study, utilized steel fibers in the concrete mixture had a substantial effect on resisting crack initiation and growth; steel fibers improved concrete tensile strength, thus minimized the crack maximum width by approximately 14% for both SFRC-CIP and SFRC-PC decks. Figure 6-18 shows the failure shape of RC, SFRC-CIP, and SFRC-PC Decks specimens (group 1).

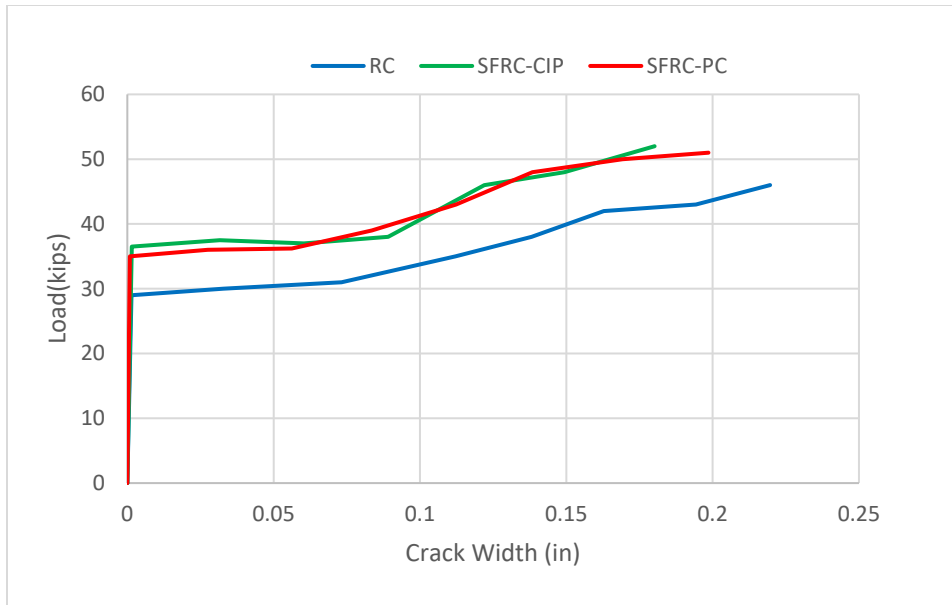


Figure 6 - 17 Crack Width Curves of RC, SFRC-CIP, SFRC-PC

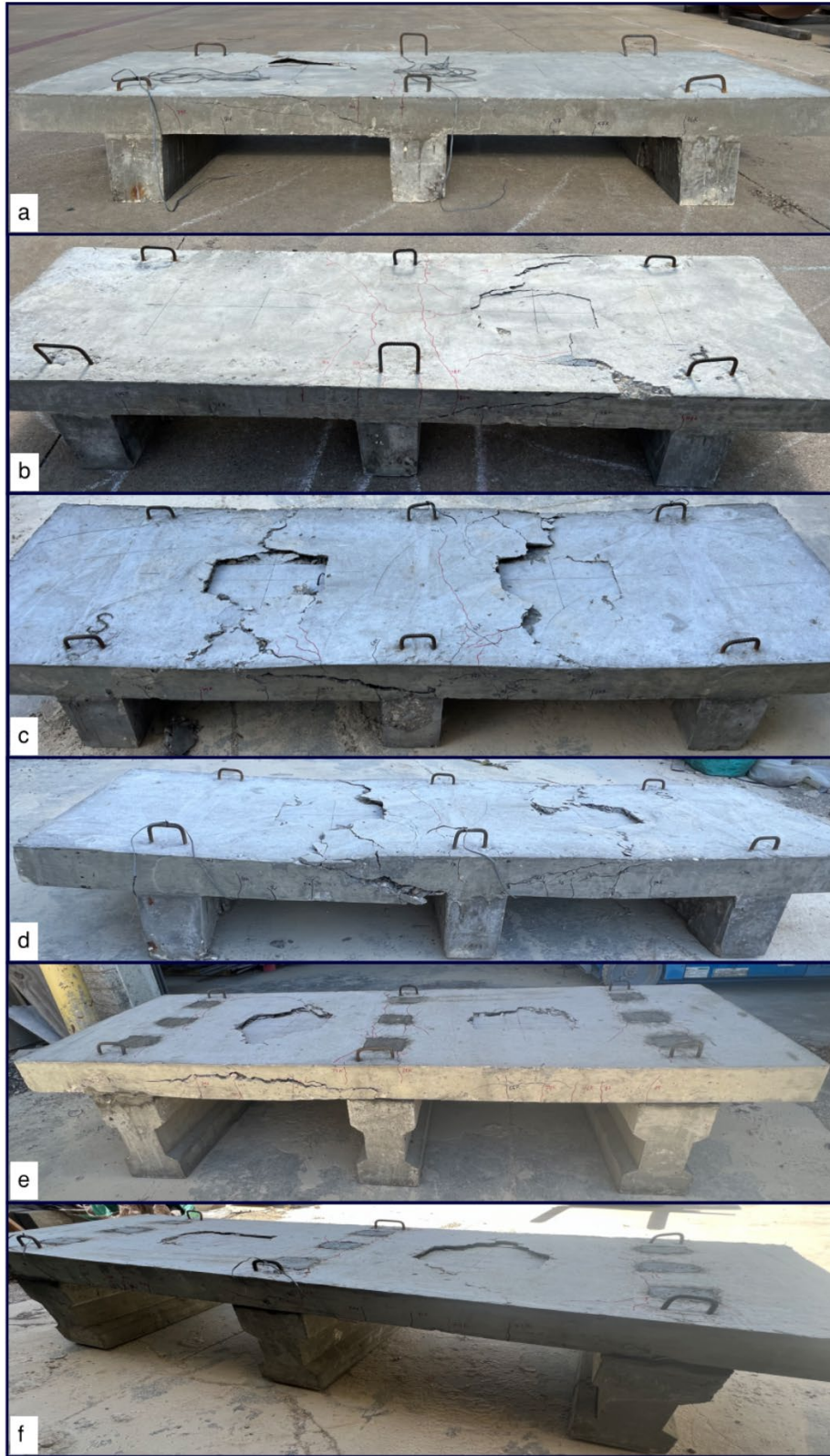


Figure 6 - 18 Concrete Specimens Failure, (a, b) RC; (c, d) SFRC-CIP; (e, f): SFRC-PC

CHAPTER 7

RESULTS AND DISCUSSIONS OF SFRC-GFRP-CIP & SFRC-GFRP-PC VS. GFRP

7.1 Results Presentation

Similar to the previous concrete deck discussed in Chapter 6, the experiment documented all the findings, encompassing the load-displacement data ($P-\Delta$), maximum loads, stresses, strains, initial cracks, and crack width. The data was gathered from six concrete decks, with each set of decks reinforced with distinct types of reinforcement, as depicted in Table 4-1.

This chapter discusses the results outcome of the second group, which are SFRC-GFRP-CIP and SFRC-GFRP-PC decks to be compared to GFRP decks.

7.1.1 Reference GFRP

Two cast-in-place concrete decks were constructed on three precast concrete girders, designed according to the AASHTO LRFD and ACI-440 codes. The main and distribution reinforcement consisted of #3 and #4 GFRP. These decks were then tested and used as a reference for comparison with other concrete decks, as illustrated in Figures 4-10 and 4-11.

1- Load – Displacement Curves

After testing GFRP decks, the initial crack was detected at an average service load of (39 kips) accompanied by a deflection of (0.03 in). The mean ultimate load was (51 kips), with a deflection of (0.15 in). At the point of failure, the maximum deflection was (0.46 in). The area under the average load-deflection curve was (18.8 area units). Figures 7-1 and 7-2 display the load-deflection curves of GFRP-1 and GFRP-2 specimens, respectively.

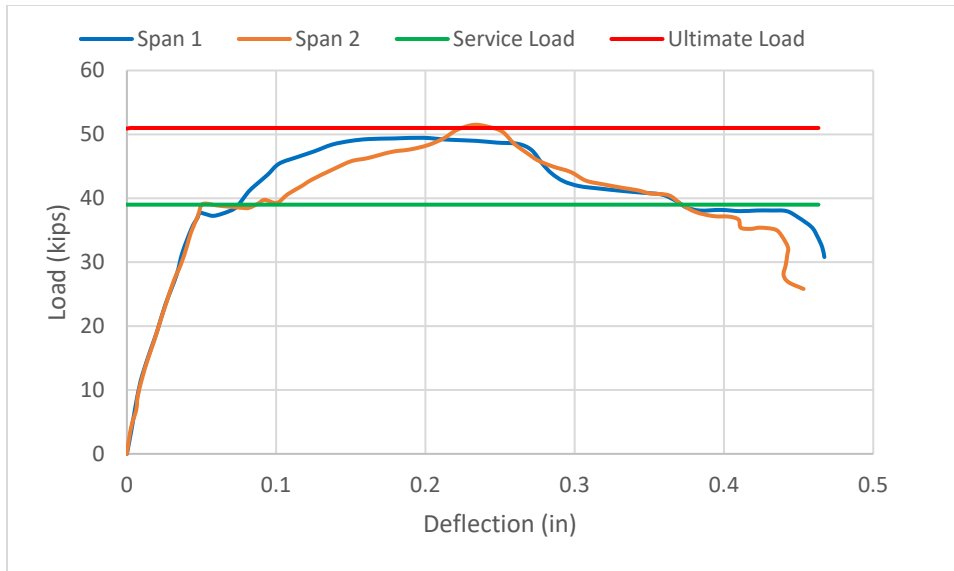


Figure 7 - 1 Load-Displacement Curve of GFRP-1 Deck

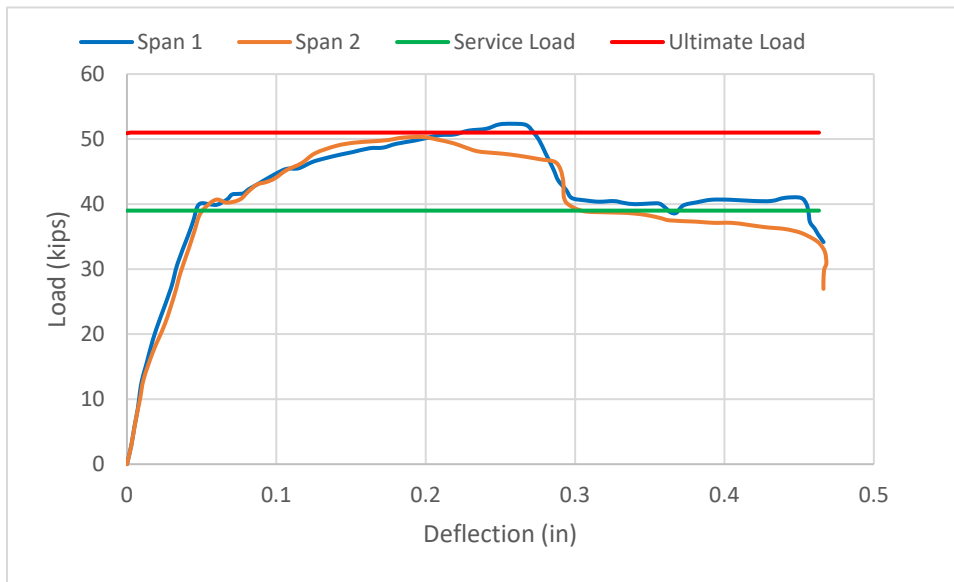


Figure 7 - 2 Load-Displacement Curve of GFRP-2 Deck

2- Stress-Strain Curves

Upon being subjected to a service stress of (3120 psi), the specimens displayed an average

strain of (0.0007 in/in). As the stress climbed to an ultimate value of (4081 psi), the average strain also rose to (0.0013 in/in). The highest strain recorded before failure was at (0.0043 in/in). Furthermore, the area below the average stress-strain curve was determined to be (13.5 area units). Figures 7-3 and 7-4 illustrate the stress-strain curves of GFRP-1 and GFRP-2 specimens, respectively. Figure 7-5 shows the failure shape of the GFRP specimen.

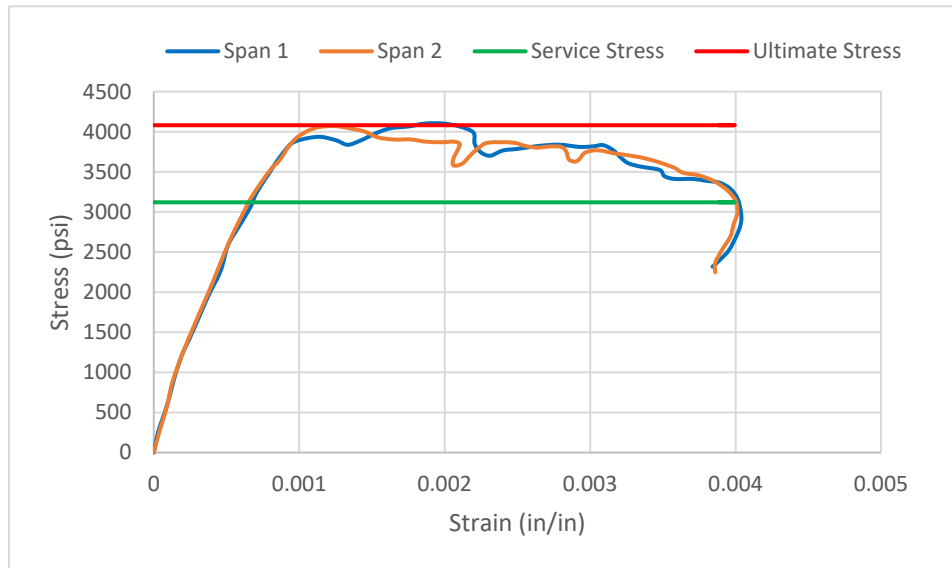


Figure 7 - 3 Stress-Strain Curve of GFRP-1 Deck

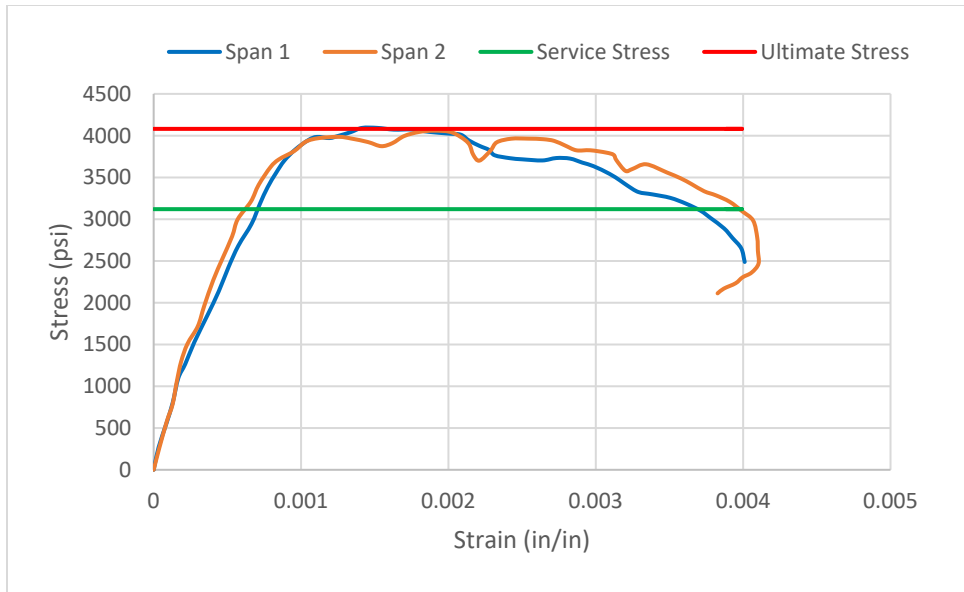


Figure 7 - 4 Stress-Strain Curve of GFRP-2 Deck



Figure 7 - 5 GFRP Concrete Deck Specimen

7.1.2 SFRC-GFRP-CIP

Two cast-in-place concrete decks were cast on top of three precast concrete girders, utilizing (70 lb/cy) steel fiber as the primary reinforcement, in addition to GFRP mesh supplementary reinforcement.

1- Load – Displacement Curves

After testing, it was observed that SFRC-GFRP-CIP decks displayed their first crack at an average service load of (41 kips), accompanied by a deflection of (0.035 in). The average ultimate load was noted to be (55 kips) with a deflection of (0.17 in). The maximum deflection at the point of failure was reported to be (0.5 in), while the area under the average load-deflection curve was measured to be (24.4 area units). To further illustrate, Figures 7-6 and 7-7 depict the load-deflection curves of SFRC-GFRP-CIP-1 and SFRC-GFRP-CIP-2 specimens, respectively.

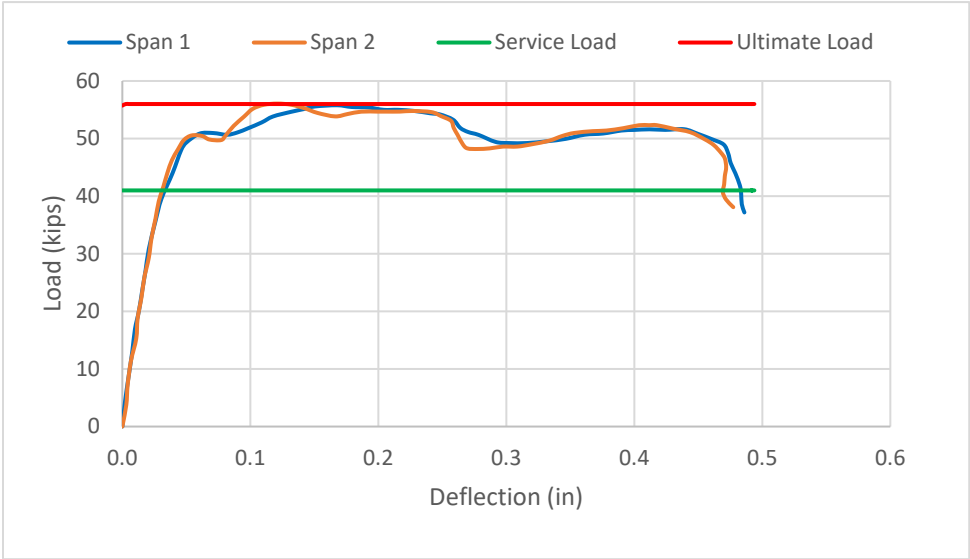


Figure 7 - 6 Load-Displacement Curve of SFRC-GFRP-CIP-1 Deck

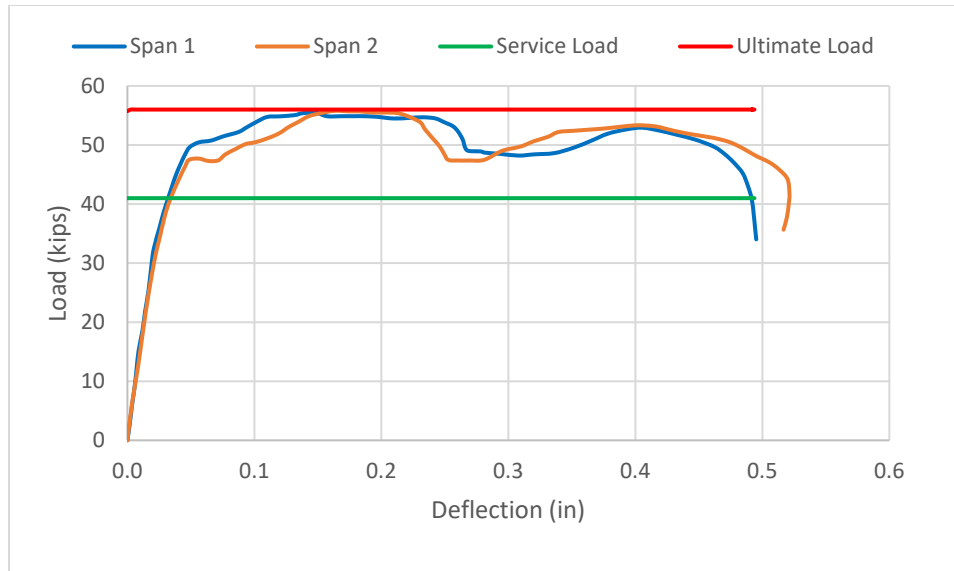


Figure 7 - 7 Load-Displacement Curve of SFRC-GFRP-CIP-2 Deck

2- Stress-Strain Curves

When the service stress reached (3524 psi), the average strain was (0.0007 in/in), while at an ultimate stress of (4828 psi), the average strain was (0.002 in/in). The highest strain before failure was recorded at (0.0048in/in). Moreover, the area under the average stress-strain curve amounts to (19.5 area units). Figures 7-8 and 7-9 depict the stress-strain curves of SFRC-GFRP-CIP-1 and SFRC-GFRP-CIP-2 specimens, respectively. Figure 7-10 shows the failure shape of the SFRC-GFRP-CIP specimen.

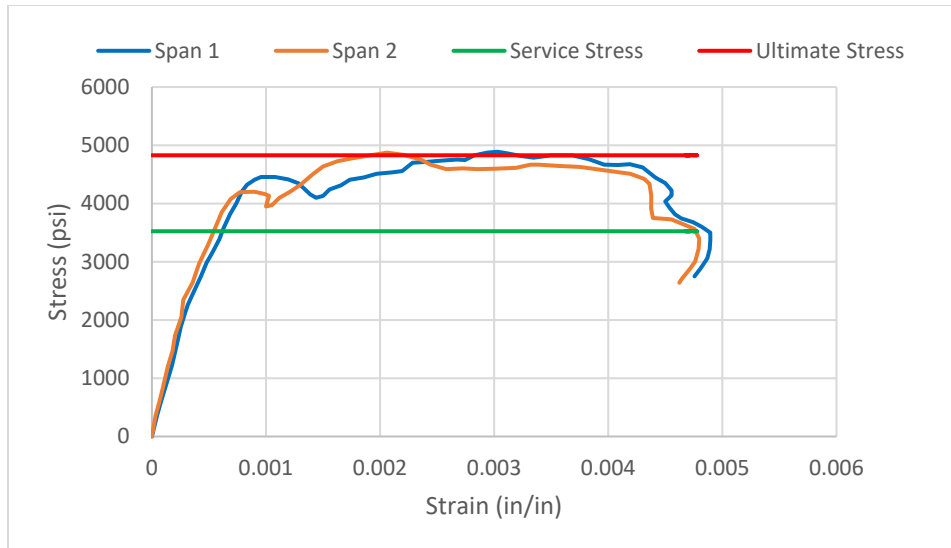


Figure 7 - 8 Stress-Strain Curve of SFRC-GFRP-CIP-1 Deck

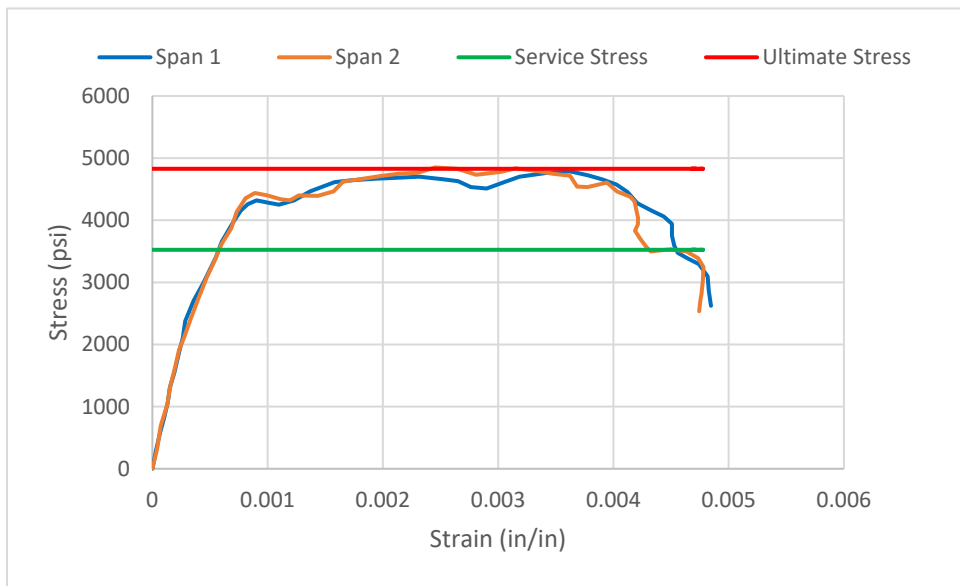


Figure 7 - 9 Stress-Strain Curve of SFRC-GFRP-CIP-2 Deck



Figure 7 - 10 SFRC-GFRP-CIP Concrete Deck Specimen

7.1.3 SFRC-GFRP-PC

The experimental setup comprised two precast concrete decks that were conjoined using three precast concrete girders in the shear pocket and connectors. The specimens were reinforced primarily with 70 pounds per cubic yard of steel fiber and were further supplemented with GFRP mesh.

1- Load – Displacement Curves

After conducting tests, it was discovered that the SFRC-GFRP-PC decks began to crack at an average service load of (42 kips), resulting in a deflection of (0.036 inches). The average ultimate load was determined to be (56 kips), with a deflection of (0.18 inches). At the point of failure, the maximum deflection reached (0.48 inches). Furthermore, the area under the average load-deflection curve was measured to be (23.3 area units). To see the load-deflection curves of the SFRC-GFRP-PC-1 and SFRC-GFRP-PC-2 specimens, please refer to Figures 7-11 and 7-12, respectively.

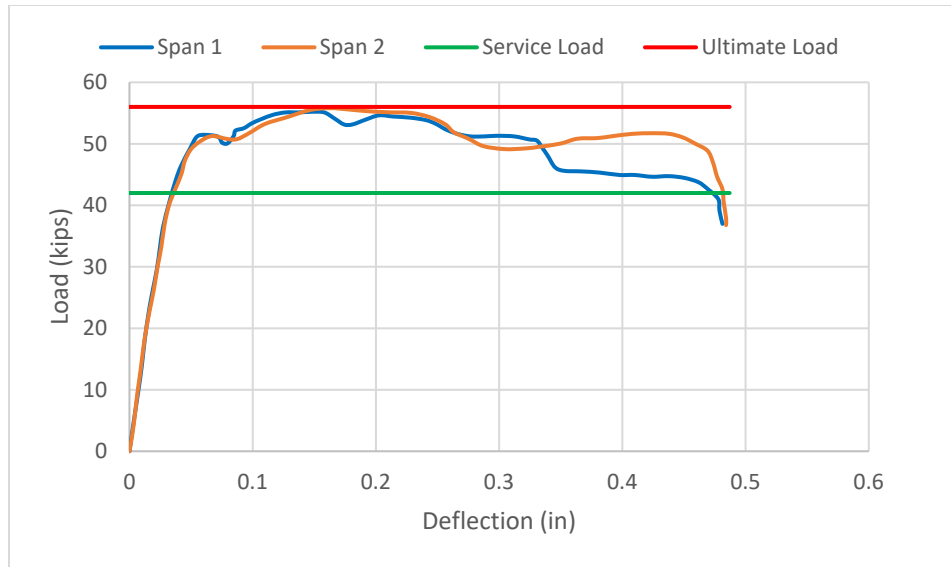


Figure 7 - 11 Load-Displacement Curve of SFRC-GFRP-PC-1 Deck

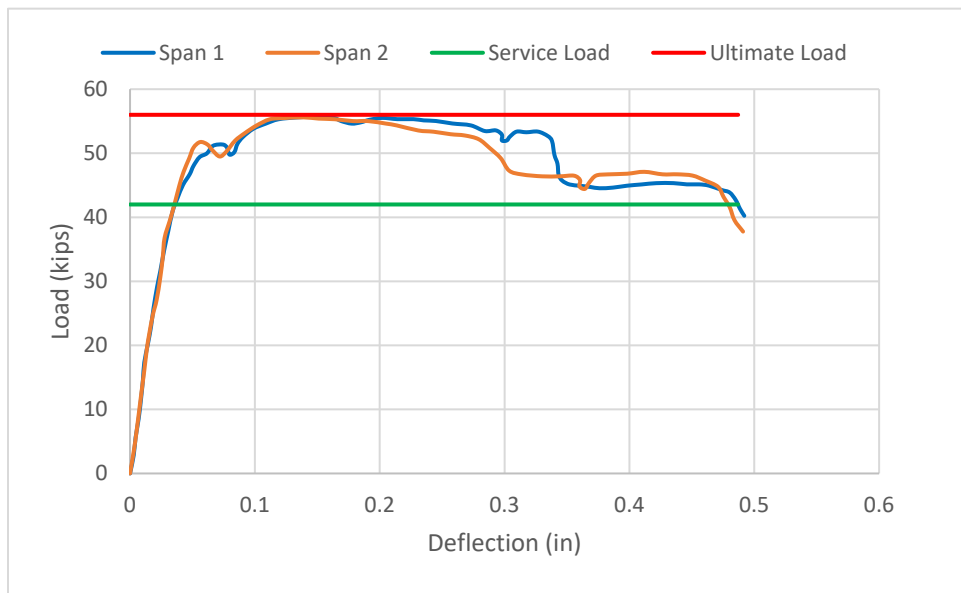


Figure 7 - 12 Load-Displacement Curve of SFRC-GFRP-PC-2 Deck

2- Stress-Strain Curves

When subjected to a service stress of (3634 psi), the specimens exhibited an average strain of (0.0007 in/in). As the stress increased to an ultimate stress of (4776 psi), the average strain

also increased to (0.002 in/in). The maximum strain observed before failure occurred at (0.0047 in/in). Moreover, the area under the average stress-strain curve was calculated to be (18.6 area units). Figures 7-13 and 7-14 depict the stress-strain curves of SFRC-GFRP-PC-1 and SFRC-GFRP-PC-2 specimens, respectively. Figure 7-15 shows the failure shape of the SFRC-GFRP-PC specimen.

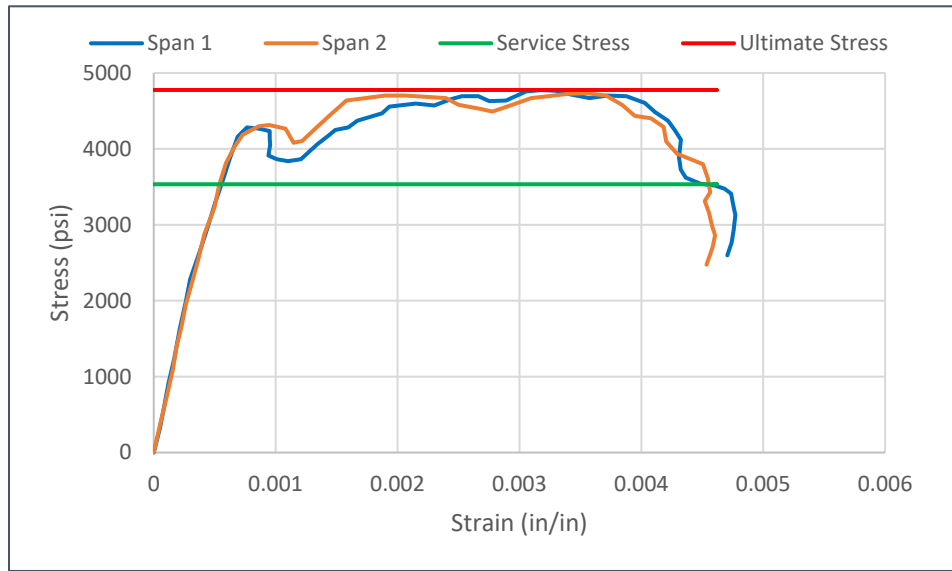


Figure 7 - 13 Stress-Strain Curve of SFRC-GFRP-PC-1 Deck

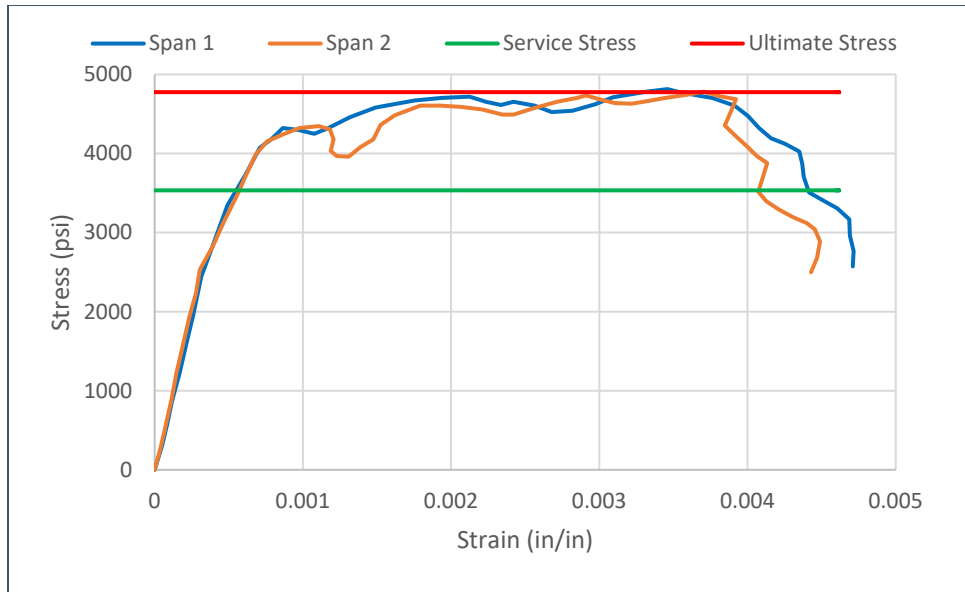


Figure 7 - 14 Stress-Strain Curve of SFRC-GFRP-PC-2 Deck

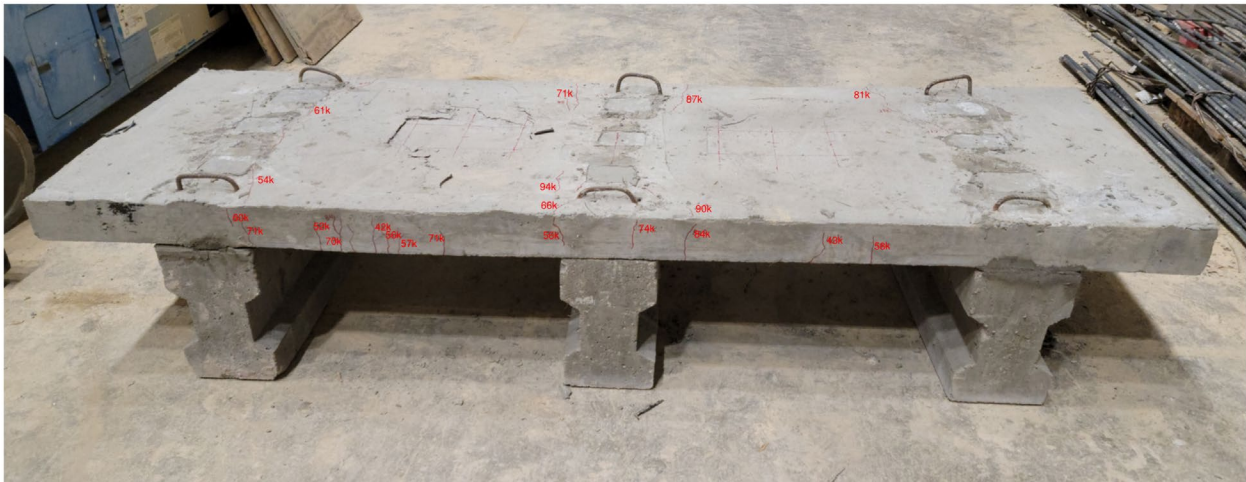


Figure 7 - 15 SFRC-GFRP-PC Concrete Deck Specimen

7.2 Results Comparison

7.2.1 Load – Displacement Characteristics

Utilizing steel fiber as the main reinforcement in concrete had a significant effect on its strength and deflection. According to the results, GFRP decks had a service load average of

(39 kips), whereas SFRC-GFRP-CIP and SFRC-GFRP-PC decks had an average service load of (41 kips) and (42 kips), respectively. Additionally, the average ultimate load for GFRP decks was (51 kips), while SFRC-GFRP-CIP and SFRC-GFRP-PC decks had an average ultimate load of (55 kips) and (56 kips), respectively. These figures indicate a (5.1%) and (7.7%) increase in the service load capacity and a (7.8%) and (9.8%) increase in the ultimate load capacity of SFRC-GFRP-CIP and SFRC-GFRP-PC decks, respectively. It is noteworthy that all decks exhibit consistent deflection at the service load. However, there was a high increase in deflection at ultimate load when subjected to GFRP, SFRC-GFRP-CIP, and SFRC-GFRP-PC decks, with a range of (0.15 in), (0.17 in) to (0.18 in), respectively. It is interesting to note that the maximum deflection prior to failure for SFRC-GFRP-CIP and SFRC-GFRP-PC decks was (0.50 in) and (0.48 in), respectively, which exceeded the (0.46 in) deflection for GFRP decks. This suggests that the steel fiber contributes to increased deflection prior to failure. Table 7-1 shows the GFRP, SFRC- GFRP-CIP, and SFRC- GFRP-PC decks load-displacement values.

Table 7 - 1 Load-Displacements of GFRP, SFRC-GFRP-CIP, and SFRC-GFRP-PC Decks

Deck ID	P _{service} kips	%P _{service} Increases	P _{Ult} kips	%P _{Ult} Increases	Δ at P _{service} in	Δ at P _{Ult} in	Δ _{Max} in
GFRP	39	5.1	51	7.8	0.030	0.15	0.46
SFRC-GFRP-CIP	41		55		0.035	0.17	0.5
SFRC-GFRP-PC	42	7.7	56	9.8	0.036	0.18	0.48

7.2.2 Ductility Index

The ductility index was derived through a rigorous analysis of the load-displacement curves. This was done by utilizing Spadea's equation (Equation 6-2), a proven and widely accepted method for calculating the index. To further support our findings, Table 7-2 provides values for the total energy at both the ultimate load and at (75%) of the ultimate load. These results have been obtained

through a thorough and systematic academic approach. The results indicate that the ductility index of the SFRC-GFRP-CIP and SFRC-GFRP-PC decks exceeded that of the GFRP decks by (35.6%) and (37.3%) respectively. The results indicate that utilizing steel fiber reinforcement as the main reinforcement in the concrete decks has substantially enhanced the ductility of concrete. This was clearly observed in the load-deflection curves, where a larger area under the curve signifies that the specimens were able to absorb more energy during load application.

Table 7 - 2 Energy Absorbed, and Ductility Index of GFRP, SFRC-GFRP-CIP, and SFRC-GFRP-PC Decks.

Deck ID	P_{Ult} kips	E_{tot} Kip-in	$E_{75\%P_{Ult}}$ Kip-in	$\%E_{tot}$ Increasing	μE	$\% \mu E$ Increasing
GFRP	51	13.5	1.5	44.4 37.8	9.0	35.6 37.3
SFRC-GFRP-CIP	55	19.5	1.6		12.2	
SFRC-GFRP-PC	56	18.6	1.5		12.4	

7.2.3 Stress-Strain Characteristics

The study has shown that utilizing steel fibers in concrete can significantly enhance its strength and durability, particularly in terms of its ability to resist cracking, withstand compression, and maintain tensile strength. Furthermore, the use of hooked-end steel fibers has proven to be more effective than conventional reinforcement methods. Reinforced concrete GFRP decks have shown average service stress of (3120 psi), whereas SFRC-GFRP-CIP and SFRC-GFRP-PC decks have demonstrated average service stresses of (3524 psi) and (3634 psi), respectively. This translates to an impressive increase in service strength of (12.9%) and (16.5%), respectively. Similarly, the GFRP decks had an average ultimate stress of (4081 psi), whereas the SFRC-GFRP-CIP and SFRC-GFRP-PC decks had (4828 psi) and (4776 psi), respectively. This indicates an increase in ultimate strength of (18.3%) and (17.0%). Additionally, the area under the SFRC-GFRP-CIP and SFRC-GFRP-PC curves was

(44.4%) and (37.8%) larger than the GFRP curve. This suggests that the decks were able to absorb and carry more energy since they behaved as a more ductile material. As a result, they were able to deflect and absorb more energy before failing as shown in Table 7-3.

Table 7 - 3 Stress-Strain of GFRP, SFRC-GFRP-CIP, and SFRC-GFRP-PC Decks.

Deck ID	Stress _{service} psi	%Stress _{service} Increases	Stress _{ult} psi	%Stress _{ult} Increases	Strain at Stress _{service}	Strain at Stress _{ult}	Area Under the Curve	%Area increases
GFRP	3120	12.9	4081	18.3	0.0007	0.0013	13.5	44.4 37.8
SFRC-GFRP-CIP	3524		4828		0.0007	0.002	19.5	
SFRC-GFRP-PC	3634	16.5	4776	17.0	0.0007	0.002	18.6	

7.2.4 Crack Width

It has been observed that the SFRC-GFRP-CIP and SFRC-GFRP-PC decks exhibited higher ductility compared to the GFRP decks. This led to the emergence of primary cracks in the SFRC-GFRP-CIP and SFRC-GFRP-PC decks after the GFRP decks. Throughout the loading process, the progression of cracks was monitored, and the width of a specific crack was measured across all specimens. During the testing, it was observed that the main cracks appeared in two locations. At the bottom of the mid spans of each deck for the positive moment, and the top of the deck near the edge of the girders for the negative moment. The load vs. crack width curve shown in Figure 7-16 indicates that the crack started appearing at a load of (32 kips) for SFRC-GFRP-CIP decks and (30 kips) for SFRC-GFRP-PC decks. On the other hand, for GFRP decks, the crack appeared at a load of (24 kips). Additionally, the maximum width of the crack in SFRC-GFRP-CIP decks was (0.26 in), while for SFRC-GFRP-PC decks, it was (0.25 in). The maximum crack width observed was (0.30 in) on the GFRP decks. Based on the experimental work results of this study, utilized steel fibers in the concrete mixture had a substantial effect on resisting crack initiation and growth; steel fibers improved concrete tensile strength, thus minimizing the crack maximum width by

approximately (20%) for both SFRC-GFRP-CIP and SFRC-GFRP-PC decks. Figure 7-17 shows the failure shape of GFRP, SFRC-GFRP-CIP, and SFRC-GFRP-PC Decks specimens (group 2).

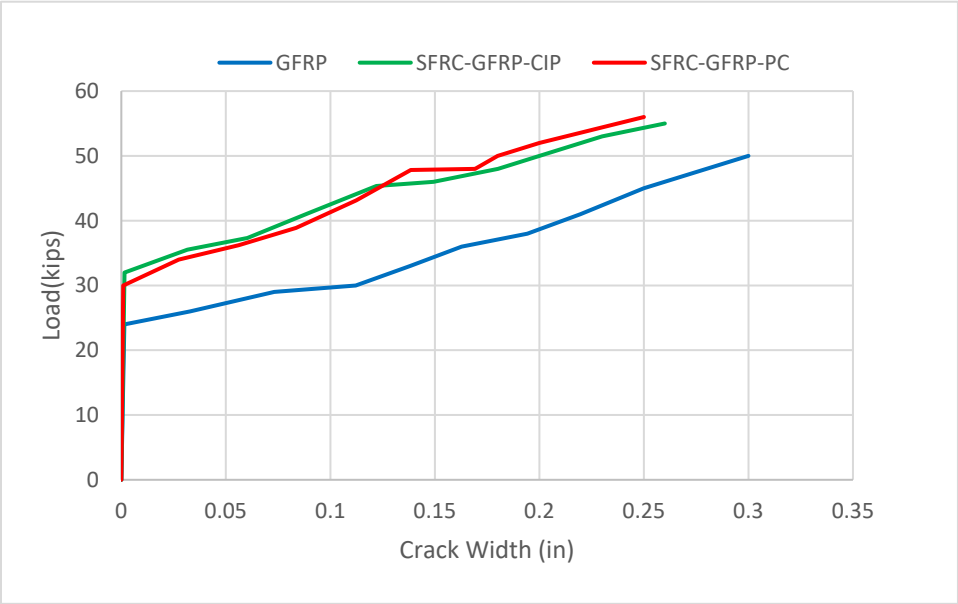


Figure 7 - 16 Crack Width Curves of GFRP, SFRC-GFRP-CIP, and SFRC-GFRP-PC

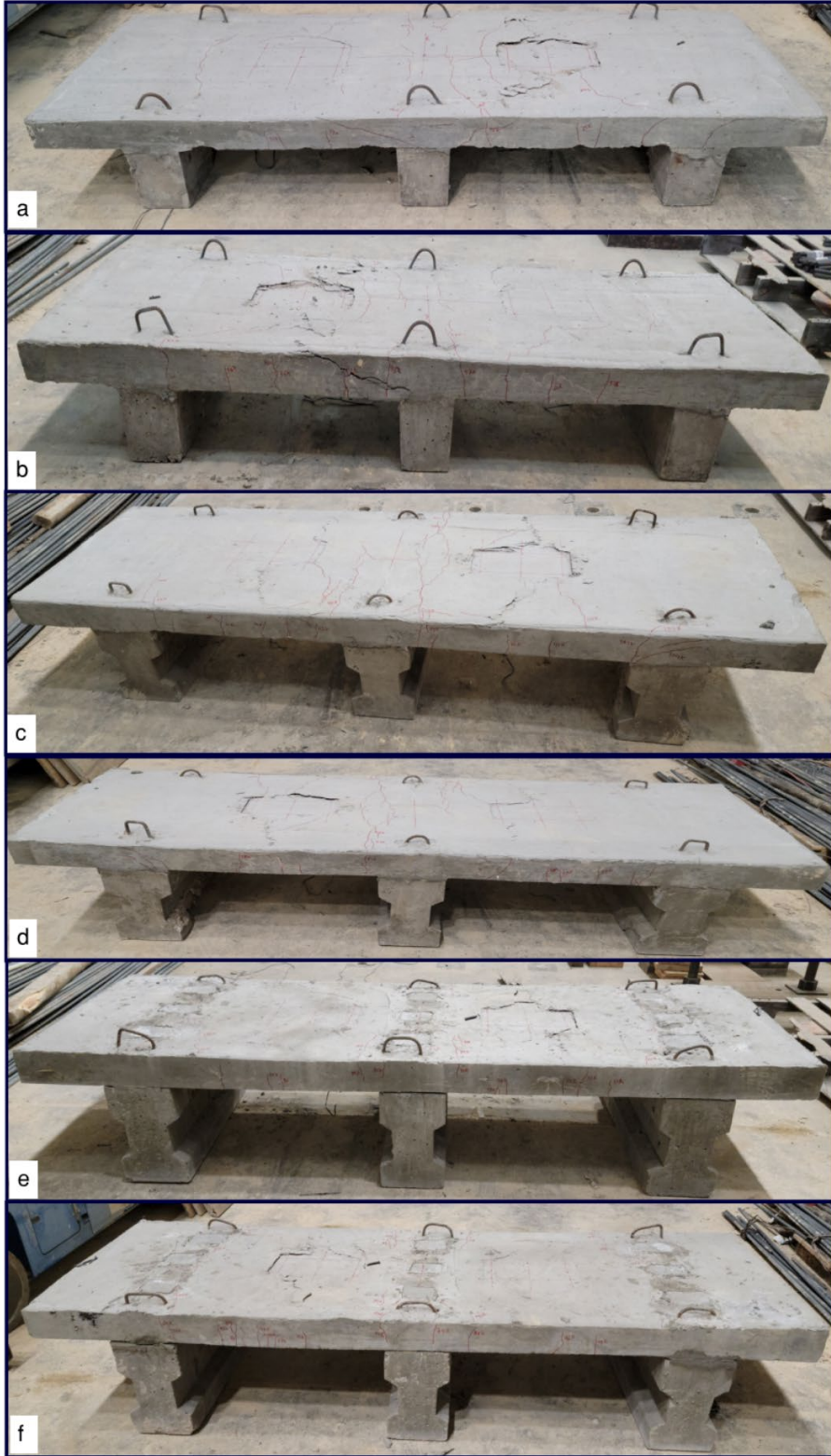


Figure 7 - 17 Concrete Specimens Failure, (a, b) GFRP; (c, d) SFRC-GFRP-CIP; (e, f): SFRC-GFRP-PC

CHAPTER 8

CONCLUSIONS AND RECOMMENDATIONS

8.1 Conclusions

The evaluation of utilizing Dramix 4D steel fiber as a mine reinforcement in bridge decks and the comparison with the conventional and GFRP reinforcement have been studied in this research. The conclusion of utilizing steel fibers significantly improved the overall structural behavior of the SFRC decks as follows:

8.1.1 SFRC-CIP Concrete Decks vs RC Concrete Decks

- The overall load capacity was improved as the average service and ultimate load capacity of SFRC-CIP were improved by utilizing the steel fiber as the main reinforcement by 14.6% and 11.8%, respectively.
- The SFRC-CIP decks exhibit more ductile behavior than RC decks since the maximum deflection was greater than the deflection of the RC decks. Moreover, the SFRC-CIP decks carried higher energy than RC decks. The ductility index (μ_E) significantly increased by 56.6%, meaning the absorbed energy exceeded the reference decks.
- The average service and ultimate stress capacity of SFRC-CIP were improved by 7.6% and 15.5%, respectively.
- The area under the stress–strain curve of SFRC-CIP decks was greater than the RC decks by 74.2%, meaning the SFRC-CIP decks could absorb more energy during the load test.
- Steel fibers were more efficient at improving tensile strength and bending behavior. The crack widths were less than the RC decks by about 14%. Steel fiber delayed the initial

main cracks in all SFRC-CIP decks. Thus, this improves the resistance of concrete decks against traffic and environmental influences.

8.1.2 SFRC-PC Concrete Decks vs RC Concrete Decks

- The overall load capacity was improved as the average service and ultimate load capacity of SFRC-CP were improved by utilizing the steel fiber as the main reinforcement by 12.2% and 11.8%, respectively.
- The SFRC-CP decks exhibit more ductile behavior than RC decks since the maximum deflection was greater than the deflection of the RC decks. Moreover, the SFRC-CIP decks carried higher energy than RC decks. The ductility index (μ_E) significantly increased by 33.3%, meaning the absorbed energy exceeded the reference decks.
- The average service and ultimate stress capacity of SFRC-CP were improved by 5.1% and 16.5%, respectively.
- The area under the stress–strain curve of SFRC-CP decks was greater than the RC decks by 65.9%, meaning the SFRC-CP decks could absorb more energy during the load test.
- Steel fibers were more efficient at improving tensile strength and bending behavior. The crack widths were less than the RC decks by about 14%. Steel fiber delayed the initial main cracks in all SFRC-CP decks. Thus, this improves the resistance of concrete decks against traffic and environmental influences.
- Utilizing steel fiber improves the opportunity for economical implementation by speeding up construction since it requires fewer work hours and requires less future maintenance since it is significantly less corrosion compared to conventional reinforcement (Tran et al. 2011).

8.1.3 SFRC-GFRP-CIP Concrete Decks vs GFRP Concrete Decks

- The overall load capacity was improved as the average service and ultimate load capacity of SFRC-GFRP-CIP were improved by utilizing the steel fiber as the main reinforcement by 5.1% and 7.8%, respectively.
- The SFRC-GFRP-CIP decks exhibit more ductile behavior than GFRP decks since the maximum deflection was greater than the deflection of the GFRP decks. Moreover, the SFRC-GFRP-CIP decks carried more energy than the GFRP decks. The ductility index (μ_E) significantly increased by 35.6%, meaning the absorbed energy exceeded the reference decks.
- The average service and ultimate stress capacity of SFRC-GFRP-CIP were improved by 12.9% and 18.3%, respectively.
- The area under the stress–strain curve of SFRC-GFRP-CIP decks was greater than the GFRP decks by 44.4%, meaning the SFRC-GFRP-CIP decks could absorb more energy during the load test.
- Steel fibers were more efficient at improving tensile strength and bending behavior. The crack widths were less than the GFRP decks by about 14%. Steel fiber delayed the initial main cracks in all SFRC-GFRP-CIP decks. Thus, this improves the resistance of concrete decks against traffic and environmental influences.

8.1.4 SFRC-GFRP-PC Concrete Decks vs GFRP Concrete Decks

- The overall load capacity was improved as the average service and ultimate load capacity of SFRC-GFRP-PC were improved by utilizing the steel fiber as the main reinforcement

by 7.7% and 9.8%, respectively.

- The SFRC-GFRP-PC decks exhibit more ductile behavior than GFRP decks since the maximum deflection was greater than the deflection of the GFRP decks. Moreover, the SFRC-GFRP-PC decks carried more energy than the GFRP decks. The ductility index (μ_E) significantly increased by 37.3%, meaning the absorbed energy exceeded the reference decks.
- The average service and ultimate stress capacity of SFRC-GFRP-PC were improved by 16.5% and 17%, respectively.
- The area under the stress–strain curve of SFRC-GFRP-PC decks was greater than the GFRP decks by 37.8%, meaning the SFRC-GFRP-PC decks could absorb more energy during the load test.
- Steel fibers were more efficient at improving tensile strength and bending behavior. The crack widths were less than the GFRP decks by about 14%. Steel fiber delayed the initial main cracks in all SFRC-GFRP-PC decks. Thus, this improves the resistance of concrete decks against traffic and environmental influences.

To summarize, utilizing Dramix 4D steel fiber as the main reinforcement in bridge decks has a positive impact on the overall structural performance. This includes enhancements in load capacity, stress-strain behavior, tensile strength, crack width, crack spacing, ductility, and energy absorption. The use of steel fiber also presents opportunities to expedite construction, as it eliminates the need for labor-intensive tasks such as laying and tying or clarifying the clear cover required with traditional reinforcement methods. This translates to reduced construction time and manpower requirements. Additionally, the corrosion resistance of steel fiber exceeds that of conventional reinforcement, leading to decreased maintenance needs and

an extended bridge lifespan. In contrast to steel fiber-reinforced decks, decks reinforced with glass fiber-reinforced polymer (GFRP) lack ductility. Therefore, it is advantageous to supplement GFRP bars with steel fiber to enhance ductility, mitigate abrupt failure, and improve crack resistance. In this approach, GFRP provides high tensile strength, while steel fiber caters to ductility and crack resistance.

8.2 Recommendations and Future Research

- The Finite Element (FE) model utilized a static model option, which applied the live load as a patch area. However, it would be more realistic to use a dynamic model to apply the moving load, as this would better reflect the real-life scenario where vehicles are driven on the bridge deck at varying speeds.
- An examination into the chipping of damaged concrete deck and subsequent overlaying of 2.5 inches of Steel Fiber Reinforced Concrete (SFRC) as a retrofitting solution for decks warrants academic attention.
- Performed other experiments to cover other concrete behaviors, including:
 - Impact tests.
 - Bending behavior under high temperatures for GFRP reinforcement.
 - Bending behavior under dynamic live load.
- Conduct a parametric study on the behavior of the SFRC deck under bending load using FE analysis investigating the following parameters:
 - Dosage fraction of steel fibers in concrete mix.
 - Aspect ratio of fibers.
 - Type of fibers.
 - Slab thickness.

- Predict the behavior of the SFRC deck under impact load with the aim of FE and material models to best predict the structural performance.
- Investigate the energy absorption of the slabs under the parametric study.

REFERENCES

- American Association of State Highway and Transportation Officials (2014). AASHTO LRFD bridge design specifications. customary U.S. units. Washington, D.C, The Association.
- Abbas, S., Nehdi, M. L., Mechanical Behavior of RC and SFRC Precast Tunnel Lining Segments under Chloride Ions Exposure, *Journal of Materials in Civil Engineering*, ASCE, 2018, 04018047-1- 04018047-13.
- AbulMaali, A., Mikhaylova, A., Wilson, A., Lundy, J., Performance of Steel Fiber-Reinforced Concrete Pipes, *Journal of the Transportation Research Board*, Volume 2313, Issue 1, January 1, 2012.
- ACI CODE-318-19, Building Code Requirements for Structural Concrete and Commentary, American Concrete Institute, 2022.
- ACI Committee 544, State-of-the-Art Report on Fiber Reinforced Concrete, May 1982, pp 411-413.
- ACI PRC-440.1-15 Guide for the Design and Construction of Structural Concrete Reinforced with Fiber-Reinforced Polymer Bars, American Concrete Institute, 2015.
- American Society of Civil Engineers (ASCE) Report Card for America's Infrastructure grades reveal widening investment gap, Bridges-2021, (infrastructurereportcard.org)
- American Society of Civil Engineers ASCE (2021) Report Card for America's Infrastructure grades reveal widening investment gap, Bridges-2021.pdf (infrastructurereportcard.org)
- ASTM A820-01 Standard Specification for Steel Fibers for Fiber-Reinforced Concrete, 2021.
- ASTM C1018 – 89 (1991) Standard test method for flexural toughness and first crack strength of fiber reinforced concrete (Using Beam with Third-Point Loading), 1991 Book of ASTM

Standards, Part 04.02. American Society for Testing and Materials, Philadelphia, p 507 – 513

ASTM C39/C39M-21 Standard Test Method for Compressive Strength of Cylindrical Concrete Specimens, 2021.

ASTM C496-96 Standard Test Method for Splitting Tensile Strength of Cylindrical Concrete Specimens, 2017.

ASTM C76-11 Standard Specification for Reinforced Concrete Culvert, Storm Drain, and Sewer Pipe, 2012.

ASTM C78-09 Standard Test Method for Flexural Strength of Concrete (Using Simple Beam with Third-Point Loading), 2010.

ASTM D7957/D7957M-22 Standard Specification for Solid Round Glass Fiber Reinforced Polymer Bars for Concrete Reinforcement, 2022.

Attari N., Amziane S., Chemrouk M., Flexural strengthening of concrete beams using CFRP, GFRP and hybrid FRP sheets, *Construction and Building Materials* Volume 37, December 2012, Pages 746-757.

Azzawi, R., Abolmaali, A., Experimental investigation of steel fiber RC hollow columns under eccentric loading, *Structures* 24 (2020) 456–463.

Bekaert, Steel Fiber 4D Dramix 65/60 BG Datasheet, Dramix® 4D technical documents - Bekaert.com 2023.

Bridge Design Guide, Texas Department of Transportation, 2023.

Bridge Design Manual - LRFD, Texas Department of Transportation, 2021.

Carrillo, J., Ramirez, J., Lizarazo-Marriaga, J., Modulus of elasticity and Poisson's ratio of fiber-reinforced concrete in Colombia from ultrasonic pulse velocities, *Journal of Building Engineering* Volume 23, May 2019, Pages 18-26

Correia J. R., Bai, Y., Keller T., A review of the fire behavior of pultruded GFRP structural profiles for civil engineering applications, *Composite Structures* Volume 127, 1 September 2015, Pages 267-287.

Dhonde, H. B., Mo, Y. H., Thomas, T. C., Fiber Reinforcement in Prestressed Concrete Beams, No. FHWA/TX-06/0-4819-1. 2005.

Ehsani, M.R., Saadatmanesh, H., Tao, S., Design Recommendations for Bond of GFRP Rebars To Concrete, *Journal of Structural Engineering* Volume 122, Issue 3, Mar 1996, Pages 227-347

Fan, L., Meng, W., Teng, L., Khayat, K.H., Effect of steel fibers with galvanized coatings on corrosion of steel bars embedded in UHPC, *Composites Part B: Engineering* Volume 177, 15 November 2019, 107445.

Fattouh, M.S., Tayeh, B. A., Agwa, I. S., Elsayed, E. K., Improvement in the flexural behavior of road pavement slab concrete containing steel fiber and silica fume, *Case Studies in Construction Materials* Volume 18, July 2023, pages 1-12.

Ferretti, E. On Poisson's ratio and volumetric strain in concrete. *International Journal of Fracture* 126, 49–55 (2004). <https://doi.org/10.1023/B:FRAC.0000026587.43467.e6>

Gilbert, R.I., The Serviceability Limit States in Reinforced Concrete Design, *Procedia Engineering* 14 (2011) 385–395

Goldston M., Remennikov A., Neaz Sheikh M., Experimental investigation of the behavior of concrete beams reinforced with GFRP bars under static and impact loading, *Engineering Structures* Volume 113, 15 April 2016, Pages 220-232

Hajiloo, H., Green, M. F., Gales, J., Mechanical Properties of GFRP Reinforcing Bars at High Temperatures, *Construction and Building Materials*, Volume 162, 20 February 2018, Pages 142-154.

- Hason, M. M., Hanoon, A. N., Saleem, S. J., Hejazi, F., Al Zand, A. W., Characteristics of Experimental Ductility Energy Index of Hybrid-CFRP Reinforced Concrete Deep Beams, SN Applied Sciences 3, 200 (2021) <https://doi.org/10.1007/s42452-021-04202-6>.
- Hwang, H., Park, H., Hong, G., Kim, G., Choi, S., Effect of Steel Fiber for Crack Control in Concrete Slabs with Steel Deck Plates, ACI Structural Journal; Farmington Hills Vol. 114, Iss. 4, (Jul/Aug 2017), Pages 851-860.
- Issa, M. S., Metwally, Elzeiny, S. M., Influence of fibers on flexural behavior and ductility of concrete beams reinforced with GFRP rebars, Engineering Structures Volume 33, Issue 5, May 2011, Pages 1754-1763.
- Johan Ahlström, Corrosion of steel in concrete at various moisture and chloride levels, ENERGIFORSK, 133-8, 2015.
- John, Corven, Post-Tensioned Box Girder Design Manual, 2016
- Kamal, M.M., El-Refai, F.E., Durability of steel fiber reinforced concrete, Proceedings of the Fourth International Conference on Durability of Building Materials and Components Singapore, November 1987, Pages 235-247
- Karabinis, A.I, Rousakis, T.C., Manolitsi, G.E., 3D finite element analysis of substandard RC columns strengthened by fiber-reinforced polymer sheets, Journal of Composites for Construction, vol. 12, no. 5, pp. 531–540, 2008.
- Kinjawadekar, T.A. Patil, S., Gopinatha Nayak, G., A Critical Review on Glass Fiber-Reinforced Polymer Bars as Reinforcement in Flexural Members, Journal of The Institution of Engineers (India): Series A, (June 2023) 104(2):501–516.
- Kirkpatrick, T.J., Weyers, R.E., Anderson-Cook, C.M., Sprinkel, M.M., Probabilistic model for the chloride-induced corrosion service life of bridge decks. Cement and Concrete Research,

- 32 (12), 2002, 1943–1960.
- Li, G., Kidane, S., Pang, S., Helms, J.E., Michael A Stubblefield, Investigation into FRP repaired RC columns, *Composite Structures* Volume 62, Issue 1, October 2003, Pages 83-89
- Mangat P.S., Gurusamy, K., Corrosion resistance of steel fibers in concrete under marine exposure. *Cement and Concrete Research*, Volume 18, Issue 1, January 1988, Pages 44-54
- Mangat, P.S., Gurusamy, K., Corrosion resistance of steel fibers in concrete under marine exposure, *Cement and Concrete Research* Volume 18, Issue 1, January 1988, Pages 44-54.
- Marcos-Meson, V., Michel, A., Solgaard, A., Fischer, G., Edvardsen, C., Skovhus, T. L., Corrosion resistance of steel fiber reinforced concrete - A literature review, *Cement and Concrete Research* Volume 103, January 2018, Pages 1-20
- Mathieu, R., Benmokrane, B., Behavior of GFRP Reinforcing Bars Subjected to Extreme Temperature, *Journal of Composites for Construction*, Vol. 14, Issue 4, August 2010, ASCE, 353–360.
- McMahon, J. A., and Birely, A. C., Experimental Performance of Steel Fiber Reinforced Concrete Bridge Deck, *Journal of Bridge Engineering*, Volume 23, Issue 10, Oct 2018, pages 1-14.
- Mirmiran, A. K. Zagers, Yuan, W., Nonlinear Finite Element Modeling of Concrete Confined by Fiber composites, *Finite Elements in Analysis and Design*, vol. 35, no. 1, pp. 79–96, 2000.
- Mohod, M. V., Performance of Steel Fiber Reinforced Concrete, *International Journal of Engineering and Science*, Vol. 1, Issue 12 (December 2012), PP 01-04
- Motter, C.J., Serviceability Analysis for Deflection of Reinforced Concrete Floor Slabs in Multi-Story High-Rise Buildings, Department of Civil and Environmental Engineering, March 2009, pp 139.
- Mu R., Wei L., Wang, X., Li, H., Qing, L., Zhou, J., Zhao, Q., Preparation of Aligned Steel Fiber

- Reinforced Cementitious Composite and Its Flexural Behavior. *Journal of Visualized Experiments*, June 2018, Vol. 136, e56307, Pages 1 to 11.
- Naaman, Antoine E., "Fiber Reinforcement for Concrete" *Concrete International Journal*, March 1985, pp 21-25.
- Odaa S.A., Hason M.M., Sharba A. A. K., Self-compacting concrete beams reinforced with steel fiber under flexural loads: a ductility index evaluation. *Materials today: Proceedings*. Volume 42, Part 5, 2021, Pages 2259-2267.
- Olivito, R.S., Zuccarello, F.A., An experimental study on the tensile strength of steel fiber reinforced concrete, *Composites Part B: Engineering* Volume 41, Issue 3, April 2010, Pages 246-255.
- Pauw, A., Static modulus of elasticity of concrete as affected by density, University of Missouri, 1960
- PCI, Precast/Prestressed Concrete Institute, *Bridge Design Manual*, 3rd Edition, 2011.
- Persson, B., Poisson's ratio of high-performance concrete, *Cement and Concrete Research* Volume 29, Issue 10, October 1999, Pages 1647-1653.
- Rousakis, T.C., Karabinis, A. I., Kiouisis, P. D., Tepfers, R., Analytical modeling of plastic behavior of uniformly FRP confined concrete members, *Composites Part B: Engineering*, vol. 39, no. 7-8, pp. 1104–1113, 2008.
- Saadeghvaziri, M. A., Hadidi, R., Transverse Cracking of Concrete Bridge Decks: Effects of Design Factors, *Journal of Bridge Engineering* Volume 10, Issue 5, 2005.
- Sideris, K.K., Manita, P., Sideris, K., Estimation of ultimate modulus of elasticity and Poisson ratio of normal concrete, *Cement and Concrete Composites* Volume 26, Issue 6, August 2004, Pages 623-631

Smith S. T., Hu S., Kim S. J., Seracino R., FRP-strengthened RC slabs anchored with FRP anchors, *Engineering Structures* Volume 33, Issue 4, April 2011, Pages 1075-1087

Spadea, G., Bencardino, F., Swamy, R., Strengthening and upgrading structures with bonded CFRP sheets design aspects for structural integrity. In: *Proceedings of 3rd International Symposium on Non-Metallic (FRP) Reinforcement for Concrete Structure*, 1997.

Subramaniam, K. V. L., Identification of Early-Age Cracking in Concrete Bridge Decks, *Journal of Performance of Constructed Facilities* Volume 30, Issue 6, 2026.

Syll A.S., Kanakubo, T., Impact of Corrosion on the Bond Strength between Concrete and Rebar: A Systematic Review. *Materials*. 15 (19), 7016, 2022, Pages 1-21.

Thomas, J. and Ramaswamy, A., Mechanical Properties of Steel Fiber-Reinforced Concrete, *Journal of Materials in Civil Engineering Archive* Vol. 19, No. 5, May 1, 2007

Tran K. K., Nakamura, H., Kawamura, K., Kunieda, M., Analysis of Crack Propagation Due to Rebar Corrosion Using RBSM, *Cem Concr Compos* 33(9), 2011, Pages 906–917.

Tuutti, K., *Corrosion of steel in concrete*, Swedish cement and concrete research institute, 1982.

Wang, H., Li, Q., Prediction of elastic modulus and Poisson's ratio for unsaturated concrete, *International Journal of Solids and Structures*, 44 (2007) 1370–1379.

Xiang, D., Liu, S., Li, Y., Liu Y., Improvement of flexural and cyclic performance of bridge deck slabs by utilizing steel fiber reinforced concrete (SFRC). *Construct Building Mater*. 2022, 329:127184

Zhang, P., Wang, C., Gao, Z., Wang, F., A review on fracture properties of steel fiber reinforced concrete, *Journal of Building Engineering* Volume 67, 15 May 2023, 105975.

ABBREVIATIONS

AASHTO	American Association of State Highway and Transportation Officials
ACI	American concrete institute
AFRP	Aramid fiber reinforced polymer
ASTM	American Society for Testing Materials
BFRP	Basalt fiber-reinforced polymer
CFRP	Carbon fiber-reinforced polymer
CIP	Cast in place
d_1	Initial diameter of the specimen
d_2	Final diameter of the specimen
DAS	Data acquisition system
DSC	Differential scanning calorimetry
$E_{75\%PUlt}$	Energy at 75% of the ultimate load
E_0	Unloading stiffness at any strain
E_c	Modulus of elasticity of concrete
EDX	Energy dispersive x-ray
E_{tot}	Energy at ultimate load
f_{b0}	Equi-biaxial compressive strength of concrete
f_{c0}	Uniaxial compressive strength

f_c'	Compressive strength
f_y	Yield strength
FEM	Fainant element model
FRC	Fiber-reinforced concrete
FTIS	Fourier transformed infrared spectroscopy
GFRP	Glass fiber reinforced polymer
HPFRC	High-performance fiber-reinforced concrete
Kips	kilo pound
Ksi	kilo pound per square inch
L ₁	Initial length of the specimen
L ₂	Final length of the specimen
lb	Pound
LRFD	Load and resistance factor design
LVDT	Linear variable differential transformer
MTS	Materials test systems
OM	Optical microscopy
P	Load
$P-\Delta$	Load-displacement

PC	Precast
PCTL	Precast concrete tunnel lining
P_{service}	Service load
Psi	Pound per square inch
P_{ult}	Ultimate load
RC	Reinforced concrete
RCP	Reinforced concrete pipe
S_1	Stress corresponding to a longitudinal strain of 50 millionths
S_2	Stress corresponding to 40% of ultimate load
SEM	Scanning electron microscopy
SFRC	Steel fiber reinforced concrete
SFRCP	Steel fiber reinforced concrete pipe
SFRC–SF	Steel fiber reinforced concrete silica fume
$\text{Strain}_{\text{service}}$	Service strain
$\text{Strain}_{\text{ult}}$	Ultimate strain
$\text{Stress}_{\text{service}}$	Service stress
$\text{Stress}_{\text{ult}}$	Ultimate stress
SW	Seawater
TW	Tap water
X_r	Value of load capacity, stiffness, stress, energy, etc., of the reference specimens
X_s	Value of load capacity, stiffness, stress, energy, etc., of the SFRC or GFRP specimens

ϵ_2	Longitudinal strain produced by stress S_2
ϵ_{axial}	Axial strain.
ϵ_{trans}	Transverse strain
μ_E	Ductility index
ν	Poisson's ratio
σ_i	Strength at any point
σ_u	Ultimate strength (compression or tension)
Δ	Displacement

APPENDIX A

Concrete Mix Design

Concrete Mix Design for Normal Strength Concrete of 4000 psi

Assumptions:

- Concrete mix for 4000 psi compressive strength.
- Maximum size of aggregate = $\frac{3}{4}$ in.
- With Fineness Modulus of sand = 2.6.
- The dry weight of aggregate = 100 lb/ft³.
- Moisture content of 3% for the coarse aggregate and 2% for the fine aggregate.
- The recommended slump for different types of construction activities is below in Table A-1.

Table A-1 Slumps for Various Types of Construction Slumps

Types of Construction	Slump (in) ^a	
	Maximum ^b	Minimum
Reinforced Foundation walls and footings	3	1
Plain footings and caissons	3	1
Slabs, beams, and reinforced walls	4	1
Building Columns	4	1
Pavements and slabs	3	1
Heavy mass construction	2	1

^a 1 in. = 25.4 mm.

^b May be increased 1 in. for methods of consolidation other than vibration.

From slump Table A-1, 3 in is required.

Max size of aggregate = $\frac{3}{4}$ in, weight of water required per cubic yard of concrete = 340 lb/yd³,
and for concrete with $f'_c = 4000$ psi

w/c = 0.57 (see Table A-2)

Amount of cement required = 340 lb/yd³ / 0.57 = 596.5 lb/yd³

Use fineness value of 2.6, the volume of coarse aggregate = 0.64 yd³, (See Table A-3)

Using the dry rodded weight of 100 lb/ft³ for coarse aggregate,

Weight of coarse aggregate = 0.64 yd³ * 27 ft³ yd³ * 100 lb/ft³ = 1728 lb/yd³

Estimated weight of fresh concrete = 3960 lb/yd³.

Weight of sand = weight of fresh concrete - weight of water - weight of cement - weight of coarse aggregate

Weight of sand = 3960 lb/yd³ - 340 lb/yd³ - 596.5 lb/yd³ - 1728 lb/yd³ = 1295.5 lb/yd³

Net weight of sand = 1.02 * 1295.5 lb/yd³ = 1321.41 lb/yd³ (moisture content 2%)

Moisture absorption 2% = 1321.41 lb/yd³

Net weight of gravel = 1.03 * 1728 lb/yd³ = 1779.84 lb/yd³

Net weight of water = 340 lb/yd³ - 0.02 * 1295.5 lb/yd³ - 0.03 * 1728 lb/yd³ = 262.25 lb/yd³

Table A-2 Relationship Between Water/Cement Ratio and Compressive Strength of Concrete

Water/Cement Ratio, by Weight		
Compressive strength at 28 days (psi)	Non-air entrained Concrete	Air-entrained Concrete
6000	0.41	
5000	0.48	0.4
4000	0.57	0.48
3000	0.68	0.59
2000	0.82	0.74

Table A-3 Volume Of Coarse Aggregate Per Unit Volume Of Concrete

	Volume Of Dry-Rodded Coarse Aggregate Per Unit Volume Of Concrete For Different Fineness Moduli Of Sand		
Maximum size of aggregate (in)	2.40	2.60	2.80
3/8	0.5	0.48	0.44
1/2	0.59	0.57	0.53
3/4	0.66	0.64	0.6
1	0.71	0.69	0.65
1 1/2	0.75	0.73	0.69
2	0.78	0.76	0.72
3	0.82	0.8	0.76
6	0.87	0.85	0.81

For 1 yd³ of concrete

Cement = 596.5 lb = 600 lb

Sand = 1321.41 lb = 1320 lb

Gravel = 1779.84 lb = 1780 lb

Water = 262.25 lb = 260 lb

APPENDIX B

AASHTO LRFD Concrete Deck Design

$$f_c' = 4000 \text{ psi}$$

$$f_{pu} = 145\,000 \text{ psi (Guaranteed Tensile Strength of GFRP)}$$

$$E_f = 6000\,000 \text{ psi}$$

$$\text{Deck thickness} = 8.5 \text{ in}$$

$$D_c = 8.5 * 1/12 * (0.15 \text{ k/ft}^3) = 0.1 \text{ k/ft}$$

$$D_w = \text{Future wearing surface load} = 0.025 \text{ k/ft}$$

1. Dead Load:

a. Positive bending moment:

$$M_{DC+} = 0.071 * D_c * S^2 \quad (\text{AASHTO Table A 4.1 P. 4-98, 102})$$

$$M_{DC+} = 0.071 * 0.1 * (5.3)^2 = 0.199 \text{ k-ft}$$

$$M_{Dw+} = 0.071 * 0.025 * (5.3)^2 = 0.05 \text{ k-ft}$$

$$\begin{aligned} \text{Strip of positive moment} &= 26 + 6.6 * S \\ &= 26 + 6.6 * 5.3 = 61 \text{ in} \end{aligned}$$

$$\begin{aligned} \text{Strip of negative moment} &= 48 + 3 * S \\ &= 48 + 3 * 5.3 = 64 \text{ in} \quad (\text{AASHTO Table 4.6.2.1.3-1}) \end{aligned}$$

$$M_{DC+} = 0.119 * \frac{144}{61} = 0.281 \text{ k-ft/ft}$$

$$M_{Dw+} = 0.05 * \frac{144}{64} = 0.113 \text{ k-ft/ft}$$

b. Negative bending moment

$$M_{DC-} = 0.1 * D_c * S^2$$

$$M_{DC-} = 0.1 * 0.1 * (5.3)^2$$

$$M_{DC-} = 0.281 \text{ k-ft}$$

$$M_{Dw-} = 0.1 * D_w * S^2$$

$$M_{Dw-} = 0.1 * 0.025 * (5.3)^2$$

$$M_{Dw-} = 0.07 \text{ k-ft}$$

$$M_{DC-} = 0.281 * \frac{144}{61} = 0.66 \text{ k-ft/ft}$$

$$M_{Dw-} = 0.07 * \frac{144}{64} = 0.61 \text{ k-ft/ft}$$

2. Live Load (HL-93)

From AASHTO Table A 4-1:

$$M_{L+} = 4.67 \text{ k-ft and } M_{L-} = 3.47 \text{ k-ft}$$

$$M_{L+} = 4.67 * \frac{144}{61} = 11 \text{ k-ft/ft}$$

$$M_{L-} = 3.47 * \frac{144}{64} = 7.8 \text{ k-ft/ft}$$

3. Load Combinations:

$$M_{f+} = 1.25 M_{DC+} + 1.5 M_{Dw+} + 1.75 M_{L+}$$

$$M_{f+} = 1.25 * 0.281 + 1.5 * 0.113 + 1.75 * 11$$

$$M_{f+} = 19.4 \text{ k-ft}$$

$$M_{f-} = 1.25 M_{DC-} + 1.5 M_{Dw-} + 1.75 M_{L-}$$

$$M_{f-} = 1.25 * 0.66 + 1.5 * 0.16 + 1.75 * 7.8$$

$$M_{f-} = 14.7 \text{ k-ft}$$

The effective depths of the slab:

$$d^+ = 8.5 - 0.5 - 0.5 - 1 - 0.5/2 = 6.75 \text{ in}$$

$$d^- = 8.5 - 1 - 0.5/2 = 7.25 \text{ in}$$

4. Positive bending moment reinforcement

$$R_n = \frac{M_u}{\phi b d^2}$$

$$R_n = \frac{19.4 * 12000}{1 * 12 * (6.75)^2}$$

$$R_n = 425.8 \text{ psi}$$

From Table A 5a (Design Concrete Structures), $\rho = 0.006$

$$S_o, A_{sp} = 0.006 * 12 * 6.75 = 0.485 \text{ in}^2/\text{ft}$$

$$\text{Using \#4 bars, } A_s = 0.375 \text{ in}^2$$

$$S^+ = 0.375 * 12 / 0.485 = 9 \text{ in c/c}$$

5. Negative bending moment reinforcement

$$R_n = \frac{M_u}{\phi b d^2}$$

$$R_n = \frac{14.7 * 12000}{1 * 12 * (7.25)^2}$$

$$R_n = 300 \text{ psi}$$

From Table A 5a (Design Concrete Structures), $\rho = 0.004$

$$S_o, A_{sp} = 0.004 * 12 * 7.25 = 0.348 \text{ in}^2/\text{ft}$$

$$\text{Using \#4 bars, } A_s = 0.375 \text{ in}^2$$

$$S^- = 0.375 * 12 / 0.348 = 12 \text{ in c/c}$$

6. Distribution reinforcement in bottom slab

$$S = 5' - 4'' - 16'' = 4 \text{ ft (clear span)}$$

$$D = \frac{220}{\sqrt{S}} = \frac{220}{\sqrt{4}} = 110\% > 67\% \text{ so use } 67\%$$

$$A_s * 0.67 = 0.486 * 0.67 = 0.326 \text{ in}^2/\text{ft}$$

Use #4 @ 13 in c/c

7. Temperature and shrinkage reinforcement (AASHTO 5.10.6)

$$A_s = \frac{1.3 \cdot b \cdot h}{2 \cdot (b+h) \cdot f_y} = \frac{1.3 \cdot 12 \cdot 8.5}{2 \cdot (12+8.5) \cdot 145}$$

$$A_s = 0.023 < 0.11 \text{ in}^2, \text{ Use } 0.11 \text{ in}^2$$

So use #4 @ 18 in C/c

4.25 in Deck Design

$$f_c' = 4000 \text{ psi}$$

$$f_{tu}^* = 145,000 \text{ psi}$$

$$E_f = 6000,000 \text{ psi}$$

Deck thickness = 4.25 in

$$D_c = 4.25 \cdot 1/12 \cdot (0.15 \text{ k/ft}^3) = 0.05 \text{ k/ft}$$

$$D_w = 0.025 \text{ k/ft (Wearing surface)}$$

1- Dead load

a. Positive bending moment

$$M_{DC+} = 0.071 \cdot D_c \cdot S^2 \quad (\text{AASHTO Table A 4.1 P. 4-98, 102})$$

$$M_{DC+} = 0.071 \cdot 0.05 \cdot (2.67)^2 = 0.025 \text{ k-ft}$$

$$M_{Dw+} = 0.071 \cdot 0.025 \cdot (2.67)^2 = 0.013 \text{ k-ft}$$

$$\begin{aligned} \text{Strip of positive moment} &= 26 + 6.6 \cdot S \\ &= 26 + 6.6 \cdot 2.67 = 44 \text{ in} \end{aligned}$$

$$\begin{aligned} \text{Strip of negative moment} &= 48 + 3 \cdot S \\ &= 48 + 3 \cdot 2.67 = 56 \text{ in} \quad (\text{AASHTO Table 4.6.2.1.3-1}) \end{aligned}$$

$$M_{DC+} = 0.025 \cdot \frac{144}{44} = 0.082 \text{ k-ft/ft}$$

$$M_{Dw+} = 0.013 * \frac{144}{56} = 0.033 \text{ k-ft/ft}$$

a. Negative bending moment

$$M_{Dc-} = 0.1 * D_c * S^2$$

$$M_{Dc-} = 0.1 * 0.05 * (2.67)^2$$

$$M_{Dc-} = 0.036 \text{ k-ft}$$

$$M_{Dw-} = 0.1 * D_w * S^2$$

$$M_{Dw-} = 0.1 * 0.025 * (2.67)^2$$

$$M_{Dw-} = 0.019 \text{ k-ft}$$

$$M_{Dc-} = 0.036 * \frac{144}{44} = 0.12 \text{ k-ft/ft}$$

$$M_{Dw-} = 0.019 * \frac{144}{56} = 0.05 \text{ k-ft/ft}$$

2- Live Load (HL-93)

From AASHTO Table A 4-1:

$$M_{L+} = 2.5 \text{ k-ft and } M_{L-} = 2.07 \text{ k-ft}$$

$$M_{L+} = 2.5 * \frac{144}{44} = 8.1 \text{ k-ft/ft}$$

$$M_{L-} = 2.07 * \frac{144}{56} = 5.3 \text{ k-ft/ft}$$

3- Load Combinations:

$$M_{f+} = 1.25 M_{Dc+} + 1.5 M_{Dw+} + 1.75 M_{L+}$$

$$M_{f+} = 1.25 * 0.082 + 1.5 * 0.033 + 1.75 * 8.1$$

$$M_{f+} = 14.3 \text{ k-ft}$$

$$M_{f-} = 1.25 M_{Dc-} + 1.5 M_{Dw-} + 1.75 M_{L-}$$

$$M_{f-} = 1.25 * 0.12 + 1.5 * 0.05 + 1.75 * 5.3$$

$$M_f = 7.275 \text{ k-ft}$$

The effective depths of the slab:

$$d^+ = 4.25 - 0.5/2 - 0.5 - 0.5/4 = 3.375 \text{ in}$$

$$d^- = 4.25 - 0.5 - 0.5/4 = 3.625 \text{ in}$$

4- Positive bending moment reinforcement

$$R_n = \frac{M_u}{\phi b d^2}$$

$$R_n = \frac{14.3 * 12000}{1 * 12 * (3.375)^2}$$

$$R_n = 1255 \text{ psi}$$

From Table A 5a (Design Concrete Structures)

$$\rho * f_y (1 - 0.588 \rho f_y / f_c')$$

$$\rho * 145000 (1 - 0.588 \rho * 145000 / 4000)$$

$$\rho = 0.0115$$

$$\text{So, } A_{sp} = 0.0115 * 12 * 3.375 = 0.46 \text{ in}^2/\text{ft}$$

$$\text{Using \#4 bars, } A_s = 0.375 \text{ in}^2$$

$$S^+ = 0.375 * 12 / 0.46 = 9 \text{ in c/c}$$

5- Negative bending moment reinforcement.

$$R_n = \frac{M_u}{\phi b d^2}$$

$$R_n = \frac{9.3 * 12000}{1 * 12 * (3.625)^2}$$

$$R_n = 553 \text{ psi}$$

From Table A 5a (Design Concrete Structures), $\rho = 0.0103$

$$\text{So, } A_{sp} = 0.0103 * 12 * 3.625 = 0.448 \text{ in}^2/\text{ft}$$

$$\text{Using \#4 bars, } A_s = 0.375 \text{ in}^2$$

$$S = 0.375 * 12/0.448 = 10 \text{ in c/c}$$

6- Distribution reinforcement in bottom slab

$$S = 2 \text{ ft (clear span)}$$

$$D = \frac{220}{\sqrt{S}} = \frac{220}{\sqrt{2}} = 155\% > 67\% \text{ so use } 67\%$$

$$A_s * 0.67 = 0.448 * 0.67 = 0.30 \text{ in}^2/\text{ft}$$

Use #4 @ 14 in c/c

7- Temperature and shrinkage reinforcement (AASHTO 5.10.6)

$$A_s = \frac{1.3 * b * h}{2 * (b + h) * f_y} = \frac{1.3 * 12 * 4.25}{2 * (12 + 4.25) * 145}$$

$$A_s = 0.014 < 0.11 \text{ in}^2, \text{ Use } 0.11 \text{ in}^2$$

So use #4 @ 18 in C/c

APPENDIX C

Load-deflection and Stress-Strain curves of all specimens of each span.

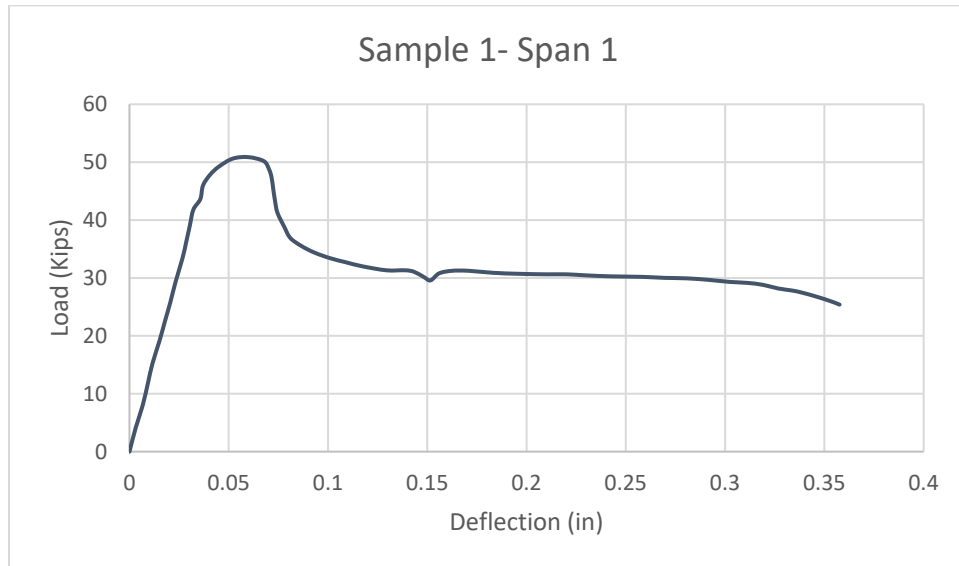


Figure C - 1 Load - Deflection Curve of RC-1 Deck

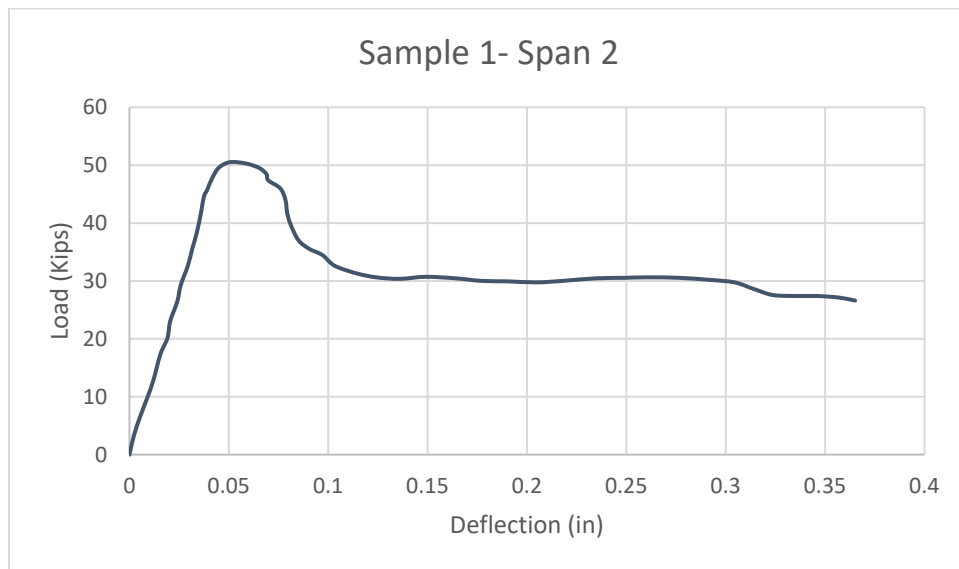


Figure C - 2 Load - Deflection Curve of RC-1 Deck

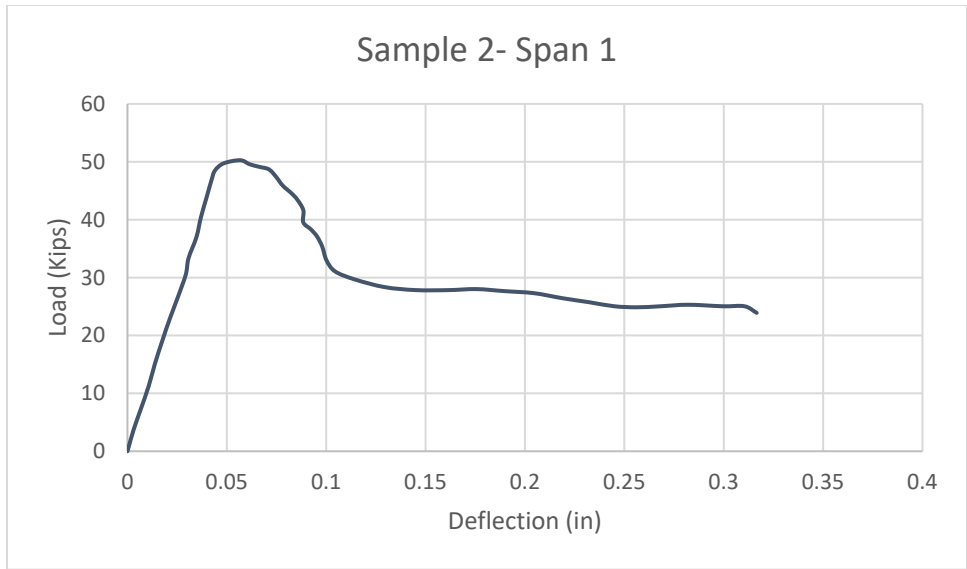


Figure C - 3 Load - Deflection Curve of RC-2 Deck

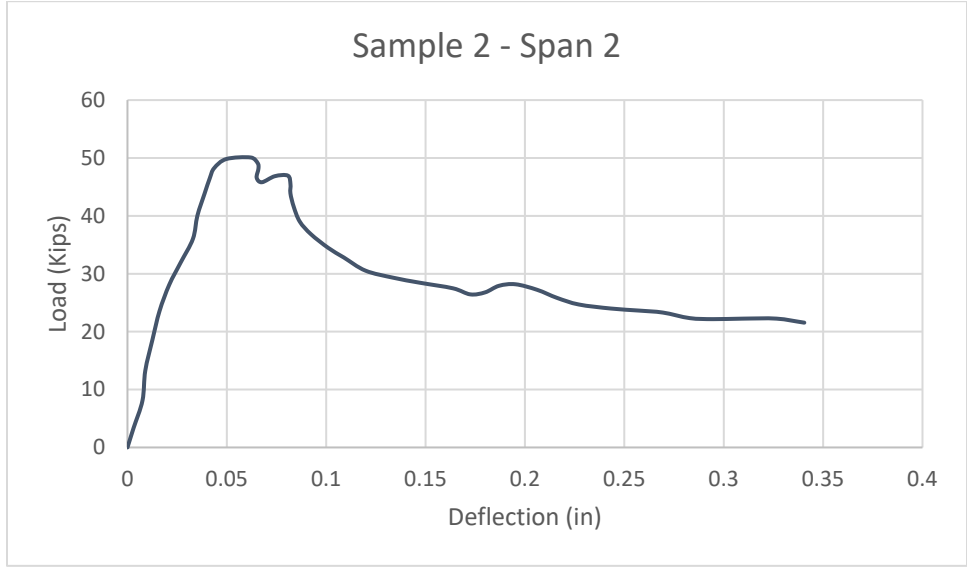


Figure C - 4 Load - Deflection Curve of RC-2 Deck

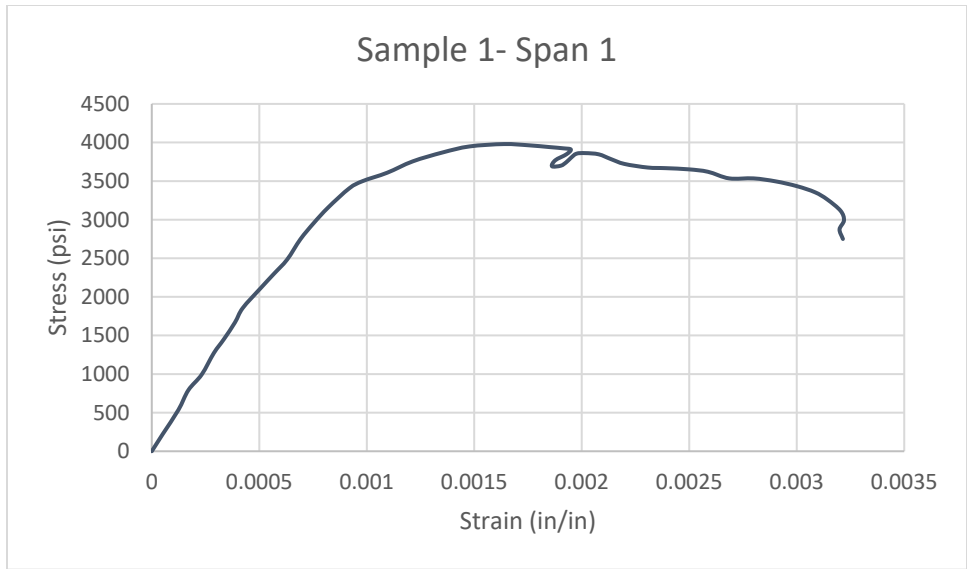


Figure C - 5 Stress – Strain Curve of RC-1 Deck

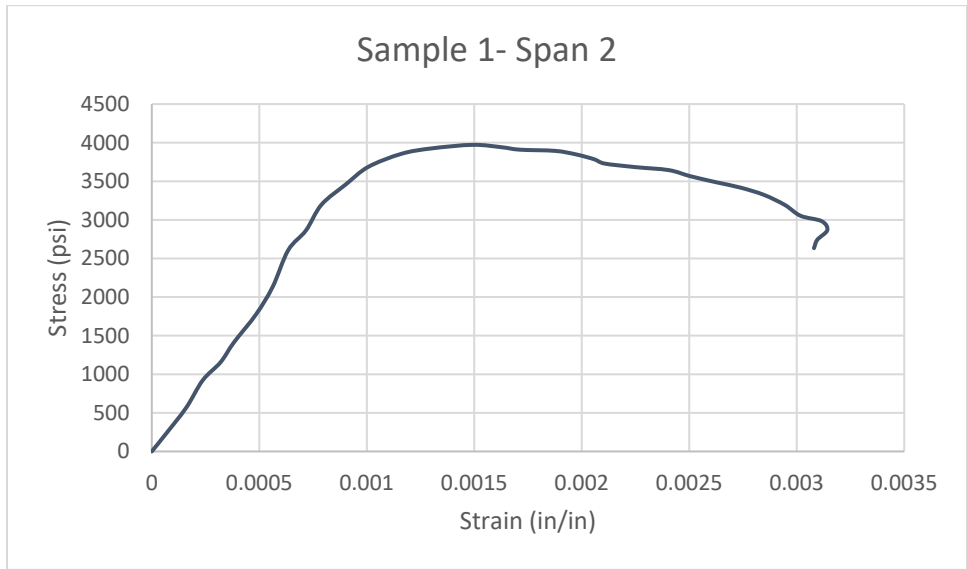


Figure C - 6 Stress – Strain Curve of RC-1 Deck

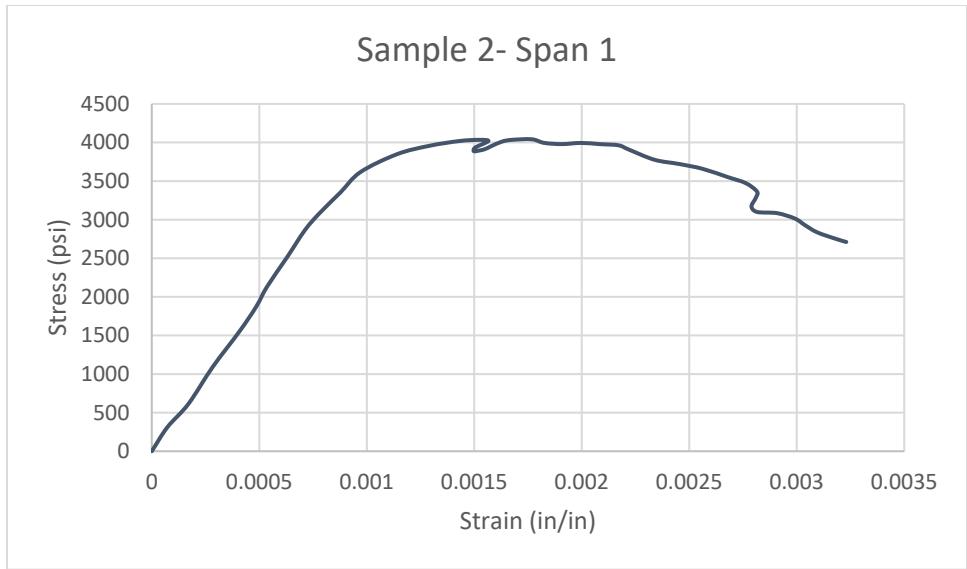


Figure C - 7 Stress – Strain Curve of RC-2 Deck

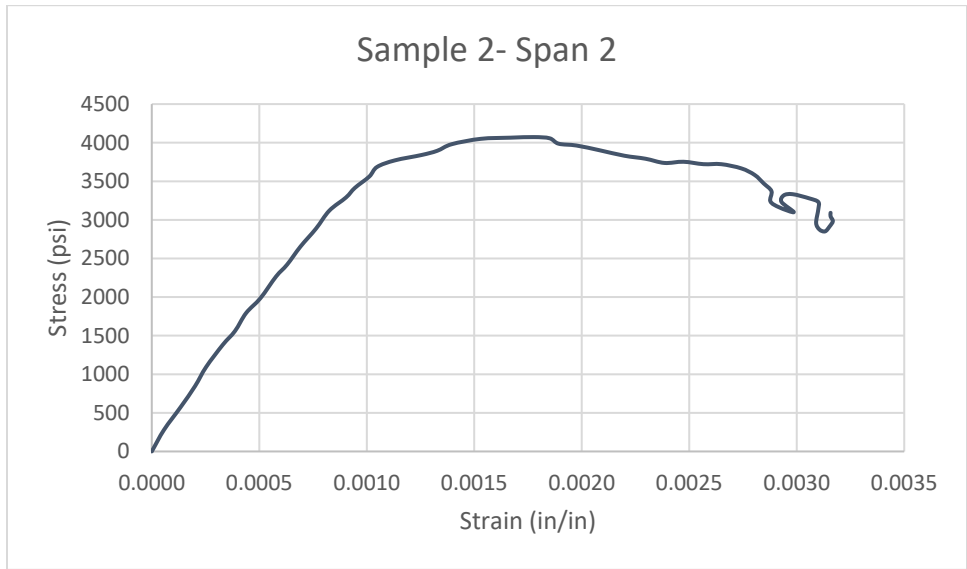


Figure C - 8 Stress – Strain Curve of RC-2 Deck

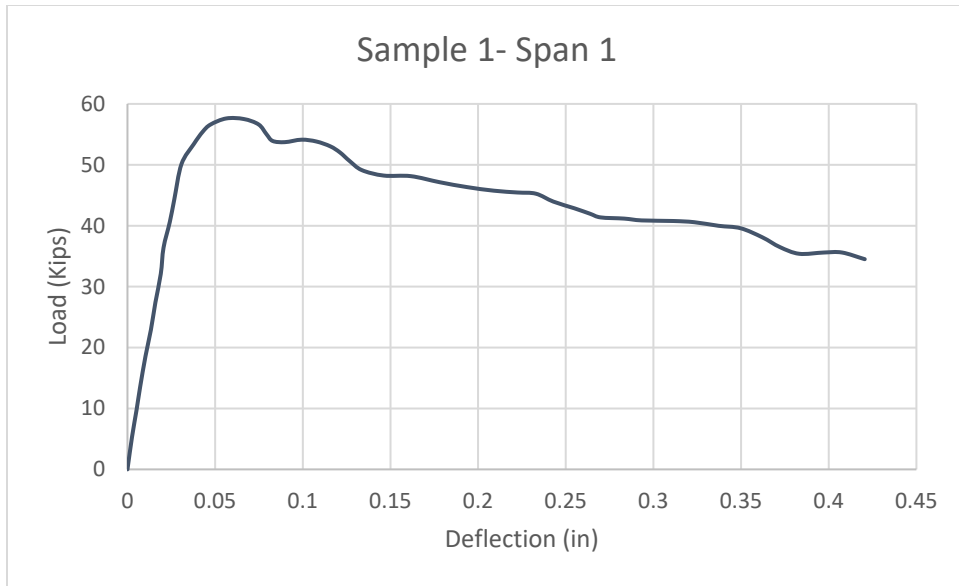


Figure C - 9 Load - Deflection Curve of SFRC-CIP-1 Deck

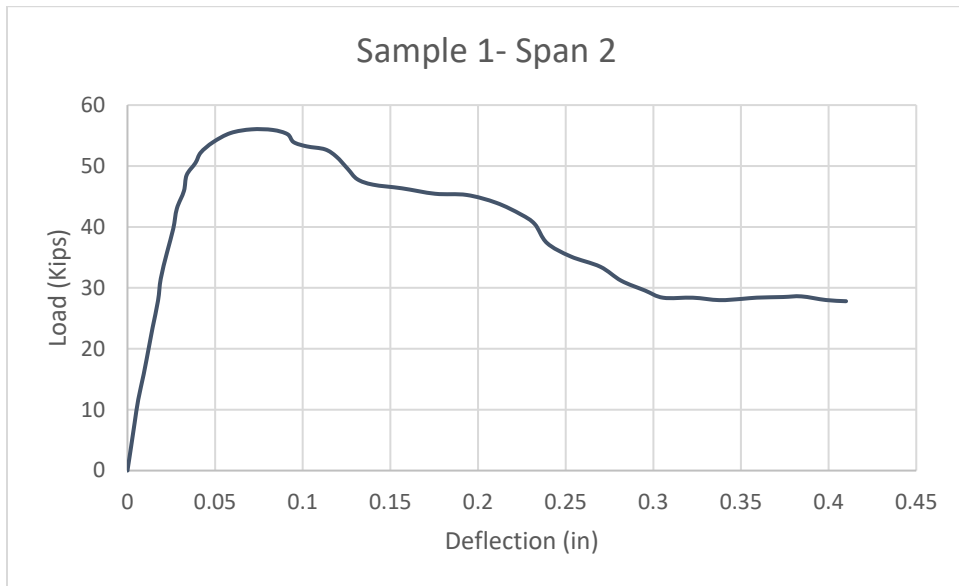


Figure C - 10 Load - Deflection Curve of SFRC-CIP-1 Deck

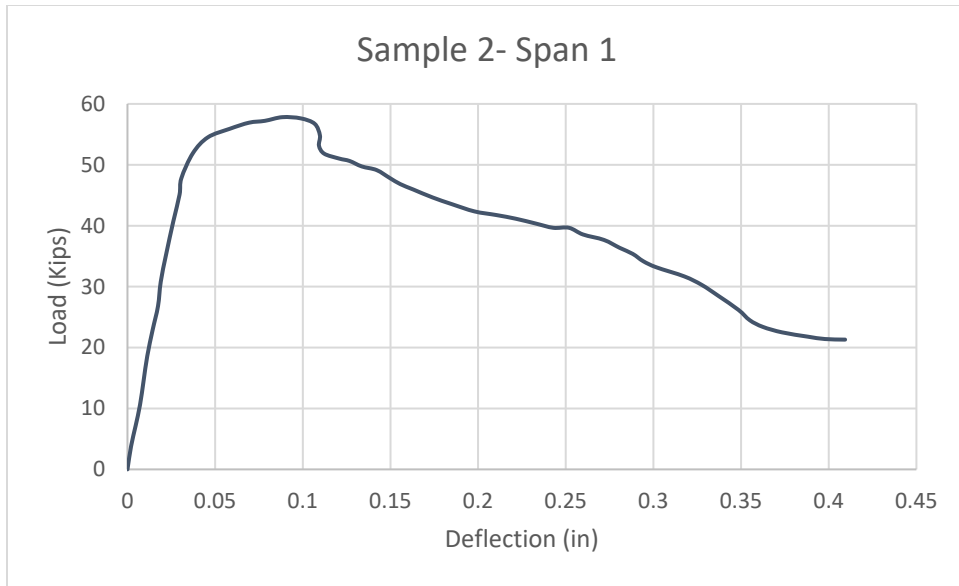


Figure C - 11 Load - Deflection Curve of SFRC-CIP-2 Deck

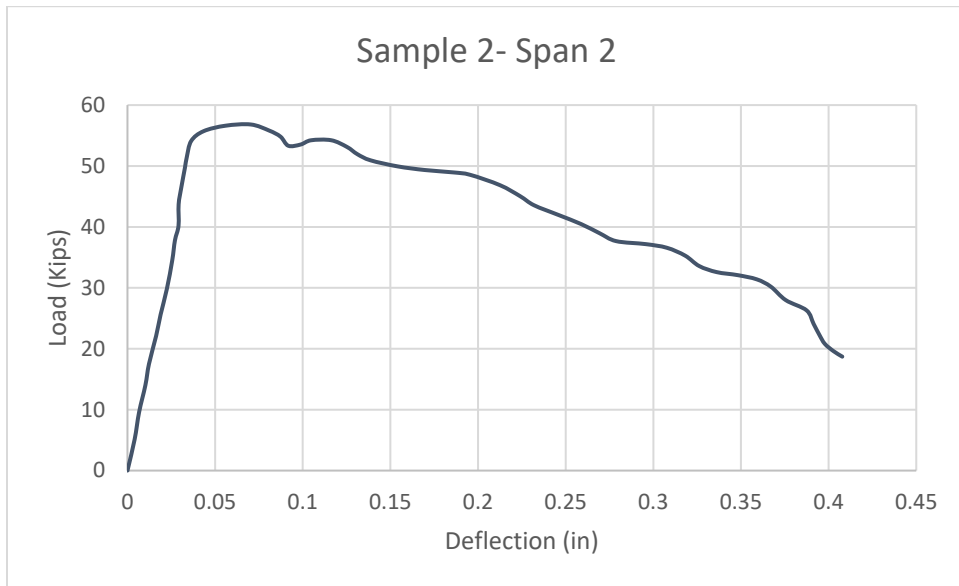


Figure C - 12 Load - Deflection Curve of SFRC-CIP-2 Deck

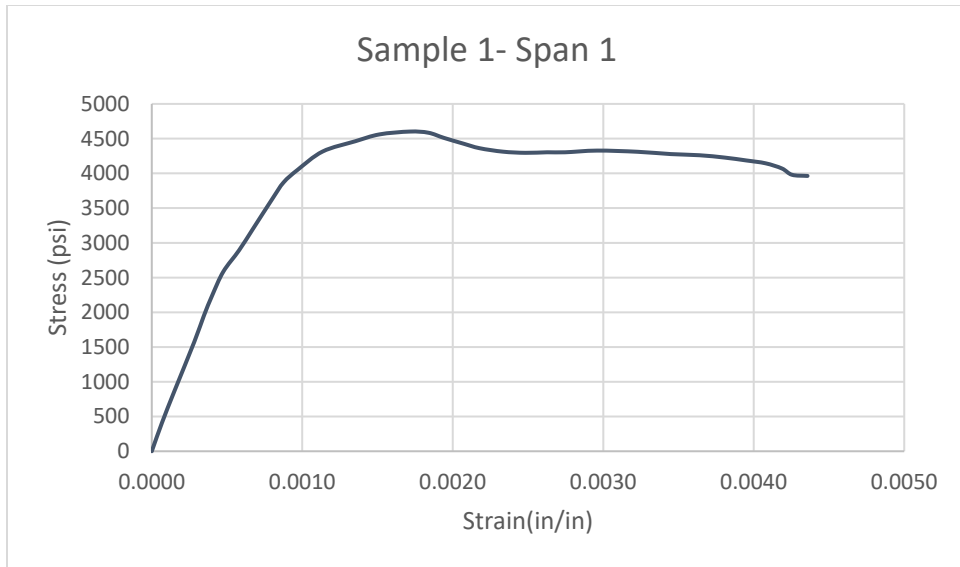


Figure C - 13 Stress - Strain Curve of SFRC-CIP-1 Deck

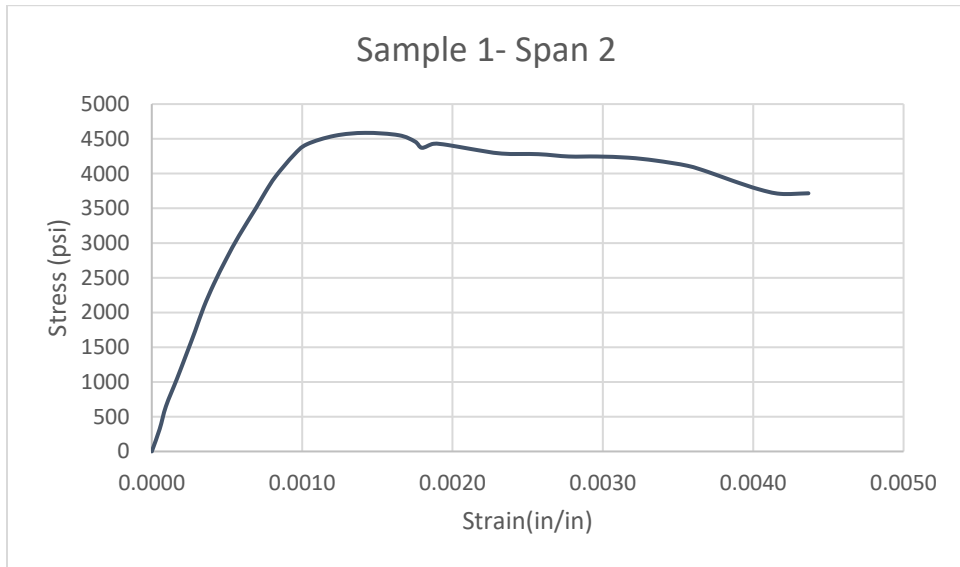


Figure C - 14 Stress - Strain Curve of SFRC-CIP-1 Deck

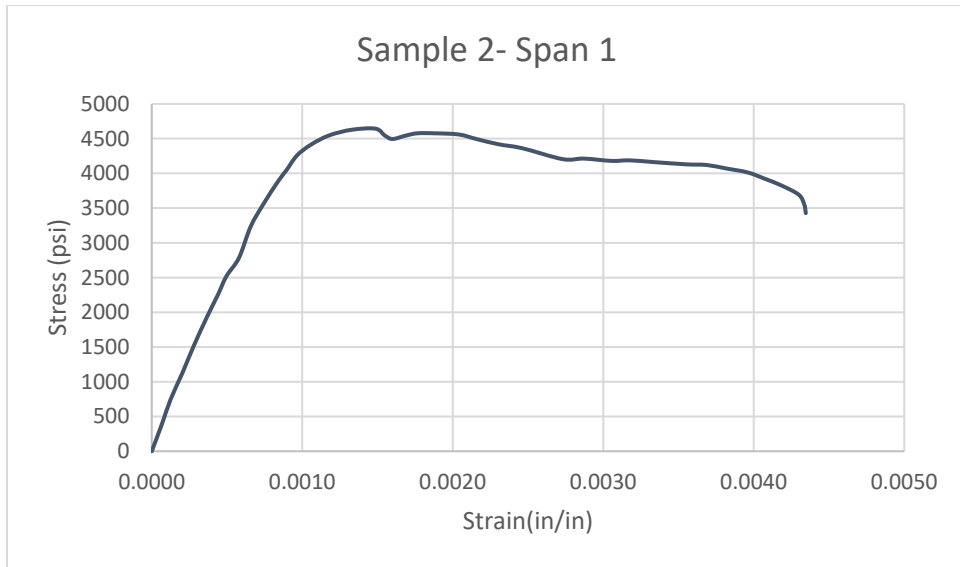


Figure C - 15 Stress - Strain Curve of SFRC-CIP-2 Deck

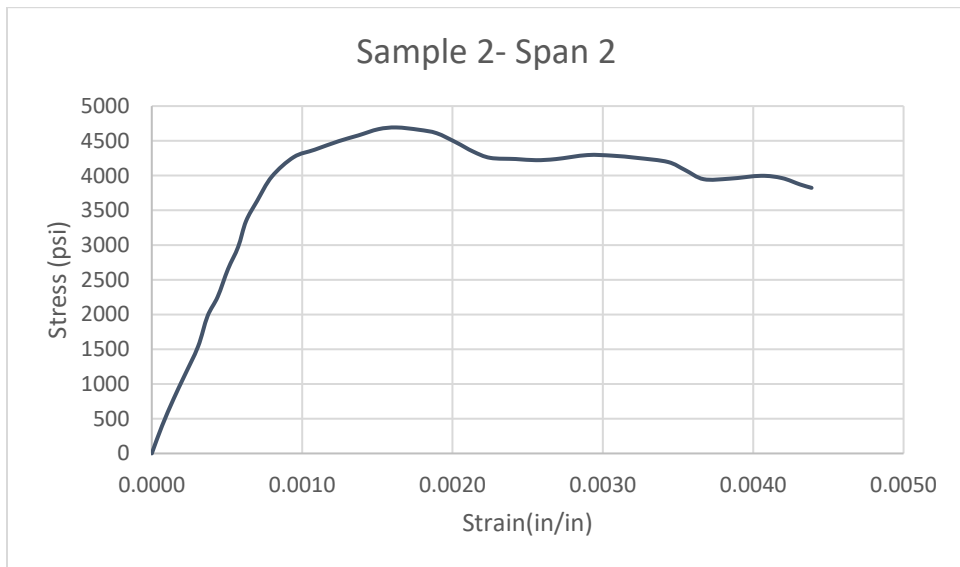


Figure C - 16 Stress - Strain Curve of SFRC-CIP-2 Deck

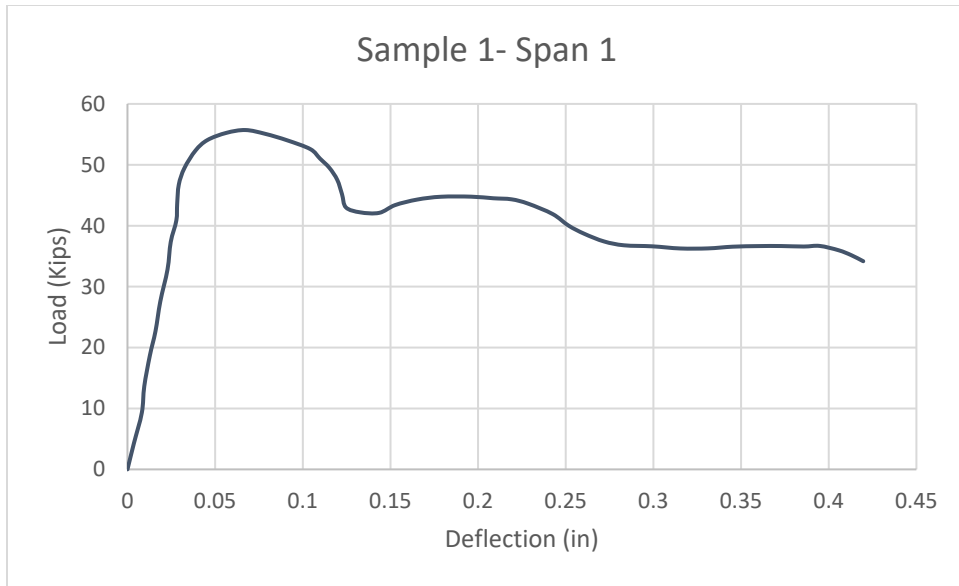


Figure C - 17 Load - Deflection Curve of SFRC-PC-1 Deck

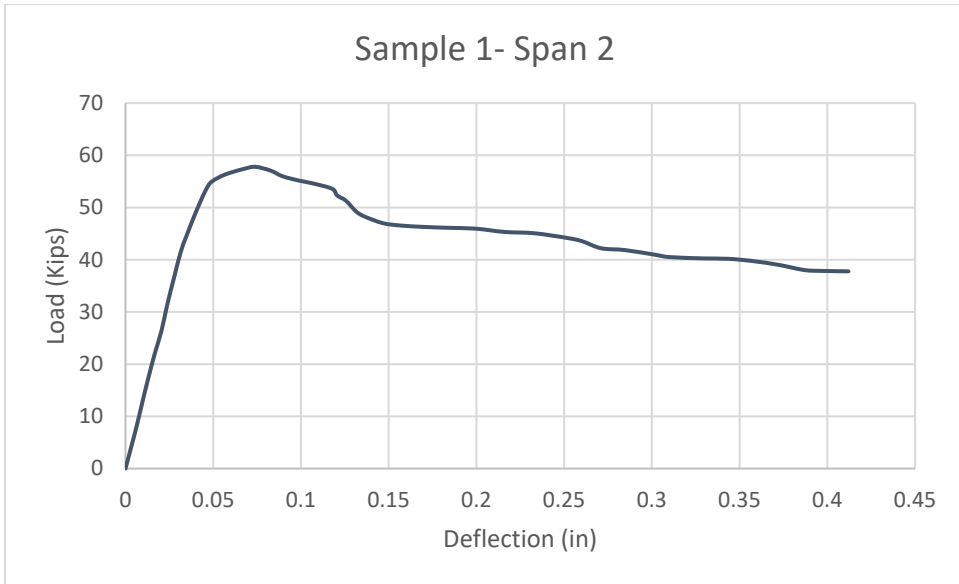


Figure C - 18 Load - Deflection Curve of SFRC-PC-1 Deck

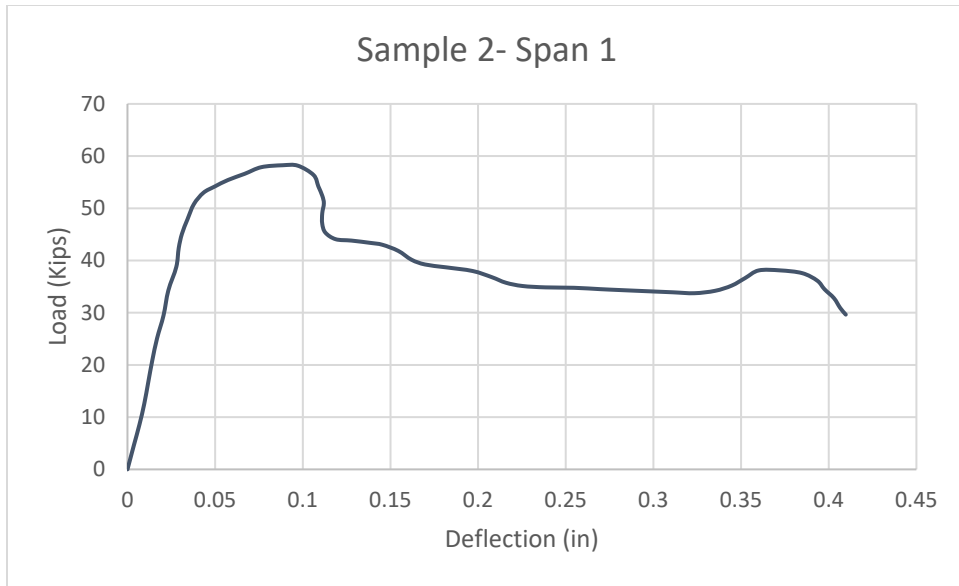


Figure C - 19 Load - Deflection Curve of SFRC-PC-2 Deck

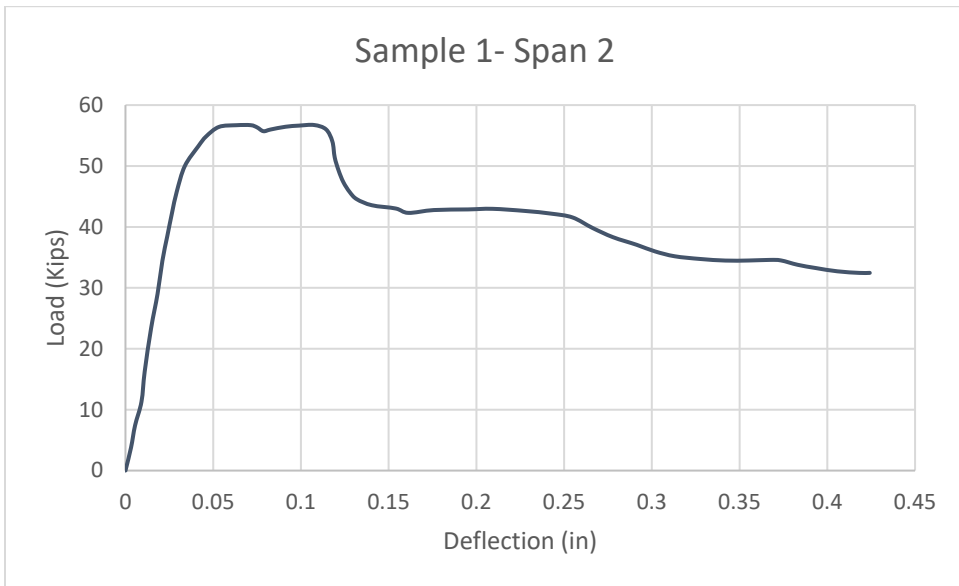


Figure C - 20 Load - Deflection Curve of SFRC-PC-2 Deck

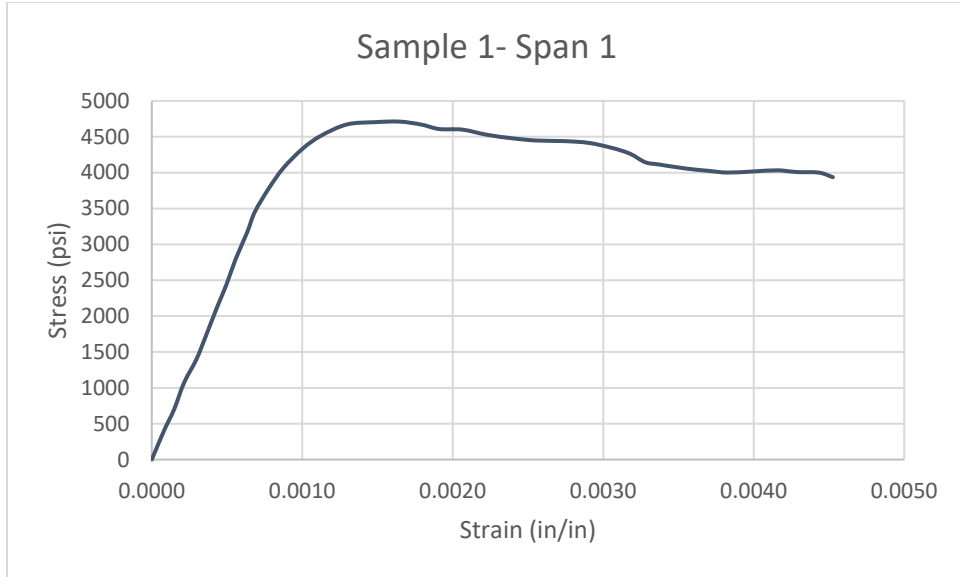


Figure C - 21 Stress – Strain Curve of SFRC-PC-1 Deck

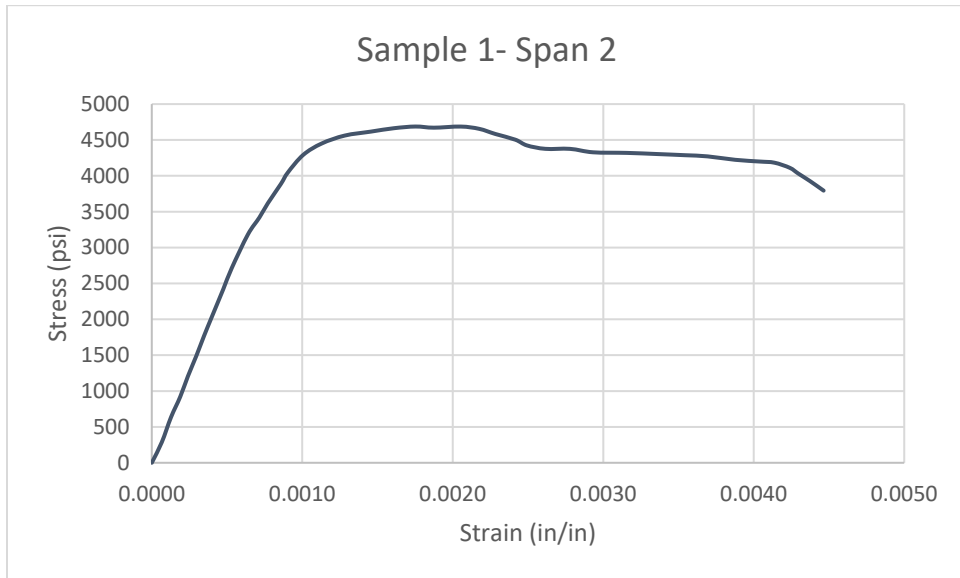


Figure C - 22 Stress – Strain Curve of SFRC-PC-1 Deck

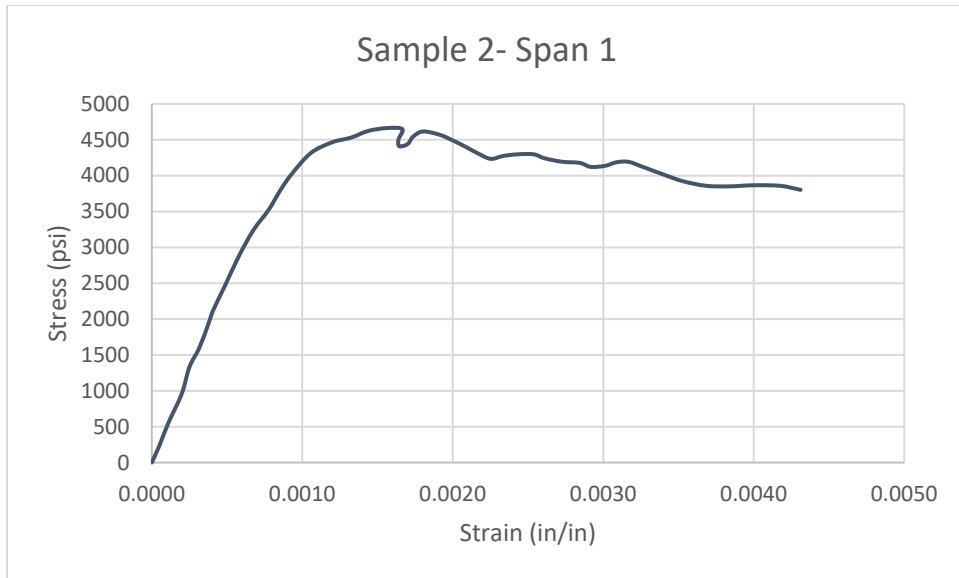


Figure C - 23 Stress – Strain Curve of SFRC-PC-2 Deck

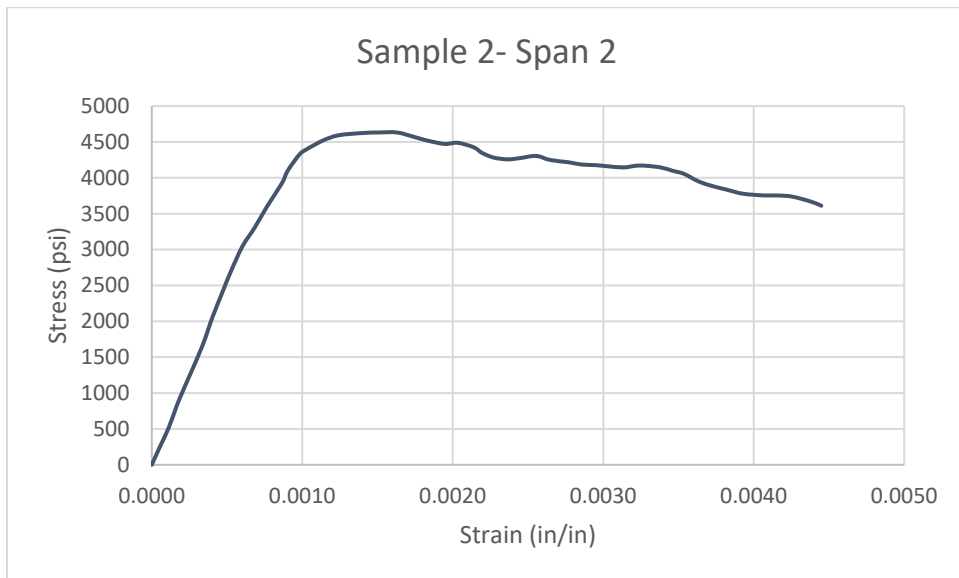


Figure C - 24 Stress – Strain Curve of SFRC-PC-2 Deck

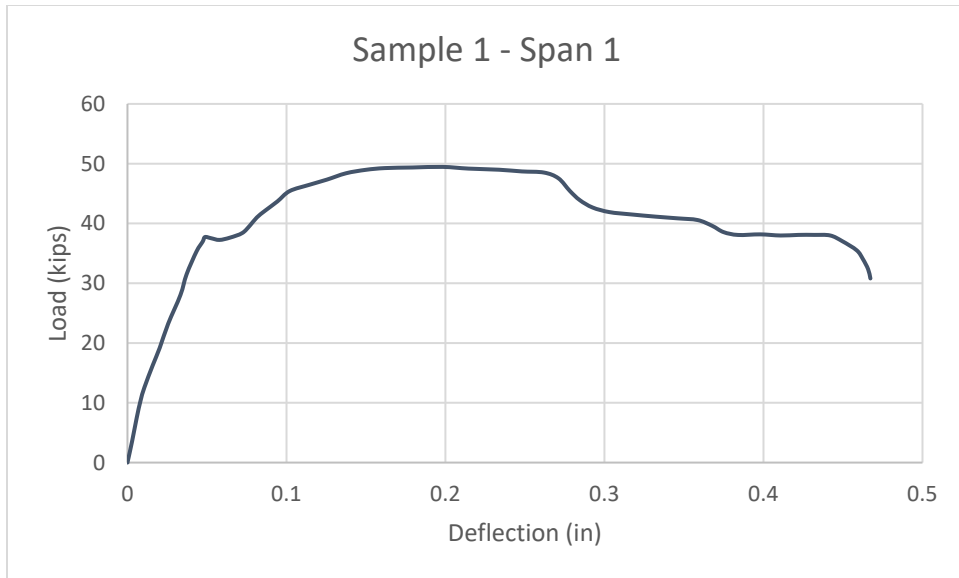


Figure C - 25 Load - Deflection Curve of GFRP-1 Deck

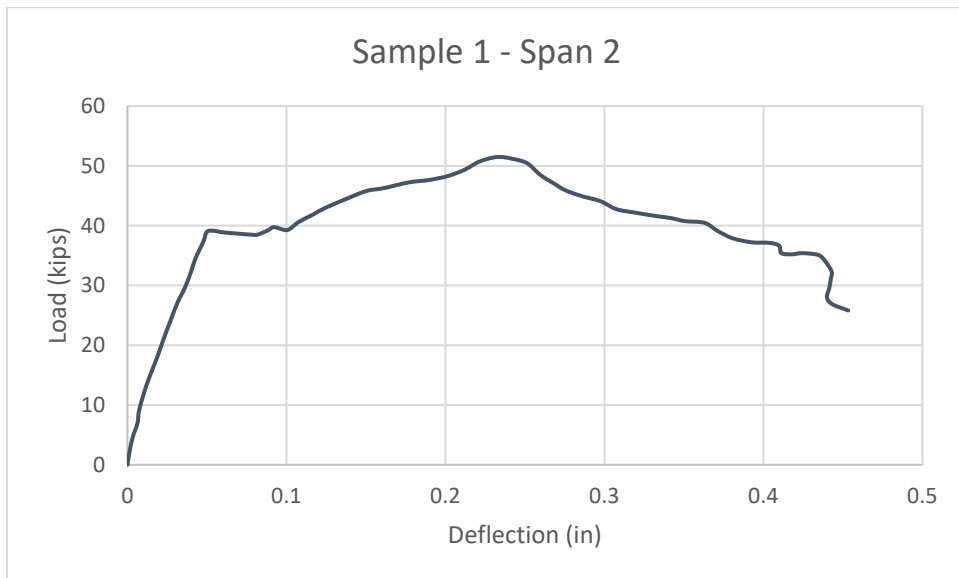


Figure C - 26 Load - Deflection Curve of GFRP-1 Deck

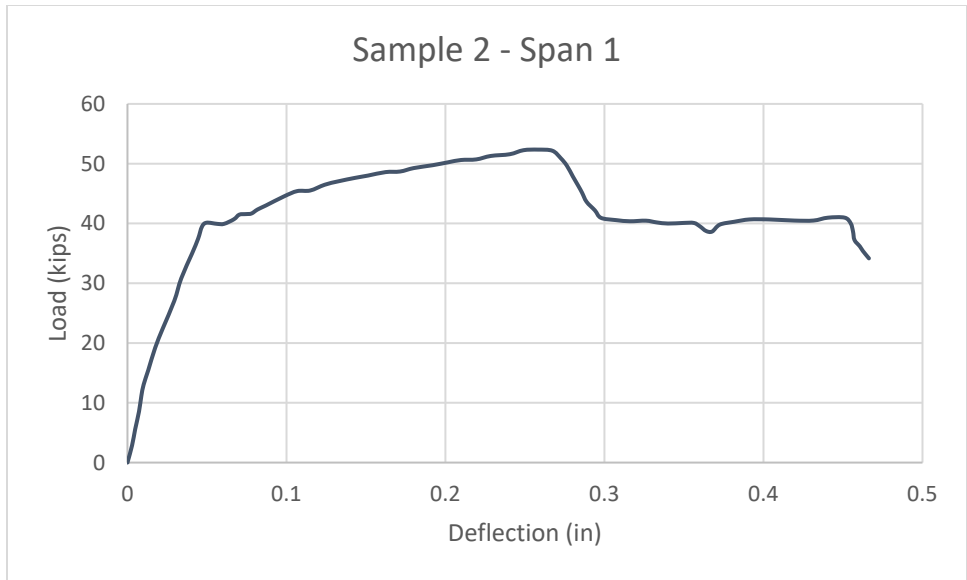


Figure C - 27 Load - Deflection Curve of GFRP-2 Deck

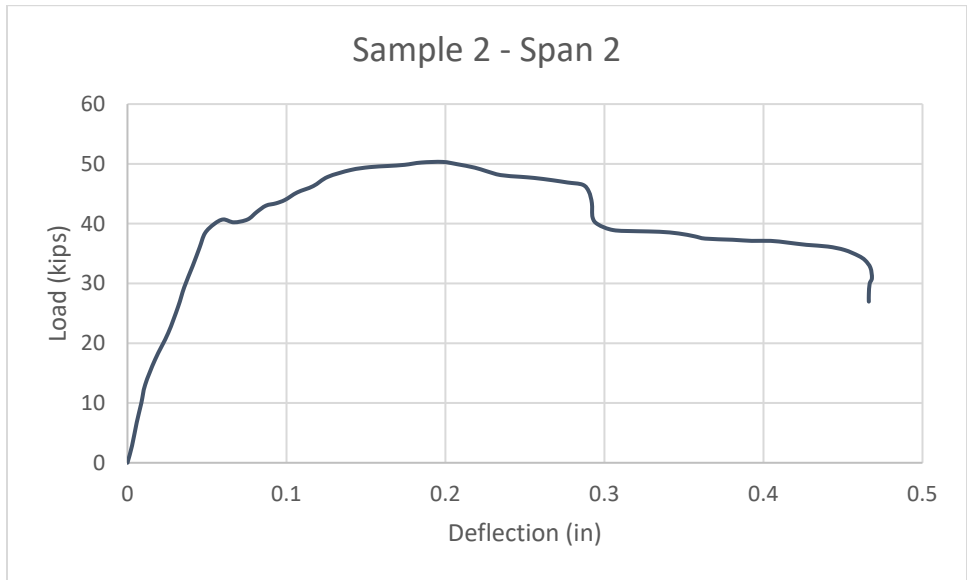


Figure C - 28 Load - Deflection Curve of GFRP-2 Deck

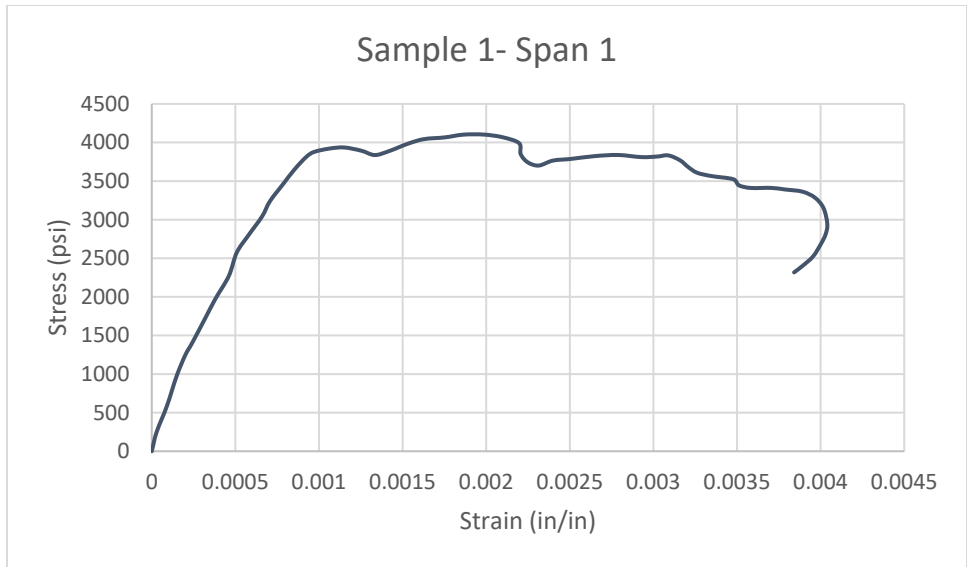


Figure C - 29 Stress-Strain Curve of GFRP-1 Deck

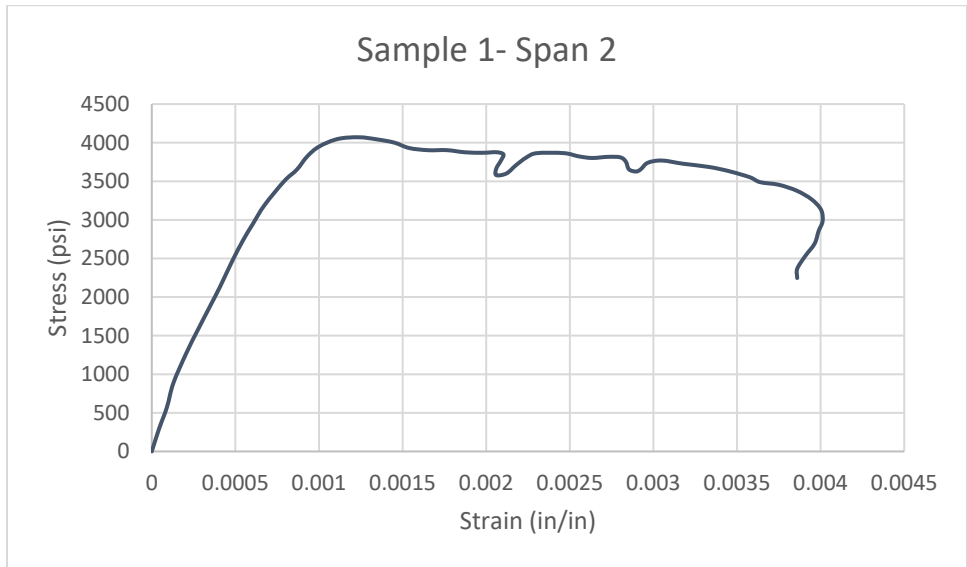


Figure C - 30 Stress-Strain Curve of GFRP-1 Deck

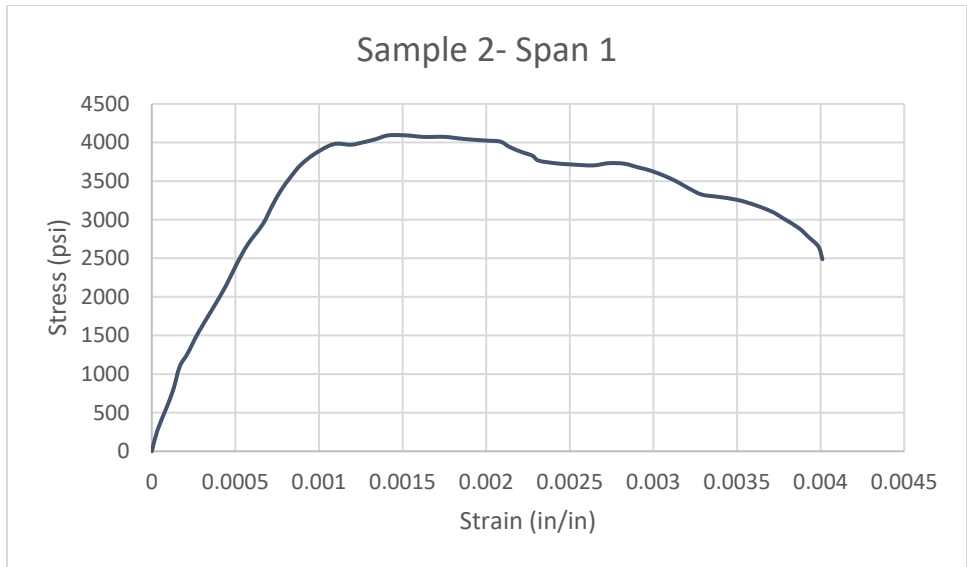


Figure C - 31 Stress-Strain Curve of GFRP-2 Deck

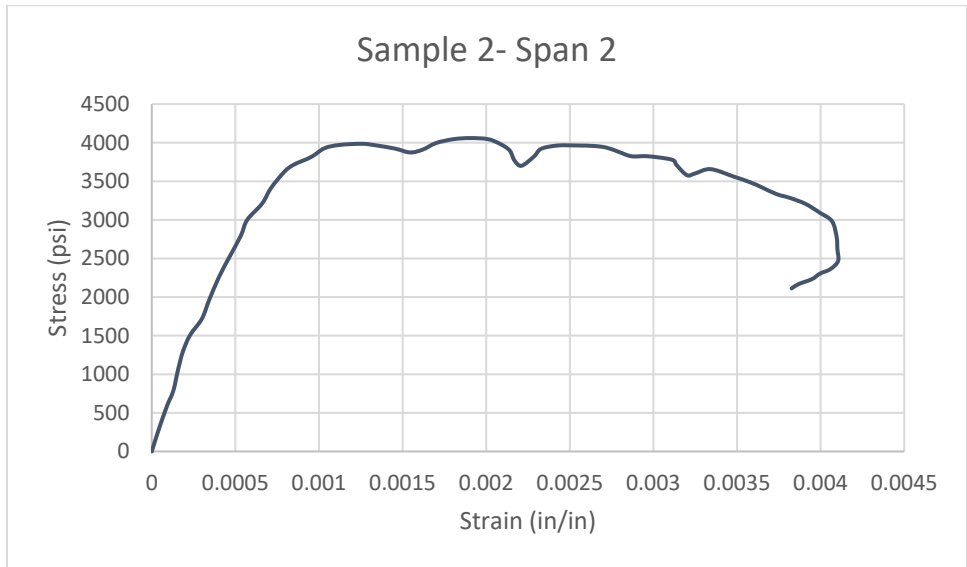


Figure C - 32 Stress-Strain Curve of GFRP-2 Deck

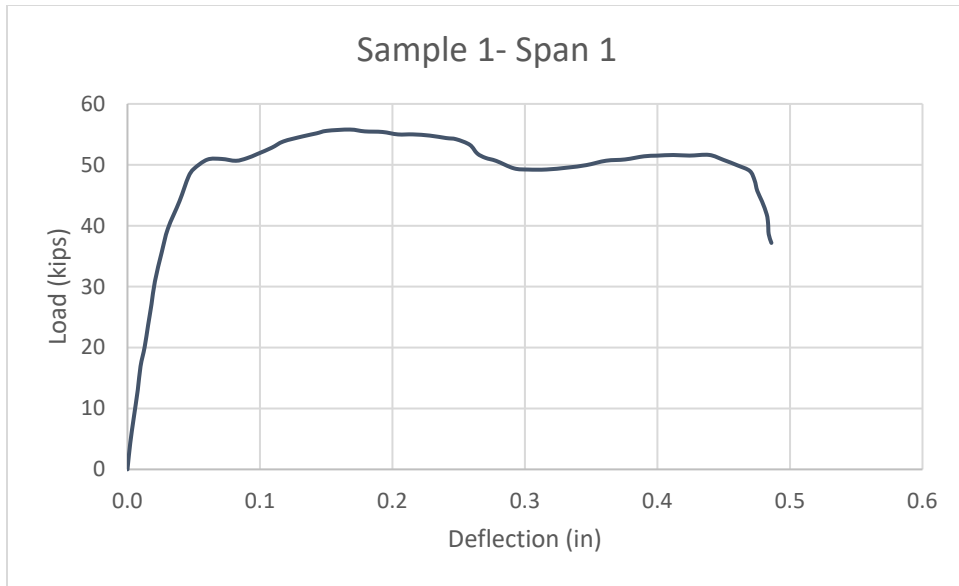


Figure C - 33 Load - Deflection Curve of SFRC-GFRP-CIP-1 Deck

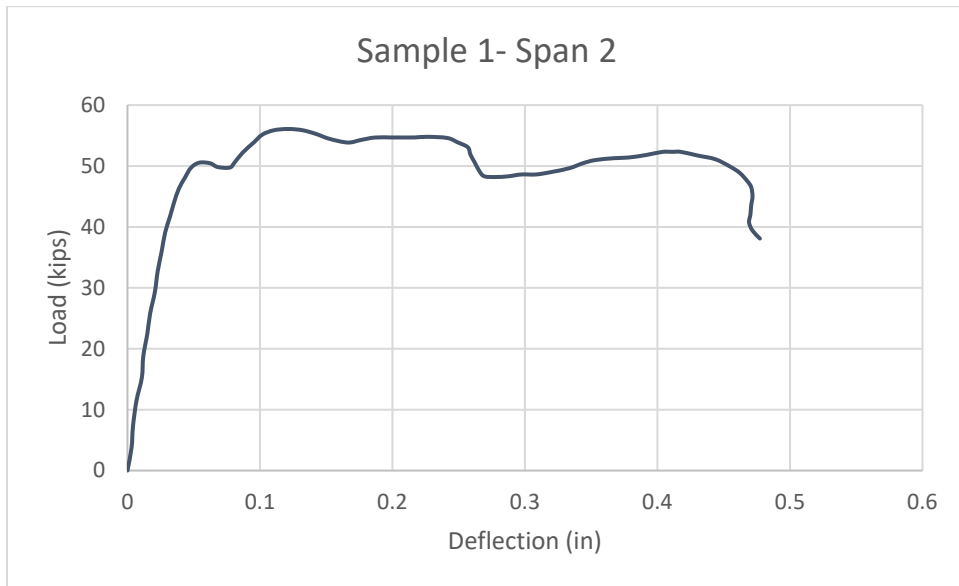


Figure C - 34 Load - Deflection Curve of SFRC-GFRP-CIP-1 Deck

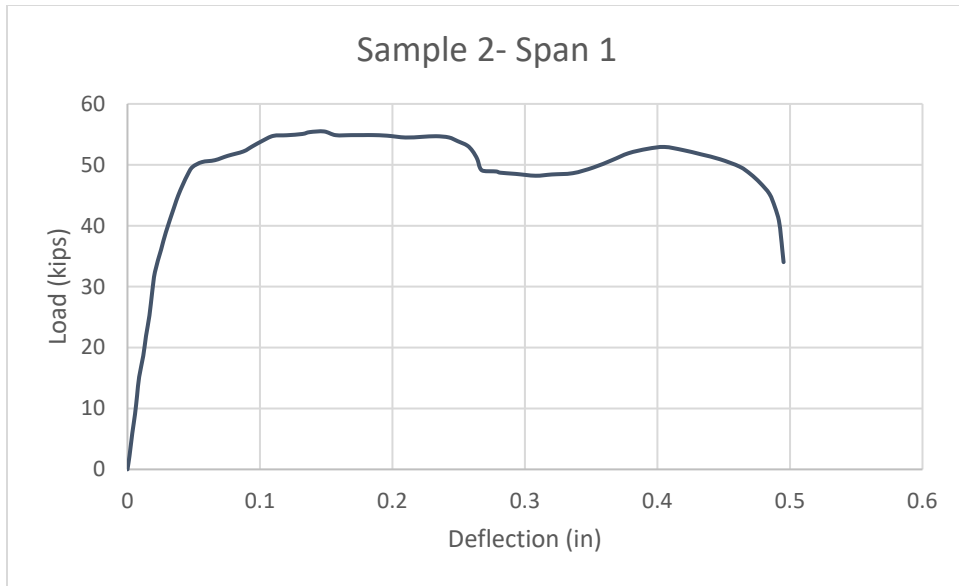


Figure C - 35 Load - Deflection Curve of SFRC-GFRP-CIP-2 Deck

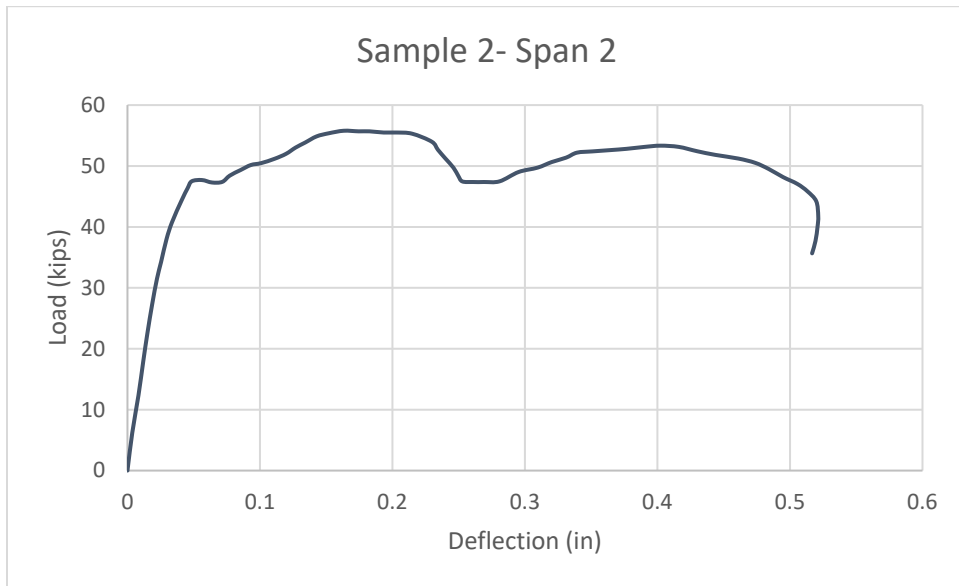


Figure C - 36 Load - Deflection Curve of SFRC-GFRP-CIP-2 Deck

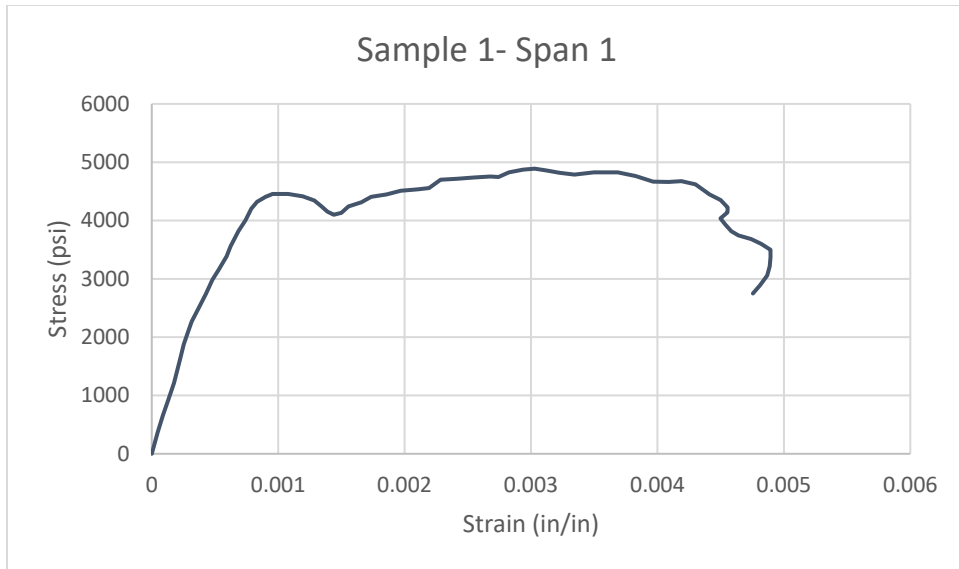


Figure C - 37 Stress - Strain Curve of SFRC-GFRP-CIP-1 Deck

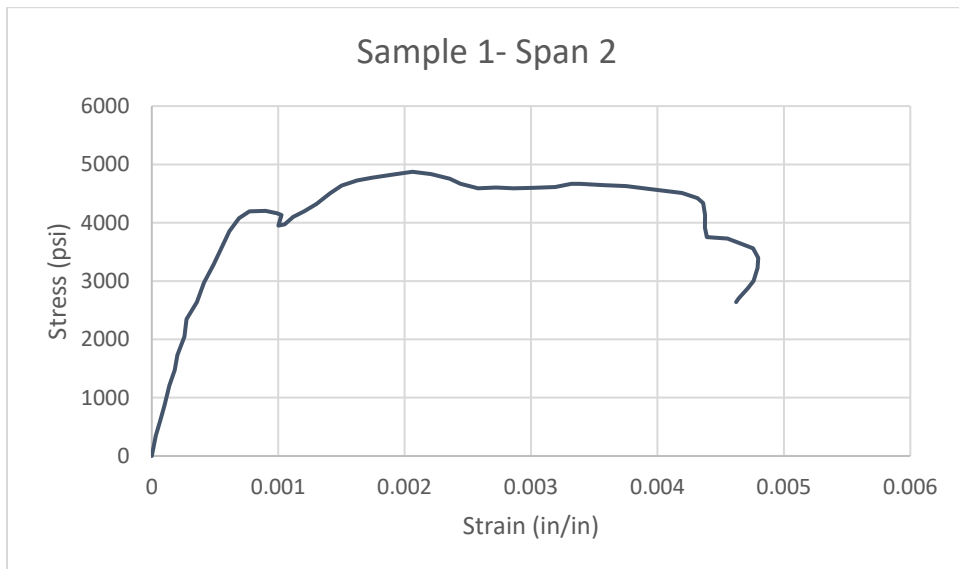


Figure C - 38 Stress - Strain Curve of SFRC-GFRP-CIP-1 Deck

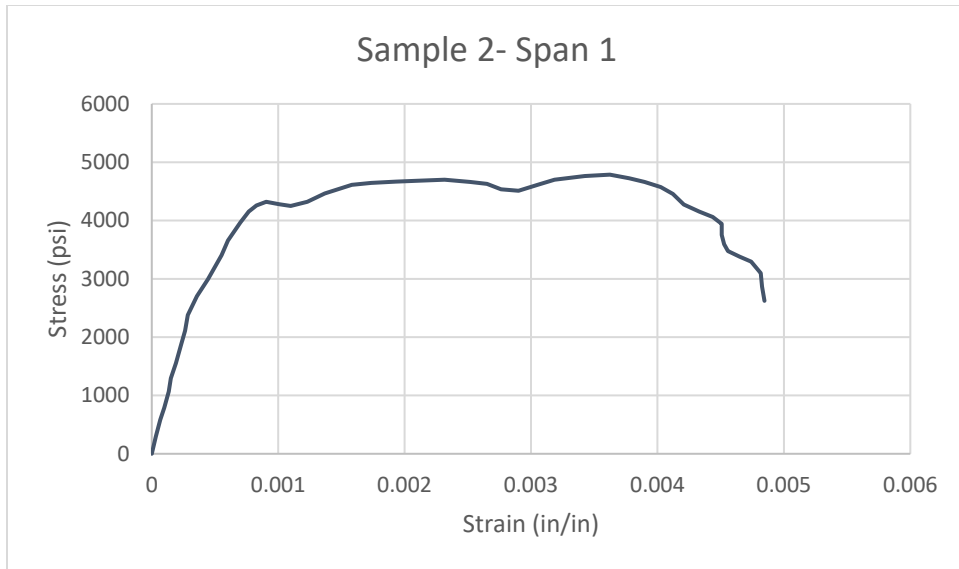


Figure C - 39 Stress - Strain Curve of SFRC-GFRP-CIP-2 Deck

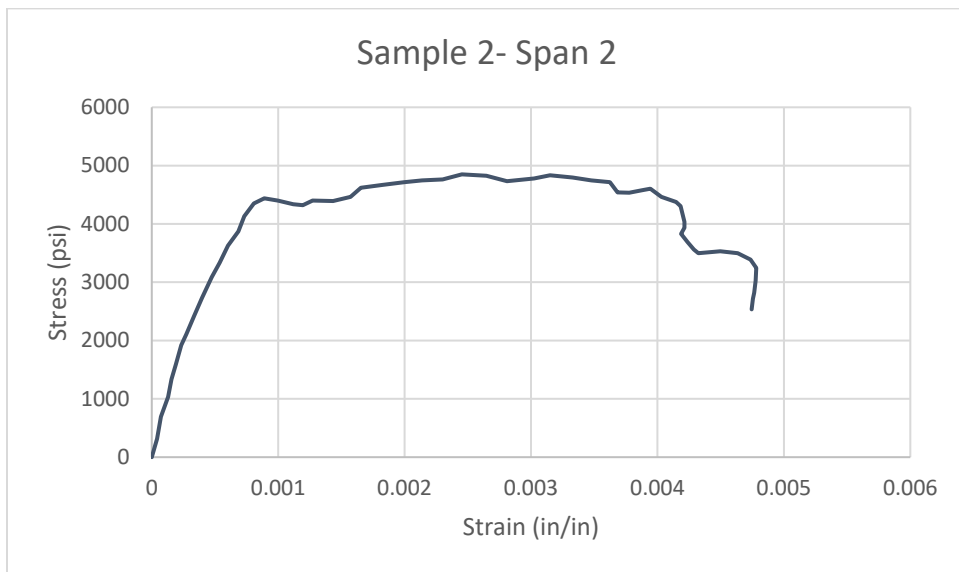


Figure C - 40 Stress - Strain Curve of SFRC-GFRP-CIP-2 Deck

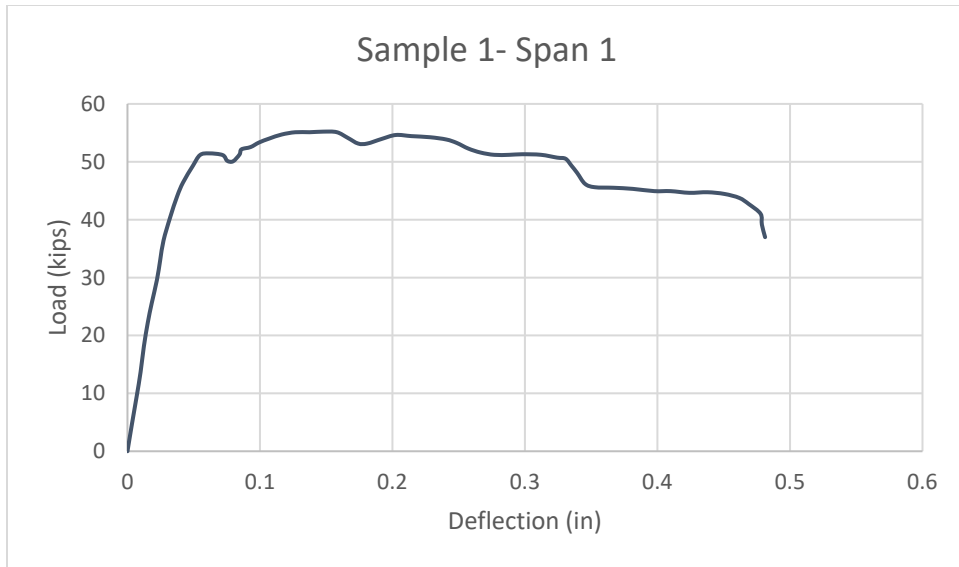


Figure C - 41 Load - Deflection Curve of SFRC-GFRP-PC-1 Deck

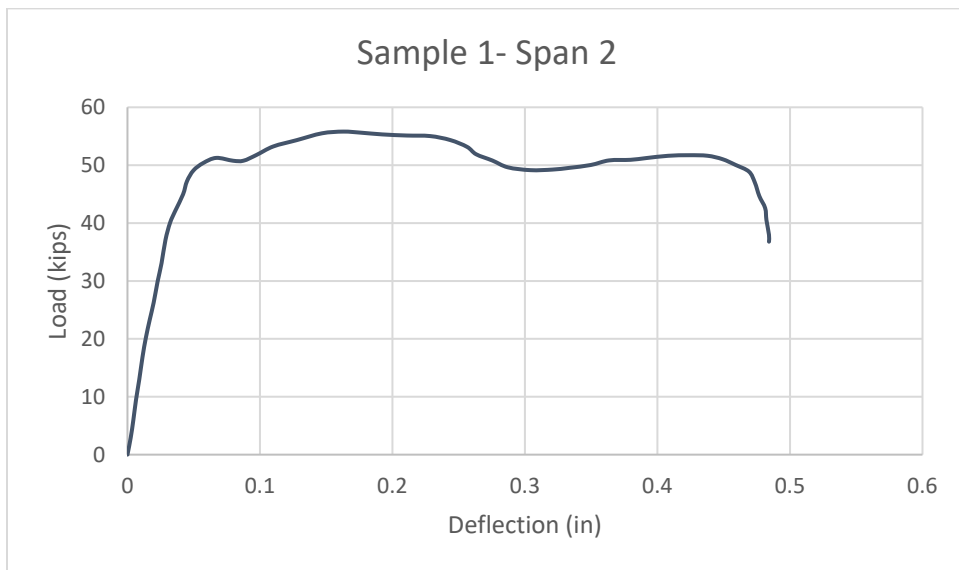


Figure C - 42 Load - Deflection Curve of SFRC-GFRP-PC-1 Deck

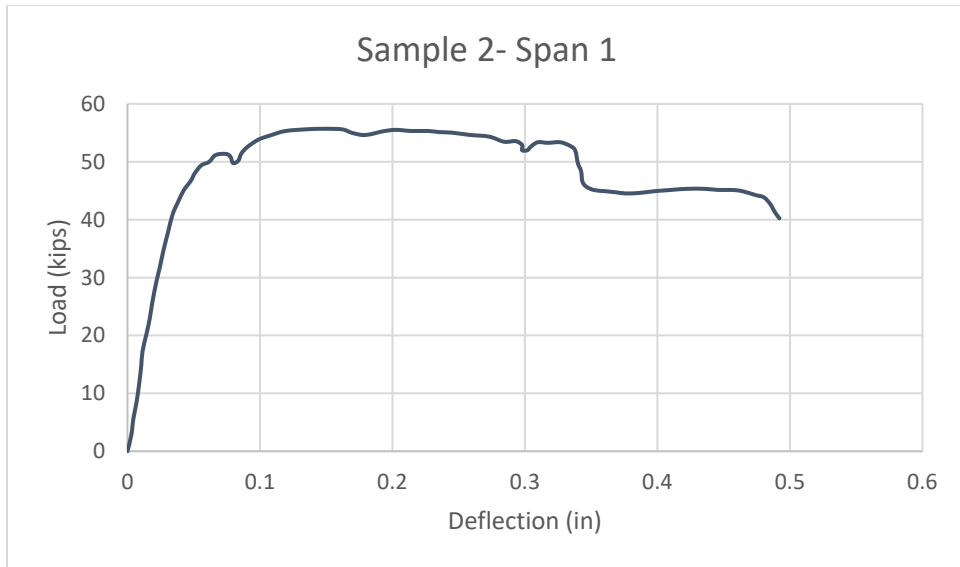


Figure C - 43 Load - Deflection Curve of SFRC-GFRP-PC-2 Deck

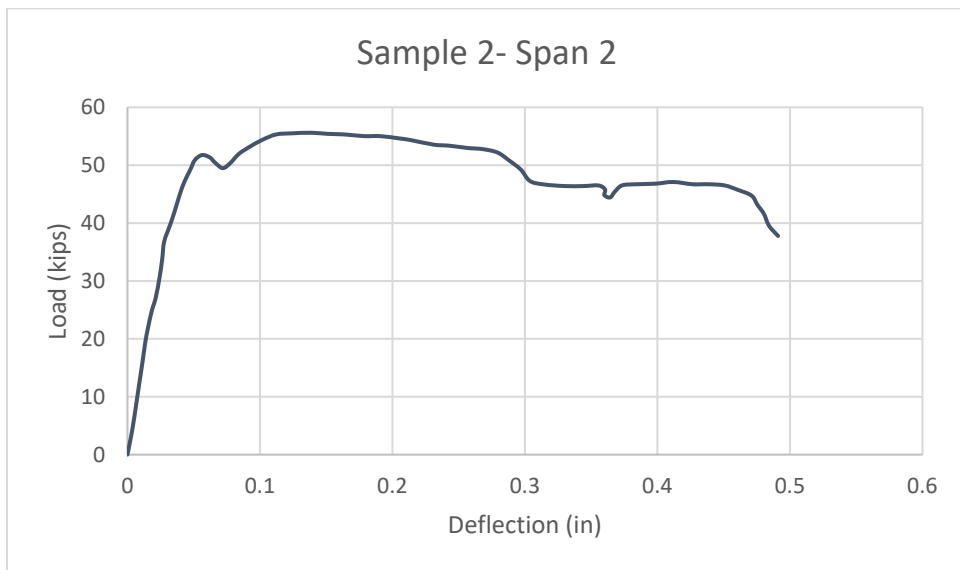


Figure C - 44 Load - Deflection Curve of SFRC-GFRP-PC-2 Deck

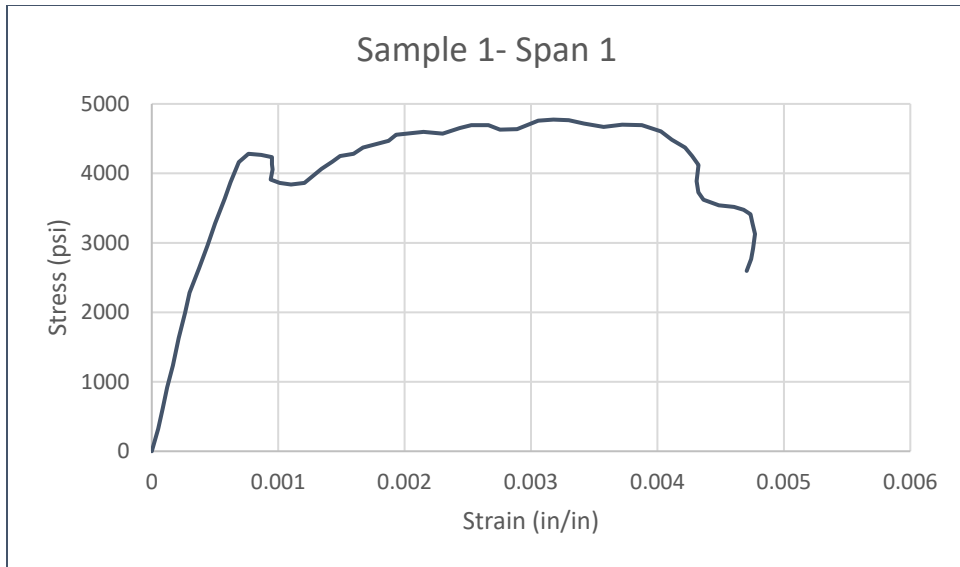


Figure C - 45 Stress - Strain Curve of SFRC-GFRP-PC-1 Deck

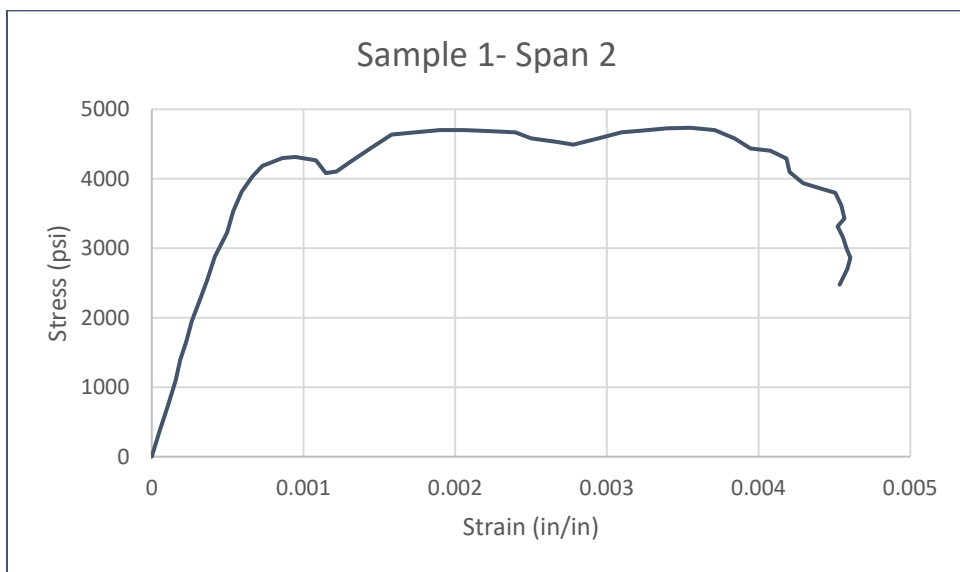


Figure C - 46 Stress - Strain Curve of SFRC-GFRP-PC-1 Deck

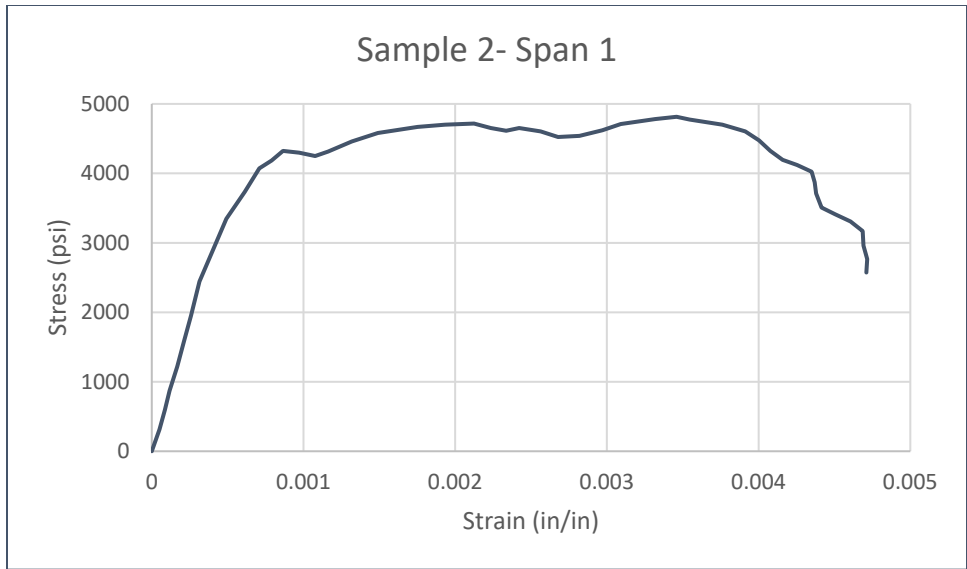


Figure C - 47 Stress - Strain Curve of SFRC-GFRP-PC-2 Deck

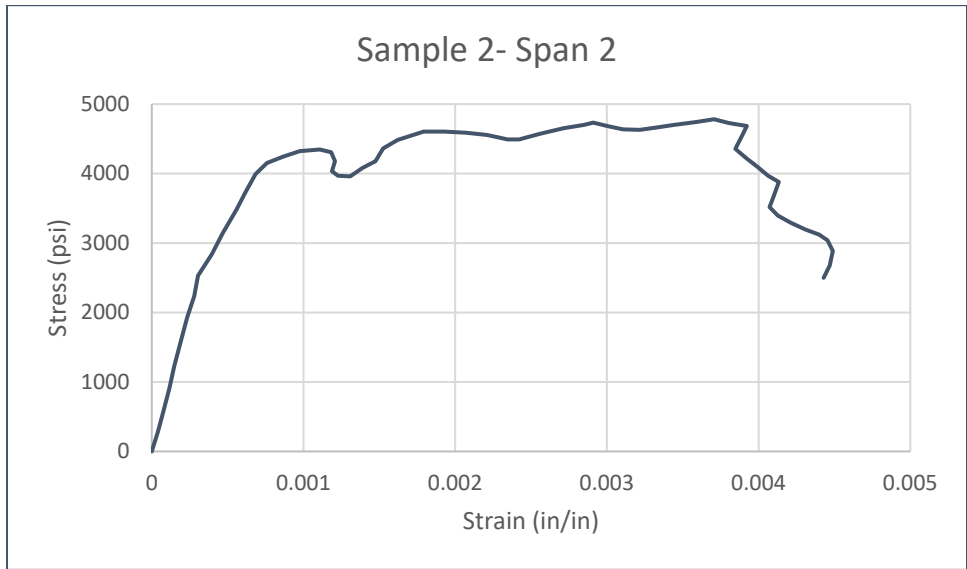


Figure C - 48 Stress - Strain Curve of SFRC-GFRP-PC-2 Deck